NACA

RESEARCH MEMORANDUM

FREE-FLIGHT MEASUREMENTS AT MACH NUMBERS FROM 0.7 TO 1.6 OF SOME EFFECTS OF AIRFOIL-THICKNESS DISTRIBUTION AND TRAILING-EDGE ANGLE ON AILERON ROLLING EFFECTIVENESS AND DRAG FOR WINGS WITH 0° AND 45° SWEEPBACK

By E. M. Fields and H. Kurt Strass

Langley Aeronautical Laboratory
Langley Field, Va.

NATIONAL ADVISORY COMMITTEE
FOR AERONAUTICS

WASHINGTON

October 8, 1951

Classification cancelled (or changed to) UNCLASSIFIED

By Authority of NASA Tech Pub Announcement #118

(OFFICER) 16 Aug 67

BY (NAME AND GRADE OF OFFICER MAKING CHANGE)

31 March

DATE

NACA RM L51G27

NATIONAL ADVISORY COMMITTEE FOR AERONAUTICS

RESEARCH MEMORANDUM

FREE-FLIGHT MEASUREMENTS AT MACH NUMBERS FROM 0.7 TO 1.6 OF SOME EFFECTS OF AIRFOIL-THICKNESS DISTRIBUTION AND TRAILING-EDGE ANGLE ON AILERON ROLLING EFFECTIVENESS AND DRAG FOR WINGS WITH 0° AND 45° SWEEPBACK

By E. M. Fields and H. Kurt Strass

SUMMARY

The wing-aileron rolling effectiveness and drag for full-span sealed ailerons deflected 5° on untapered wings with 0° and 45° sweepback have been investigated over the Mach number range from 0.7 to 1.6 by means of rocket-propelled test vehicles in free flight. The test wings had an aspect ratio of 3.7 and the ailerons were hinged at 0.8 chord. The basic 6-percent-thick symmetrical circular-arc airfoil was modified in thickness distribution to produce a range of trailing-edge angles from 0° to approximately 30°.

In addition, data from previous tests of 3-percent-, 6-percent-, and 9-percent-thick airfoils having the same plan forms and aspect ratio, but with various profiles and trailing-edge angles, are presented and correlated with the results from the present tests to show the effect of trailing-edge angle on rolling effectiveness at various Mach numbers.

For unswept wings having airfoil profiles with flat-sided rearward portions, the results show that increasing the thickness of the trailing edge (decreasing the trailing-edge angle) resulted in large drag increases with small rolling-effectiveness changes.

For unswept wings with profiles having curved rearward portions, increasing the thickness near the trailing edge (increasing the trailing-edge angle) generally resulted in rolling-effectiveness decreases. Trailing-edge angles of 7° or less gave relatively high rolling effectiveness throughout the speed range tested; whereas trailing-edge angles between 7° and 30° gave control-effectiveness losses and sometimes control-effectiveness reversal in the high subsonic speed range.

For wings swept back 45° and having profiles with curved rearward portions, increasing the thickness near the trailing edge (increasing the trailing-edge angle) resulted in rolling-effectiveness decreases. No control reversal occurred for trailing-edge angles between 3° and 33°, but the rolling effectiveness was near zero in the transonic region for the larger trailing-edge angles.

The drag generally increased with increases in thickness near the trailing edge.

INTRODUCTION

Previous research (reference 1) has shown that the loss of wing-aileron rolling effectiveness in the transonic region which may occur for some wings with plain true-contour ailerons can be largely eliminated by increasing the thickness of the aileron trailing edge. The purpose of the present investigation was to obtain additional information on wing-aileron rolling effectiveness and drag as affected by varying the thickness distribution over the rearward portion of the airfoil. A 6-percent-thick symmetrical circular-arc airfoil, equipped with sealed full-span ailerons, was modified in thickness distribution to produce a range of trailing-edge angles from 0° to 30°. Most of these modifications were tested at both 0° and 45° sweepback.

The wing-aileron rolling-effectiveness results of the present investigation are correlated with results of previous investigations, with an arbitrarily defined trailing-edge angle used as a basis, to show the effect of trailing-edge angle on wing-aileron rolling effectiveness.

The flight tests were made at the Langley Pilotless Aircraft Research Station at Wallops Island, Va. The testing technique is described in reference 2.

SYMBOLS

A	aspect ratio, 3.7, (b/c)
b	diameter of circle swept by wing tips, 2.185 feet
c	streamwise wing chord, 0.59 feet
C_L	wing lift coefficient

S	total exposed wing area for three wings, 1.563 square feet
C_{D_T}	test-vehicle total-drag coefficient, based on S
ΔC_{D_W}	wing-drag increment due to increase in thickness of aileron trailing edge, based on S
M	free-stream Mach number
M_a	free-stream Mach number at which rapid rate of loss of wing-aileron rolling effectiveness begins as Mach number increases from subsonic speeds
M_b	free-stream Mach number at which the wing-aileron rolling effectiveness may be a minimum in the transonic region
M_c	free-stream Mach number for recovery of wing-aileron rolling effectiveness going into low supersonic region when wing has experienced effectiveness loss in transonic region
p	test-vehicle rolling velocity, radians per second
$pb/2V$	wing-tip helix angle, radians
R	Reynolds number based on wing chord of 0.59 feet
V	flight path velocity, feet per second
i_w	average incidence for each wing streamwise, degrees
δ_a	average streamwise deflection of each aileron, degrees
ϕ	angle between straight lines drawn between 0.97 chord and 1.00 chord on upper and lower surfaces, defined as trailing-edge angle, degrees
h	thickness at trailing edge

TEST VEHICLES AND PROCEDURES

The general arrangement of typical test vehicles is shown in the photographs presented as figure 1 and in figure 2. Figure 3 presents details of the unswept- and sweptback-wing plan forms and full-span sealed ailerons. Figure 4 shows the 6-percent-thick symmetrical

[redacted]

circular-arc profile and its modifications used in the present investigation. Additional information is presented in table I.

The fuselages, ordinates for which may be found in reference 2, were made of balsa and mahogany and were finished fair and smooth with lacquer.

A two-stage rocket-propulsion system resulted in a maximum Mach number of approximately 1.7 at the end of thrusting period. During 10 to 12 seconds of coasting flight, time-histories of the rolling velocity and flight-path velocity were obtained. From these data and atmospheric data obtained from radiosondes, the rolling-effectiveness parameter $pb/2V$ and test-vehicle total-drag coefficient C_{D_T} were computed.

The variation of Reynolds number with Mach number is shown in figure 5.

ACCURACY AND CORRECTIONS

From mathematical analysis and previous experience, the maximum experimental uncertainties are believed to be within the following limits:

	Subsonic	Supersonic
M	±0.005	±0.005
C_{D_T}	±0.005	±0.005
$pb/2V$ (figs. 6 and 7)	±0.005	±0.003
$pb/2V$ (figs. 8, 9, 13, 14, 15, and 18)	±0.007	±0.004

The larger rolling-effectiveness uncertainties indicated for figures other than 6 and 7 are the result of multiplying measured rolling-effectiveness values by factors larger than 1.0 in the process of correcting to rigid-wing values.

Except for figures 6 and 7, the rolling-effectiveness data have been corrected to rigid-wing values by utilizing the data of reference 3 for the determination of wing-aileron rolling-effectiveness loss due to wing flexibility.

All the rolling-effectiveness data have been corrected to $i_w = 0^\circ$ and $\delta_a = 5.0^\circ$ (see reference 3).

RESULTS AND DISCUSSION OF PRESENT INVESTIGATION

Figures 6 and 7 contain wing-aileron rolling effectiveness and drag coefficients obtained with 6-percent-thick wings having 0° wing incidence and sealed full-span ailerons deflected 5° streamwise. The basic symmetrical circular-arc airfoil was modified in thickness distribution with the most extreme modification consisting of a wedge forward portion and a flat-plate rearward portion; the resulting trailing-edge angles varied from 0° to approximately 30°. Most of the modifications were tested at both 0° sweepback (models 1, 2, 4, 6, 16, 17, 18, 25, 26, and 29) and 45° sweepback (models 41, 44, 50, 58, 59, 60, and 61).

Rolling Effectiveness

Wings with 0° sweepback.- Contained in figure 8 are the rolling-effectiveness data of figure 6 corrected to rigid-wing values. Figure 8(a) shows that as the trailing-edge angle increased, the rolling effectiveness $pb/2V$ decreased except in the transonic and supersonic regions for the largest value of ϕ tested. Increasing the trailing-edge angle generally decreased the Mach number M_a at which the aileron began losing its rolling effectiveness. A minimum rolling effectiveness occurred in the transonic region for all except the smaller values of ϕ; the Mach number at which this minimum occurred M_b decreased with increasing ϕ. Changes in ϕ for $M \geq 1.3$ did not have an appreciable effect on $pb/2V$ except for small values of ϕ.

In figure 8(b) a comparison of wing-aileron rolling effectiveness is given for a flat-plate type of airfoil having wedge and circular-arc forward portions. The effectiveness was high throughout the speed range and, as indicated by reference 1, shows that moderate changes in thickness distribution over the forward portion of the airfoil did not appreciably affect the rolling effectiveness.

Wings with 45° sweepback.- Figure 9 summarizes the rolling-effectiveness data of figure 7, which have been corrected to rigid-wing values, and shows that increasing ϕ decreases $pb/2V$ throughout the speed range tested except in the supersonic region for the largest value of ϕ tested. Increasing ϕ decreased the Mach number at which a minimum transonic effectiveness occurred for the two largest trailing-edge angles tested. These results, when compared with those of figure 8 (unswept wings), indicate that changes in trailing-edge angle result in the same general trends of effectiveness change for wings with 0° or 45° sweepback.

[redacted]

Drag

Wings with 0° sweepback.- Figure 10 summarizes the drag data of figure 6 for profiles having finite and zero trailing-edge thickness. Figure 10(a) shows that large drag increases result when the trailing-edge thickness is increased from zero to the maximum thickness of the wing. The substitution of a wedge forward portion for a circular-arc forward portion (models 1 and 2) increased the drag at some speeds and decreased it at others. Figure 10(b) shows that in general the drag increased with increases in trailing-edge angle for the profiles having zero trailing-edge thickness. Thus, it can be seen that the drag increased with increases in thickness near or at the trailing edge.

Figure 11 shows the drag increases resulting when the thickness ratio h/c of the trailing edge is increased. To obtain the values shown, the drag coefficients of model 6 were subtracted from those of models 1 and 4. Shown for comparison are values calculated from the base-pressure data of reference 4.

Wings with 45° sweepback.- Figure 12 summarizes the drag data of figure 7 for profiles having zero trailing-edge thickness. The largest and smallest trailing-edge angles resulted in the largest and smallest drag values, respectively, but the intermediate ϕ values did not show consistency within the group. Overall, the drag variations were small, and generally near the limits of accuracy.

CORRELATION OF EFFECTS OF TRAILING-EDGE ANGLE ON ROLLING EFFECTIVENESS

Contained in figures 13 and 14 are the rolling-effectiveness data from figures 6 and 7 (present investigation) plus additional data from sources identified in table I (previous investigations), all corrected to rigid-wing values. All models have the same dimensions as shown in figures 2 and 3, with the only variables being the airfoil streamwise thickness distributions and ratios and trailing-edge angles. While it is realized that the trailing-edge angle is not the only factor affecting the wing-aileron rolling effectiveness, the data presented in this correlation section show that changes in trailing-edge angle generally had strong effects on changes in wing-aileron rolling power.

Rolling effectiveness, unswept wings.- Figure 15 contains $pb/2V$, obtained from figure 13, plotted against trailing-edge angle ϕ for several Mach numbers. Included for comparison are values calculated from

references 5, 6, and 7 (subsonic), and 8 and 9 (supersonic); the agreement between experimental and calculated values is generally good. For $M < 0.88$ the correlation of the experimental data is rather good and shows that increasing ϕ tends to decrease rolling effectiveness. For $0.88 \leq M \leq 0.94$ the correlation is generally poor but the data seem to indicate that increasing the trailing-edge angle results in a rolling-effectiveness decrease and reversal with some positive effectiveness recovery for the largest ϕ tested. For $0.94 < M \leq 1.6$, the correlation is again rather good and shows that the effect of increasing the trailing-edge angle is generally to decrease $pb/2V$ for $\phi < 16^\circ$; further increasing ϕ has negligible effect on rolling effectiveness. The values from the faired curves of figure 15 have been utilized in figure 16 where $pb/2V$ is plotted against Mach number for several arbitrary trailing-edge angles to show the types of rolling-effectiveness curves that can be obtained from figure 15. From these two figures it can be seen that ailerons having $\phi \leq 7^\circ$ will provide high positive rolling effectiveness in the speed range $0.7 \leq M \leq 1.6$. Ailerons having $\phi > 7^\circ$ will encounter varying amounts of control-effectiveness loss in the transonic range, with complete reversal probable at some speeds for $16^\circ \leq \phi \leq 26^\circ$.

In figure 17 is shown the Mach numbers at which major changes occur in the curves of rolling effectiveness against Mach number for unswept wings having various trailing-edge angles; the method of obtaining the test points is shown in the upper part of figure 17. The faired lines enclose a region of undesirable control-effectiveness loss, where the trailing-edge angle ϕ determines the maximum subsonic and minimum supersonic Mach number at which relatively high positive control is retained.

Rolling effectiveness, wings swept back 45°.- Figure 18 contains $pb/2V$, obtained from figure 14, plotted against trailing-edge angle ϕ for several Mach numbers. Included for comparison are values calculated from references 6, 7, and 10. It can be seen that the rolling effectiveness was positive throughout the speed range tested for trailing-edge angles between 3° and 33°. The rolling effectiveness, highest for the lowest trailing-edge angle, decreased with increasing ϕ and was near zero at $M = 1.0$ for the larger trailing-edge angles. For $M > 1.4$, variations in ϕ had a negligible effect on the rolling effectiveness. The effects of ϕ on rolling effectiveness for the 45° sweptback wings were not as severe as for the unswept wings.

The values from the faired curves of figure 18 have been utilized in constructing the curves of figure 19 where $pb/2V$ is plotted against Mach number for several arbitrary values of ϕ to show the general types of curves obtainable from figure 18.

[redacted]

GENERAL COMMENT

The magnitudes of the rolling effectiveness $pb/2V$ shown in this paper are intended to apply specifically to wing-body combinations similar to those shown in figures 2 and 3. Although the rolling moment per unit aileron deflection C_{l_δ} may change with wing angle of attack (reference 11) and the control-effectiveness reversal may sometimes be eliminated by increasing the aileron deflection (reference 12), it is felt that the trends established in the present paper will, in general, apply to other configurations and conditions where the major variable is the trailing-edge angle.

CONCLUSIONS

Wing-aileron rolling effectiveness and drag were obtained over the Mach number range from 0.7 to 1.6 for 6-percent-thick wings. In addition, rolling-effectiveness data from previous tests were correlated to show the effects of trailing-edge angle on wing-aileron rolling effectiveness for thickness ratios of 3 percent, 6 percent, and 9 percent. From these data the following conclusions may be drawn:

1. For the unswept wings, the wing-aileron rolling effectiveness was positive and relatively high for aileron trailing-edge angles between 0° and 7°. Trailing-edge angles between 7° and 30° caused rolling-effectiveness losses in the transonic and high subsonic region, with the magnitude and duration of the loss generally increasing with increasing trailing-edge angle; control reversal was indicated at some speeds for trailing-edge angles between 16° and 26°.

2. For wings swept back 45° the rolling effectiveness was positive for all trailing-edge angles between 3° and 33°. The rolling effectiveness, highest for the lowest trailing-edge angles, decreased with increasing trailing-edge angle and was near zero at a Mach number of 1.0 for the highest trailing-edge angles. The effects of trailing-edge angle on rolling effectiveness for the 45° sweptback wings were not as severe as for the unswept wings.

3. Increases in thickness near the aileron trailing edge generally increased the drag for wings both unswept and swept back 45°. For unswept wings having flat surfaces over the rearward portion of the

airfoil, increases in the thickness of the aileron trailing edge resulted in large drag increases but did not materially affect the rolling effectiveness.

Langley Aeronautical Laboratory
National Advisory Committee for Aeronautics
Langley Field, Va.

[redacted]

REFERENCES

1. Strass, H. Kurt, and Fields, Edison M.: Flight Investigation of the Effect of Thickening the Aileron Trailing Edge on Control Effectiveness for Sweptback Tapered Wings Having Sharp- and Round-Nose Sections. NACA RM L9L19, 1950.

2. Sandahl, Carl A., and Marino, Alfred A.: Free-Flight Investigation of Control Effectiveness of Full-Span 0.2-Chord Plain Ailerons at High Subsonic, Transonic, and Supersonic Speeds to Determine Some Effects of Section Thickness and Wing Sweepback. NACA RM L7D02, 1947.

3. Strass, H. Kurt, Fields, E. M., and Purser, Paul E.: Experimental Determination of Effect of Structural Rigidity on Rolling Effectiveness of Some Straight and Swept Wings at Mach Numbers from 0.7 to 1.7. NACA RM L50G14b, 1950.

4. Morrow, John D., and Katz, Ellis: Flight Investigation at Mach Numbers from 0.6 to 1.7 to Determine Drag and Base Pressures on a Blunt-Trailing-Edge Airfoil and Drag of Diamond and Circular-Arc Airfoils at Zero Lift. NACA RM L50E19a, 1950.

5. Toll, Thomas A., and Queijo, M. J.: Approximate Relations and Charts for Low-Speed Stability Derivatives of Swept Wings. NACA TN 1581, 1948.

6. Lowry, John G., and Schneiter, Leslie E.: Estimation of Effectiveness of Flap-Type Controls on Sweptback Wings. NACA TN 1674, 1948.

7. Langley Research Staff (Compiled by Thomas A. Toll): Summary of Lateral-Control Research. NACA Rep. 868, 1947. (Formerly NACA TN 1245.)

8. Tucker, Warren A., and Nelson, Robert L.: Theoretical Characteristics in Supersonic Flow of Constant-Chord Partial-Span Control Surfaces on Rectangular Wings Having Finite Thickness. NACA TN 1708, 1948.

9. Piland, Robert O.: Summary of the Theoretical Lift, Damping-in-Roll, and Center-of-Pressure Characteristics of Various Wing Plan Forms at Supersonic Speeds. NACA TN 1977, 1949.

10. Polhamus, Edward C.: A Simple Method of Estimating the Subsonic Lift and Damping in Roll of Sweptback Wings. NACA TN 1862, 1949.

11. Spearman, M. Leroy, and Webster, Robert A.: An Investigation at Mach Numbers of 1.40 and 1.59 of the Effects of Aileron Profile on the Aerodynamic Characteristics of a Complete Model of a Supersonic Aircraft Configuration. NACA RM L50J31, 1951.

12. Sandahl, Carl A., Bland, William M., Jr., and Strass, H. Kurt: Effects of Some Airfoil-Section Variations on Wing-Aileron Rolling Effectiveness and Drag as Determined in Free Flight at Transonic and Supersonic Speeds. NACA RM L9D12, 1949.

13. Sandahl, Carl A., and Strass, H. Kurt: Additional Results in a Free-Flight Investigation of Control Effectiveness of Full-Span, 0.2-Chord Plain Ailerons at High Subsonic, Transonic, and Supersonic Speeds to Determine Some Effects of Wing Sweepback, Aspect Ratio, Taper, and Section Thickness Ratio. NACA RM L7L01, 1948.

14. Sandahl, Carl A.: Preliminary Free-Flight Investigation of the Effect of Airfoil Section on Aileron Rolling Effectiveness at Transonic and Supersonic Speeds. NACA RM L8B26, 1948.

[redacted]

TABLE I

SYMBOLS USED IN FIGURES, TRAILING-EDGE ANGLE ϕ, AIRFOIL PROFILE, AND SOURCE OF DATA FOR ALL MODELS

(a) Unswept Wings

Model	Symbol	ϕ (deg)	Airfoil proffle (a)	Source of data
1	○	0	[b]Special	Present investigation
2	□	0	[b]Special	Present investigation
3	◇	3.0	NACA 65-006	Reference 13
4	△	3.2	[b]Special	Present investigation
5	▷	3.5	NACA 65A003	Reference 3
6	▽	6.2	[b]Special	Present investigation
7	▷	7.9	NACA 65A006	Unpublished data
8	◁	8.0	NACA 65A006	Unpublished data
9	▽	9.6	9-percent-thick DW	Unpublished data
10	◁	9.8	9-percent-thick DW	Unpublished data
11	▷	10.5	NACA 65A009	Unpublished data
12	◇	11.7	NACA 65A009	Reference 3
13	△	12.9	6-percent-thick CA	Unpublished data
14	✕	13.2	6-percent-thick CA	Unpublished data
15	▽	13.5	[b]Modified 6-percent-thick CA	Unpublished data
16	□	13.6	6-percent-thick CA	Present investigation
17	□	13.6	6-percent-thick CA	Present investigation
18	□	16.6	[b]Modified 6-percent-thick CA	Present investigation
19	□	17.4	NACA 16-009	Reference 12
20	□	19.8	NACA 16-009	Reference 12
21	□	20.0	9-percent-thick CA	Unpublished data
22	□	20.0	9-percent-thick CA	Reference 12
23	◇	20.4	9-percent-thick CA	Reference 12
24	◇	21.0	NACA 16-009	Unpublished data
25	◇	21.2	[b]Modified 6-percent-thick CA	Present investigation
26	◇	21.2	[b]Modified 6-percent-thick CA	Present investigation
27	◇	24.3	NACA 16-009	Unpublished data
28	◇	24.8	NACA 16-009	Unpublished data
29	□	30.2	[b]Modified 6-percent-thick CA	Present investigation
30	□	31.2	[b]Modified 6-percent-thick CA	Unpublished data

[a]Abbreviations used:
DW - Symmetrical double wedge
CA - Symmetrical circular arc

[b]See figure 4.

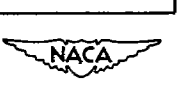

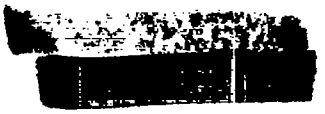

TABLE I

SYMBOLS USED IN FIGURES, TRAILING-EDGE ANGLE ϕ, AIRFOIL PROFILE, AND SOURCE OF DATA FOR ALL MODELS - Concluded

(b) Wings swept back 45°

Model	Symbol	ϕ (deg)	Airfoil profile (a)	Source of data
31	○	3.0	NACA 65-006	Reference 13
32	□	4.5	NACA 65-009	Reference 14
33	◇	4.5	NACA 65-009	Reference 14
34	△	8.2	NACA 65A006	Unpublished data
35	▽	10.2	9-percent-thick DW	Reference 12
36	▷	10.2	9-percent-thick DW	Unpublished data
37	◁	10.4	9-percent-thick DW	Reference 12
38	▽	11.3	NACA 65A009	Unpublished data
39	◁	11.7	NACA 65A009	Unpublished data
40	○	11.9	NACA 65A009	Reference 3
41	△	12.3	6-percent-thick CA	Present investigation
42	✕	12.7	NACA 65A009	Unpublished data
43	▽	12.7	6-percent-thick CA	Unpublished data
44	▷	12.9	6-percent-thick CA	Present investigation
45	◁	12.9	NACA 65A009	Unpublished data
46	⌓	13.0	NACA 65A009	Unpublished data
47	⌓	13.5	[b]Modified 6-percent-thick CA	Unpublished data
48	⌓	15.3	[b]Modified 6-percent-thick CA	Present investigation
49	⌓	16.4	9-percent-thick CA	Reference 12
50	⌓	17.2	[b]Modified 6-percent-thick CA	Present investigation
51	◇	17.3	9-percent-thick CA	Reference 12
52	◇	17.4	9-percent-thick CA	Reference 12
53	◇	17.5	[b]Modified 6-percent-thick CA	Present investigation
54	◇	19.7	NACA 16-009	Reference 12
55	◇	20.2	[b]Modified 6-percent-thick CA	Unpublished data
56	◇	20.3	NACA 16-009	Reference 12
57	⌓	20.6	[b]Modified 6-percent-thick CA	Unpublished data
58	⌓	21.9	[b]Modified 6-percent-thick CA	Present investigation
59	⌓	22.0	[b]Modified 6-percent-thick CA	Present investigation
60	⌓	30.1	[b]Modified 6-percent-thick CA	Present investigation
61	⊕	30.2	[b]Modified 6-percent-thick CA	Present investigation
62	⌓	33.3	[b]Modified 6-percent-thick CA	Unpublished data

[a]Abbreviations used:
DW - Symmetrical double wedge
CA - Symmetrical circular arc

[b]See figure 4.

[redacted]

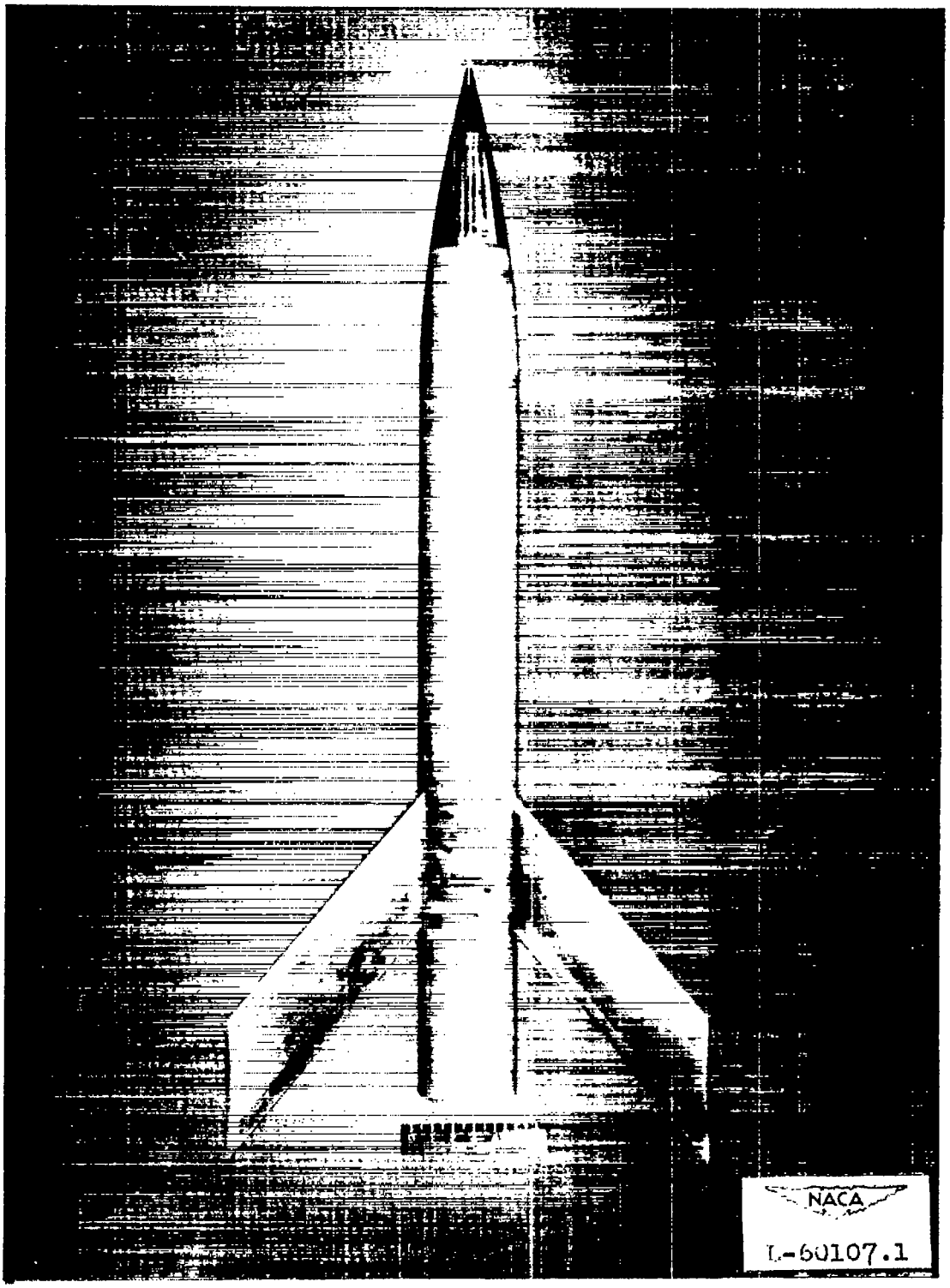

Figure 1.- Photographs of typical test vehicles.

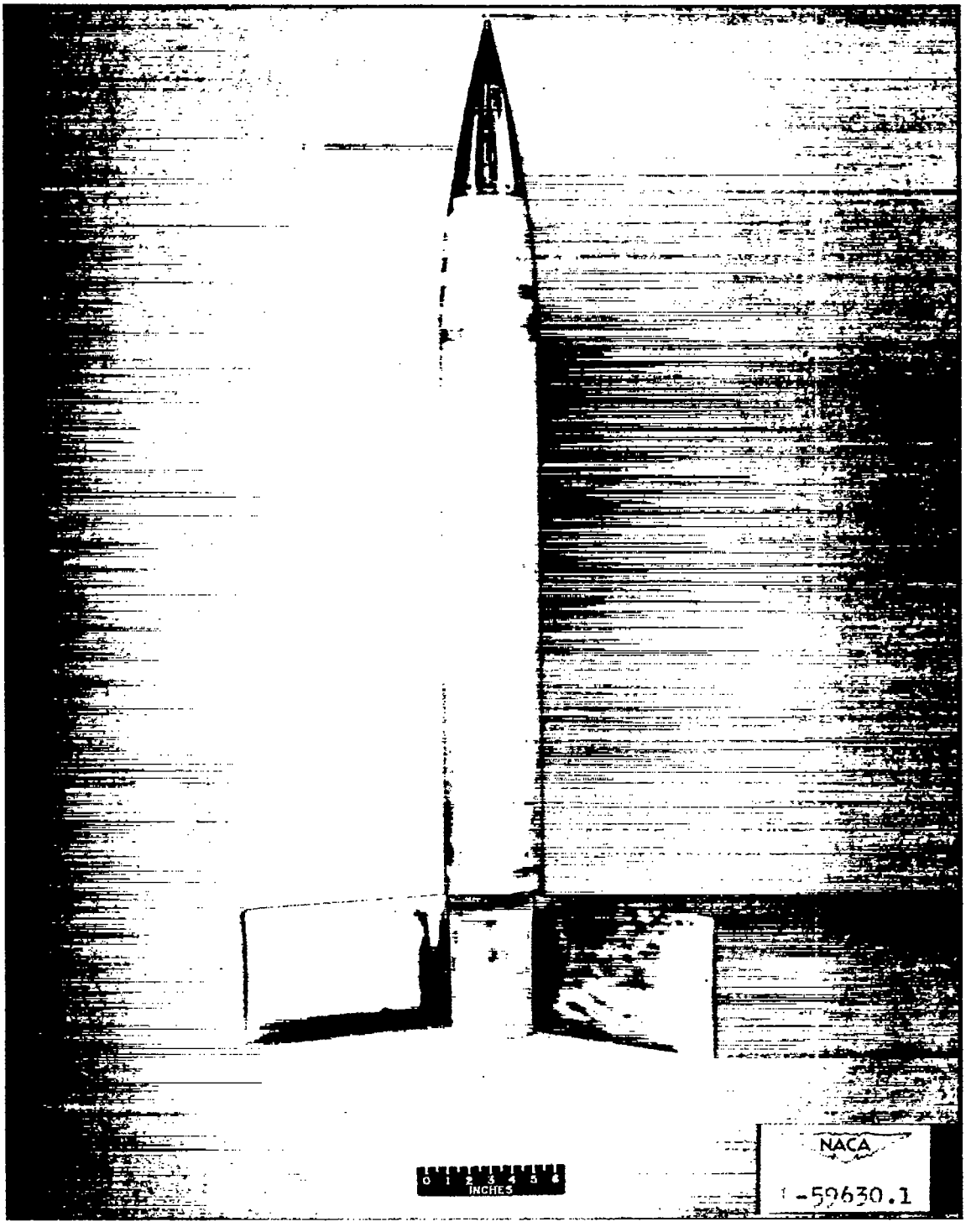

Figure 1.- Concluded.

[redacted]

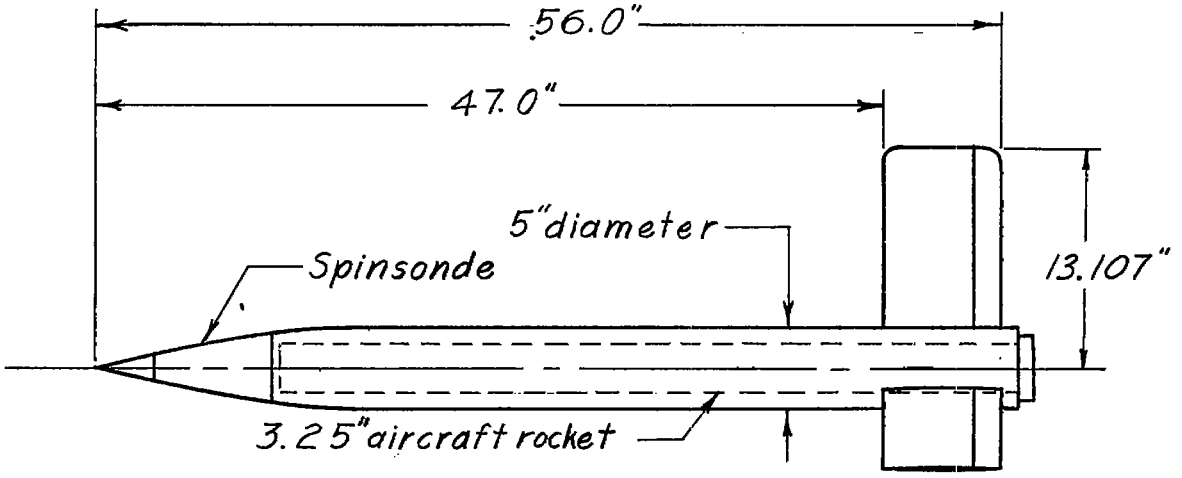

(a) Unswept wings.

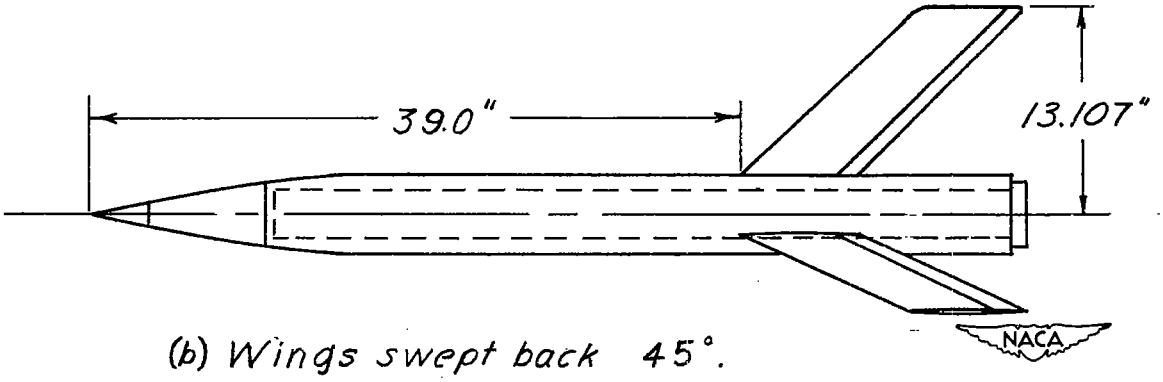

(b) Wings swept back 45°.

Figure 2.- Geometric arrangement and dimensions of typical test vehicles.

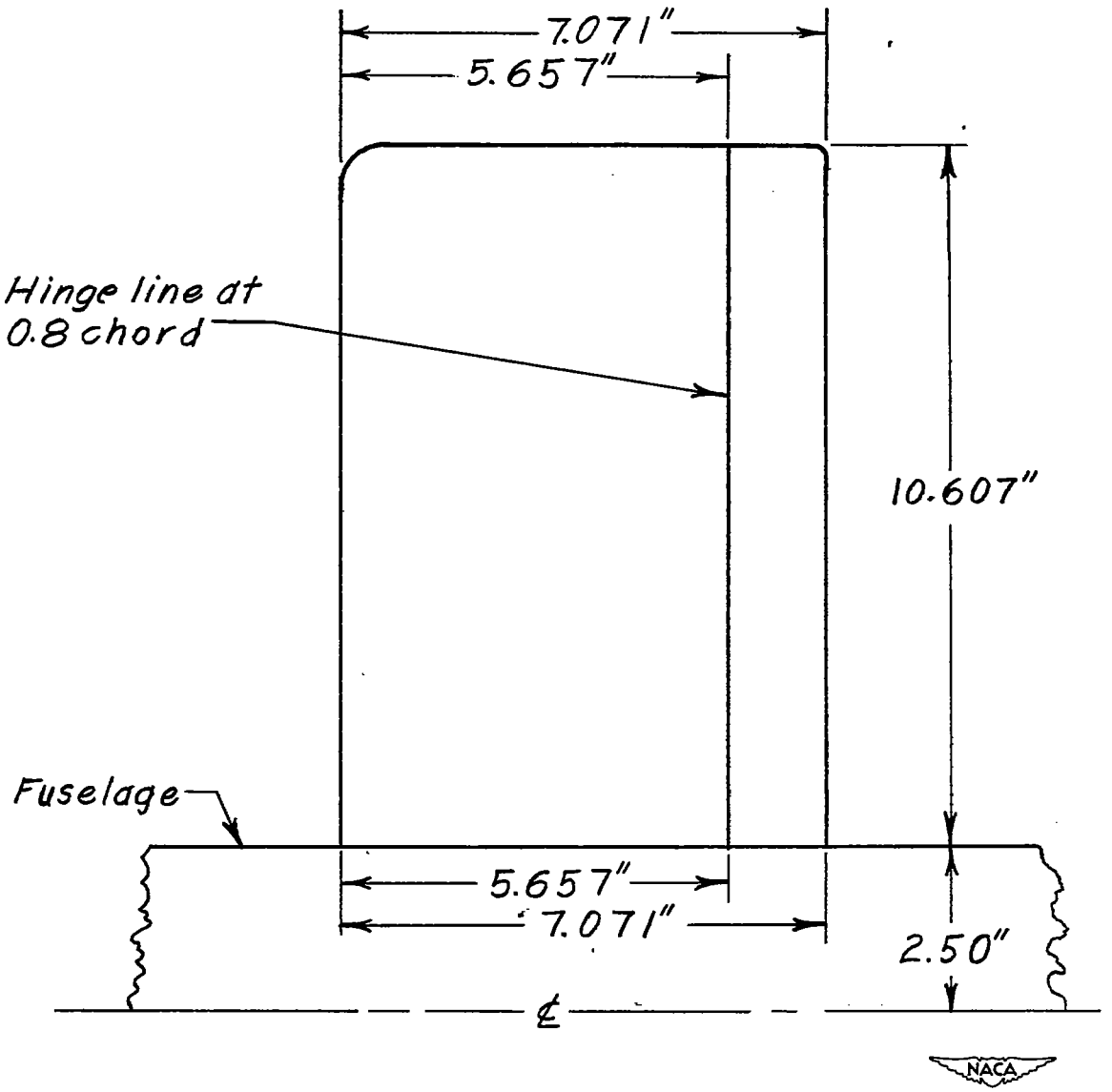

(a) Unswept wings.

Figure 3.- Geometry and dimensions of typical wings.

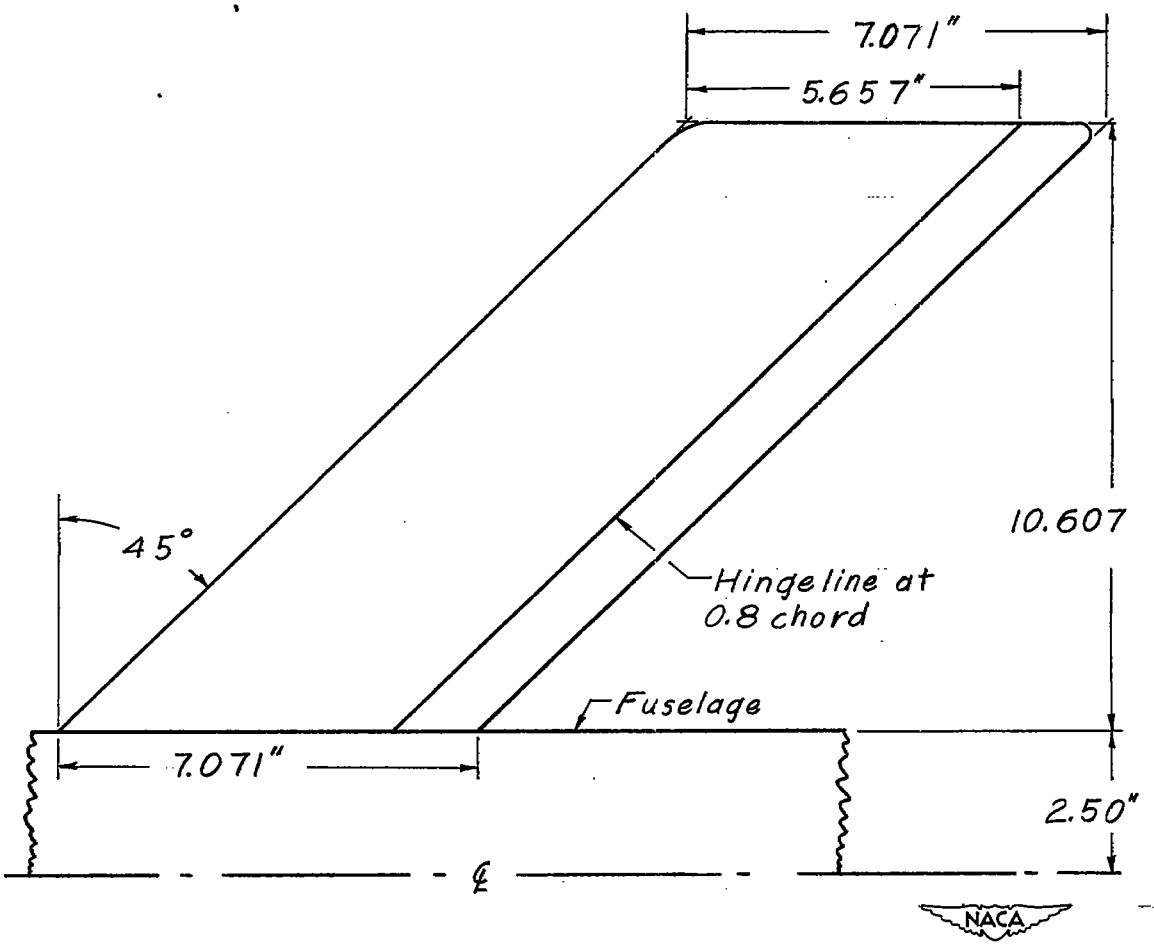

(b) Wings swept back 45°.

Figure 3.- Concluded.

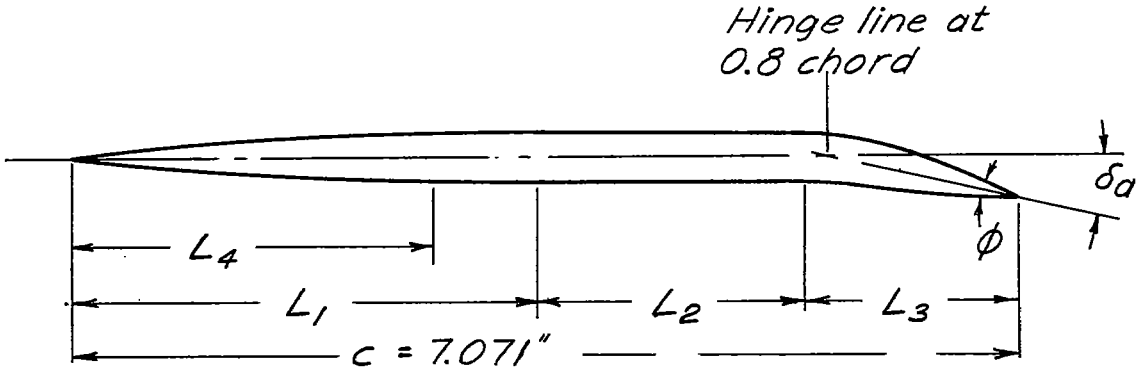

L_1 = length of circular-arc forward portion

L_2 = length of flat-sided portion (sides parallel except for models 4 and 6)

L_3 = length of circular-arc rear portion

L_4 = length of wedge forward portion, model 2

h = thickness at aileron trailing edge

(a) Definition of profiles.

Figure 4.- Six-percent-thick circular-arc profile and modifications utilized in present investigation to produce a range of trailing-edge angles and thickness distributions.

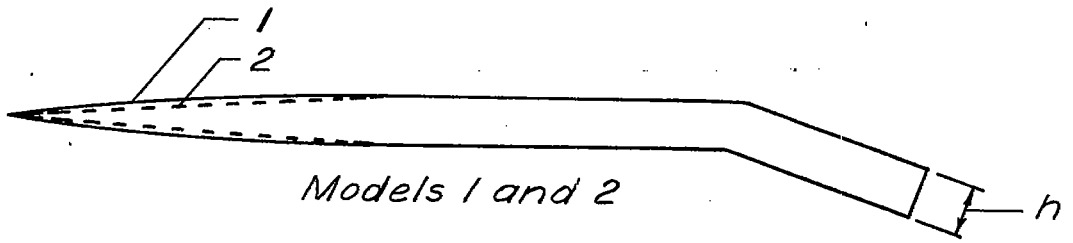

Models 1 and 2

Model 1: $L_1/c = 0.4$, $L_2/c = 0.6$, $h/c = 0.06$

Model 2: $L_4/c = 0.4$, $L_2/c = 0.6$, $h/c = 0.06$

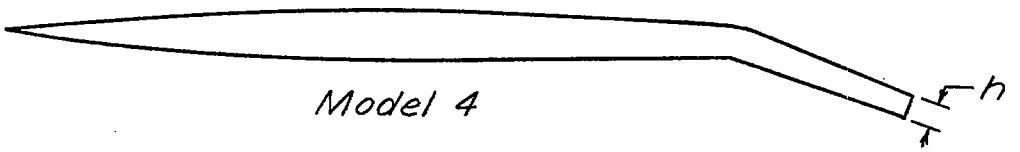

Model 4

$L_1/c = 0.4$, $L_2/c = 0.6$, $h/c = 0.03$

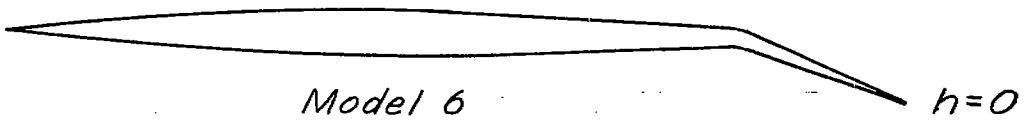

Model 6

$L_1/c = 0.4$, $L_2/c = 0.6$, $h/c = 0$

(b) Models 1, 2, 4, and 6.

Figure 4.- Continued.

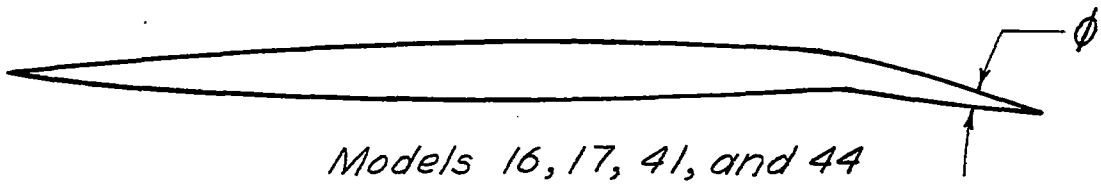

Models 16, 17, 41, and 44
(circular arc)
$L_1/c = 0.5$, $L_3/c = 0.5$, $h/c = 0$

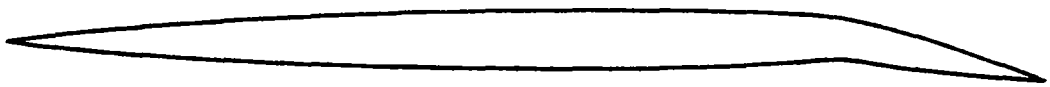

Models 18 and 50
(modified circular arc)
$L_1/c = 0.5$, $L_2/c = 0.1$, $L_3/c = 0.4$, $h/c = 0$

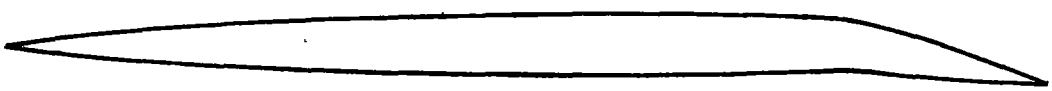

Models 25, 26, 58, and 59
(modified circular arc)
$L_1/c = 0.5$, $L_2/c = 0.2$, $L_3/c = 0.3$, $h/c = 0$

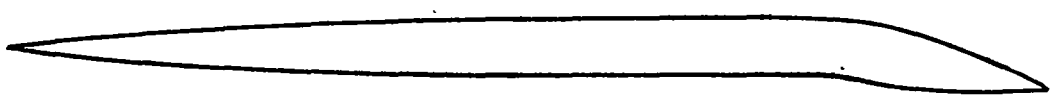

Models 29, 60, and 61
(modified circular arc)
$L_1/c = 0.5$, $L_2/c = 0.3$, $L_3/c = 0.2$, $h/c = 0$

(c) Models 16, 17, 18, 25, 26, 29, 41, 44, 50, 58, 59, 60, and 61.

Figure 4.- Concluded.

[redacted]

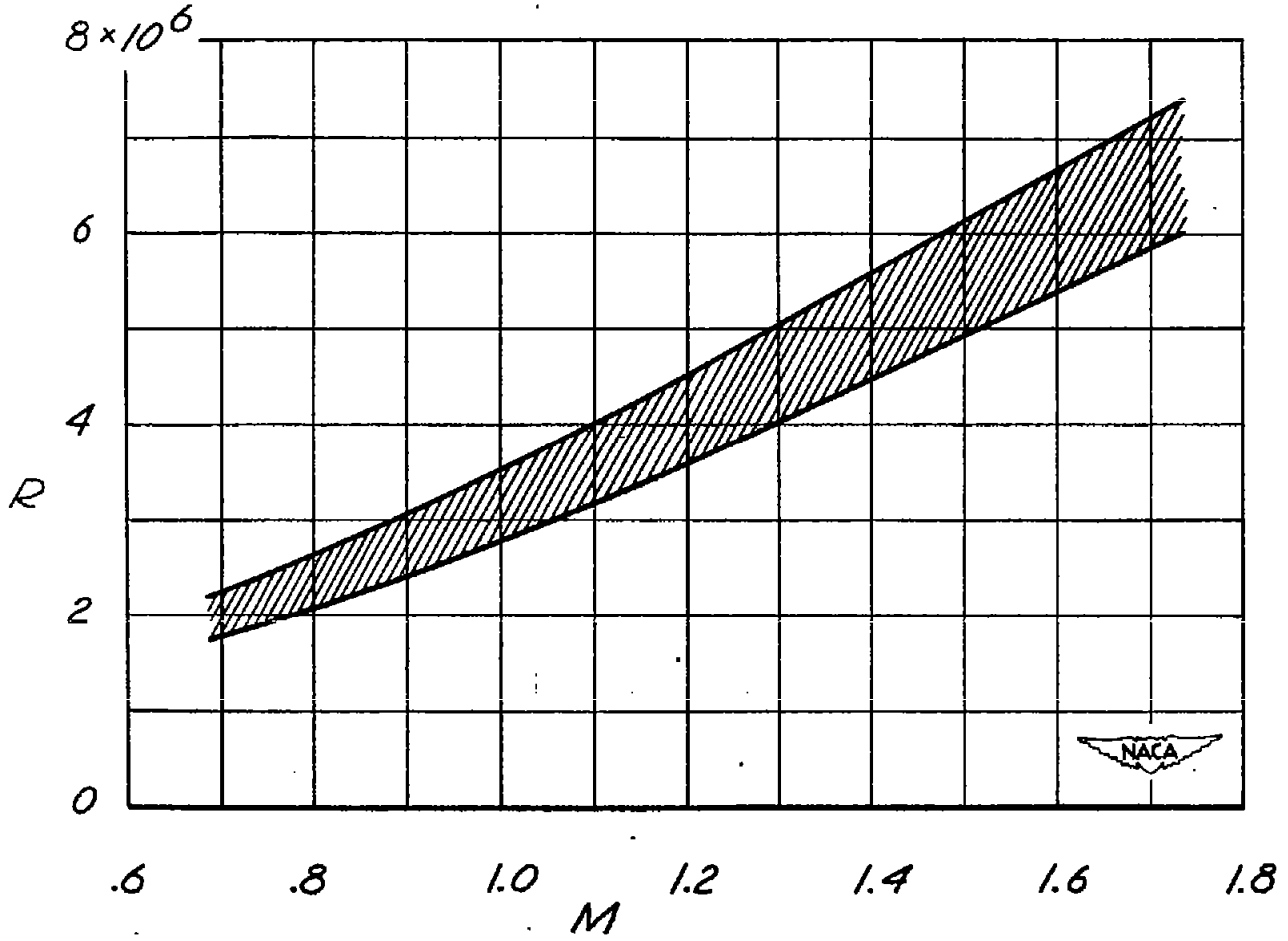

Figure 5.- Range of Reynolds numbers based on a streamwise chord of 0.59 foot.

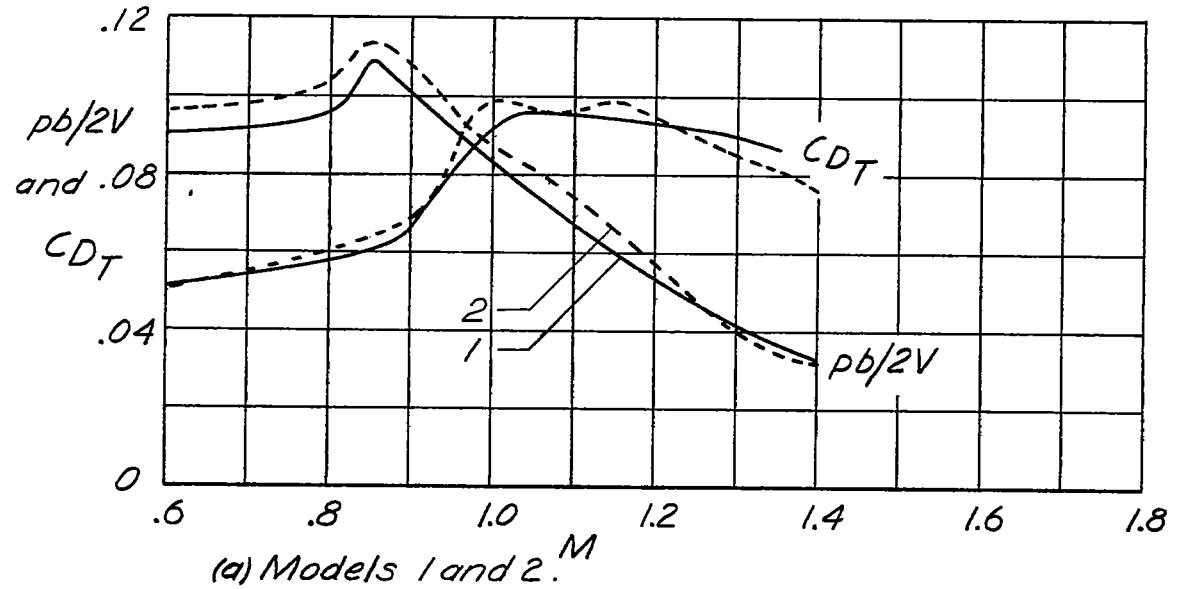

(a) Models 1 and 2.

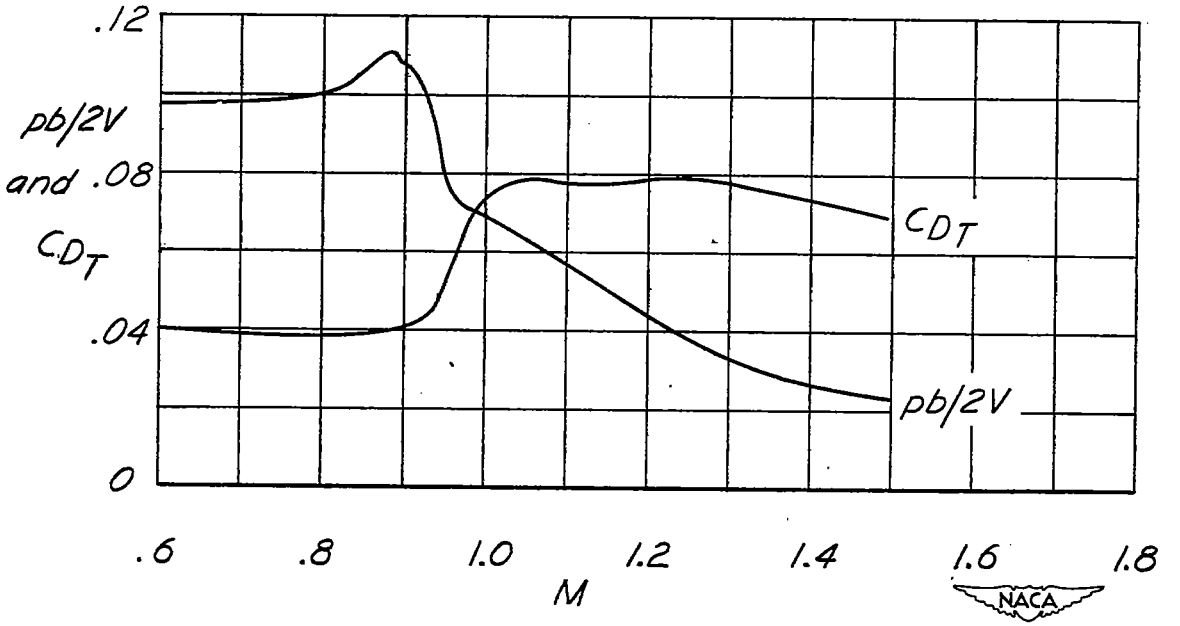

(b) Model 4.

Figure 6.- Variation with Mach number of wing-aileron rolling-effectiveness parameter pb/2V and test-vehicle total-drag coefficient C_{D_T} for unswept wings. $i_w = 0^\circ$ and $\delta_a = 5.0^\circ$; pb/2V not corrected to rigid-wing values.

[redacted]

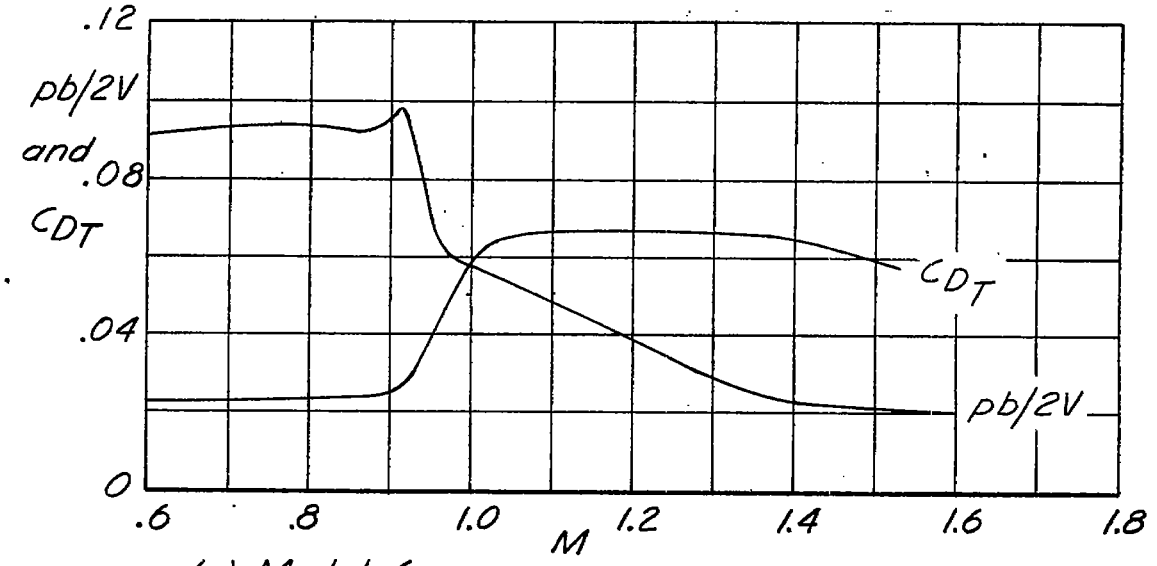

(c) Model 6.

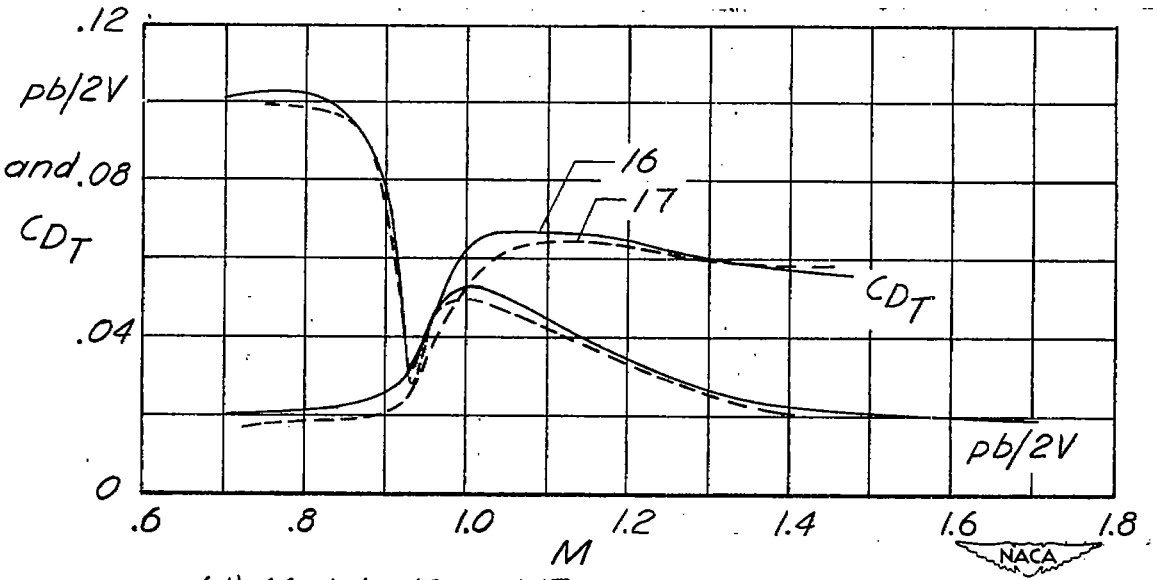

(d) Models 16 and 17.

Figure 6.- Continued.

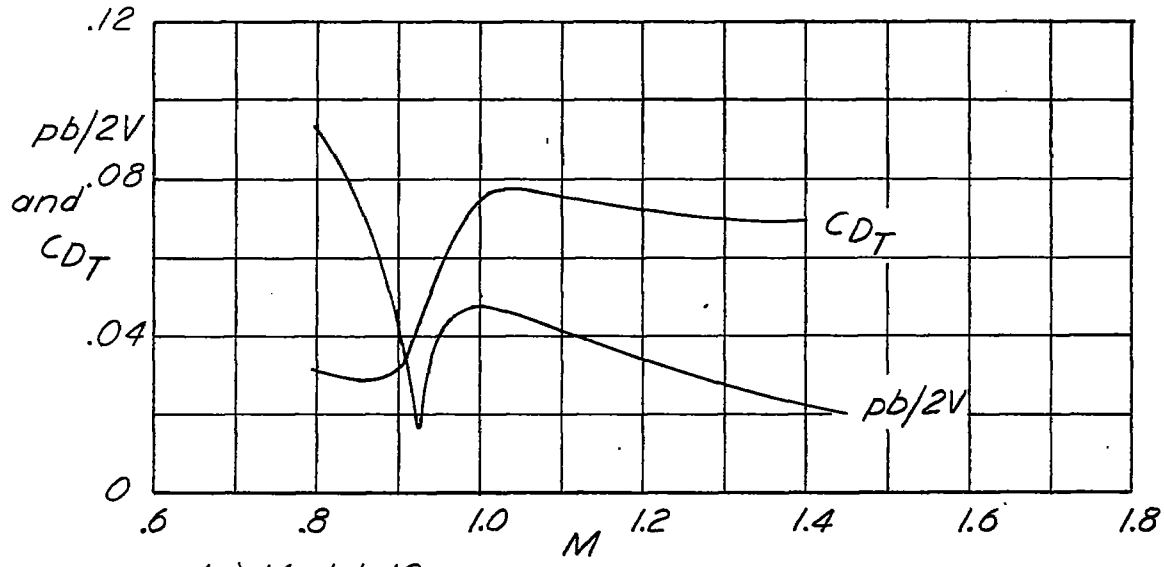

(e) Model 18.

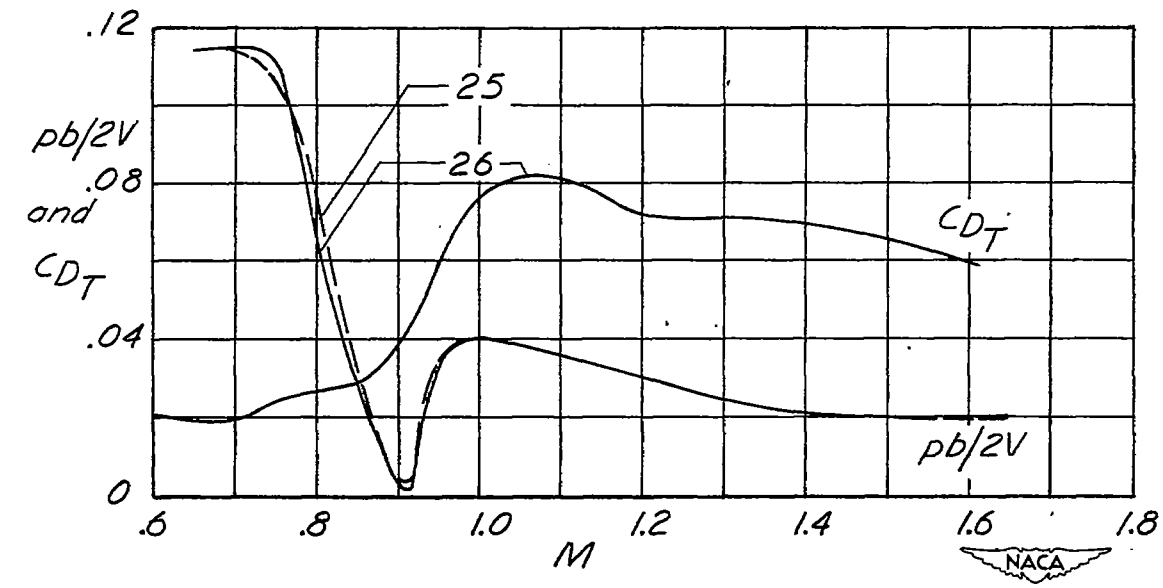

(f) Models 25 and 26.

Figure 6.- Continued.

[redacted]

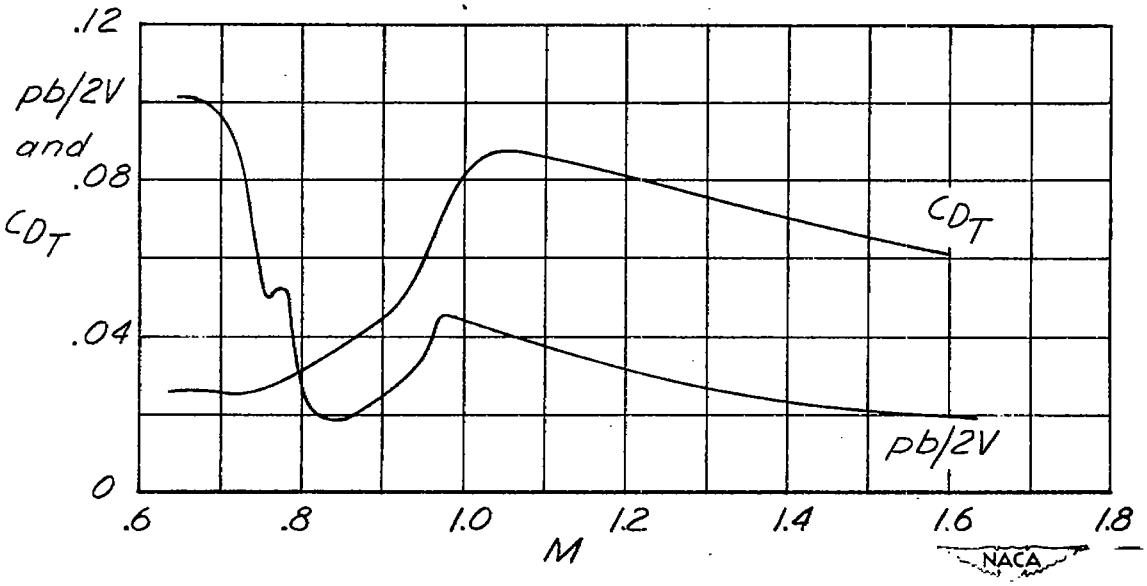

(g) Model 29.

Figure 6.- Concluded.

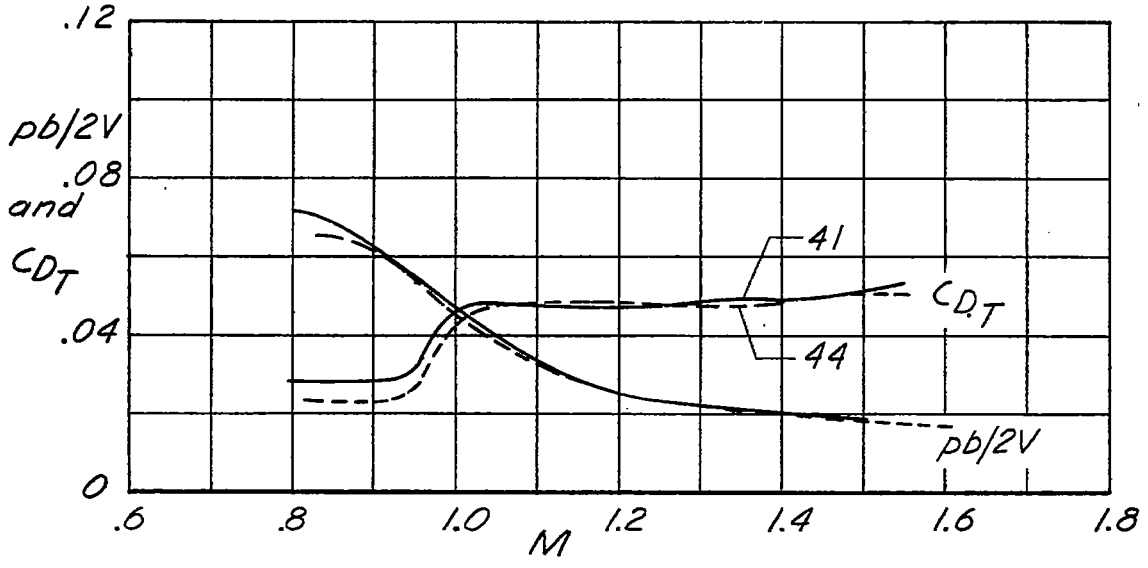

(a) Models 41 and 44.

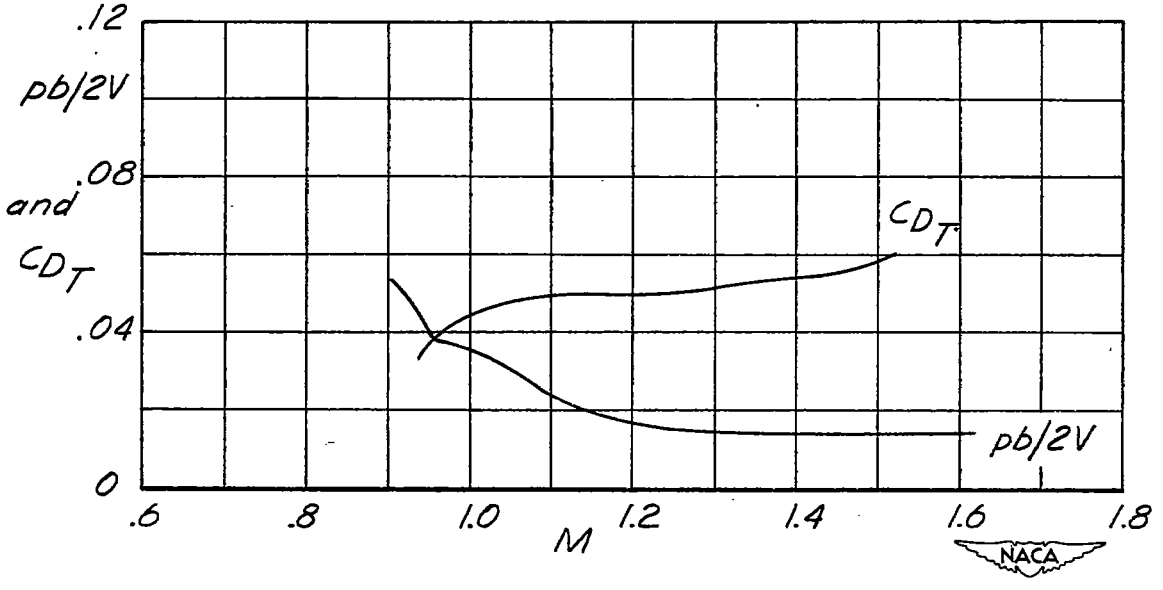

(b) Model 50.

Figure 7.- Variation with Mach number of wing-aileron rolling-effectiveness parameter pb/2V and test-vehicle total-drag coefficient C_{D_T} for wings swept back 45°. $i_w = 0°$ and $\delta_a = 5.0°$; pb/2V not corrected to rigid-wing values.

[redacted]

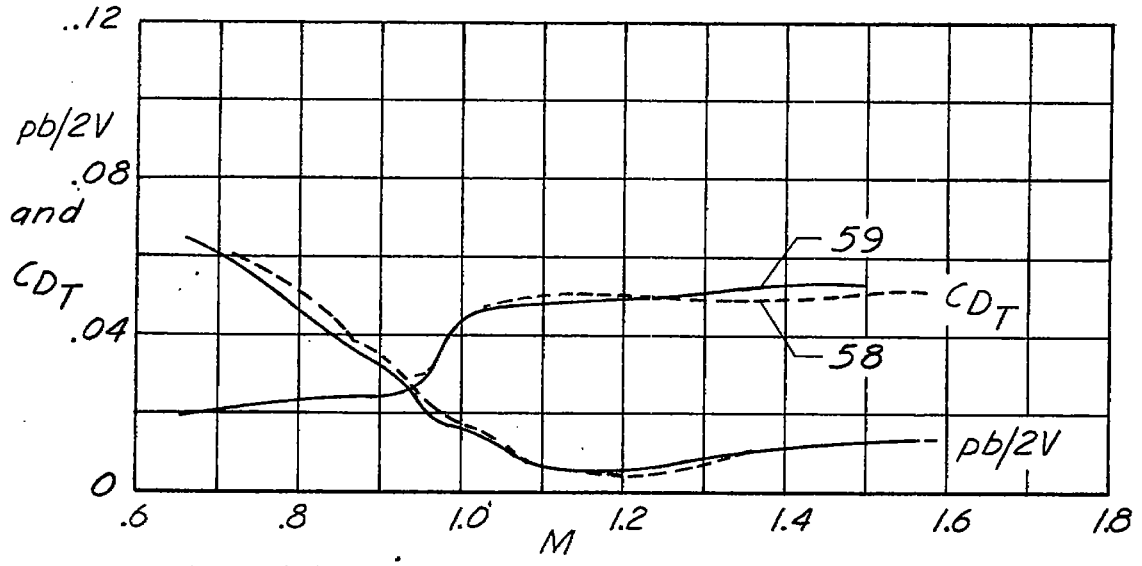

(c) Models 58 and 59.

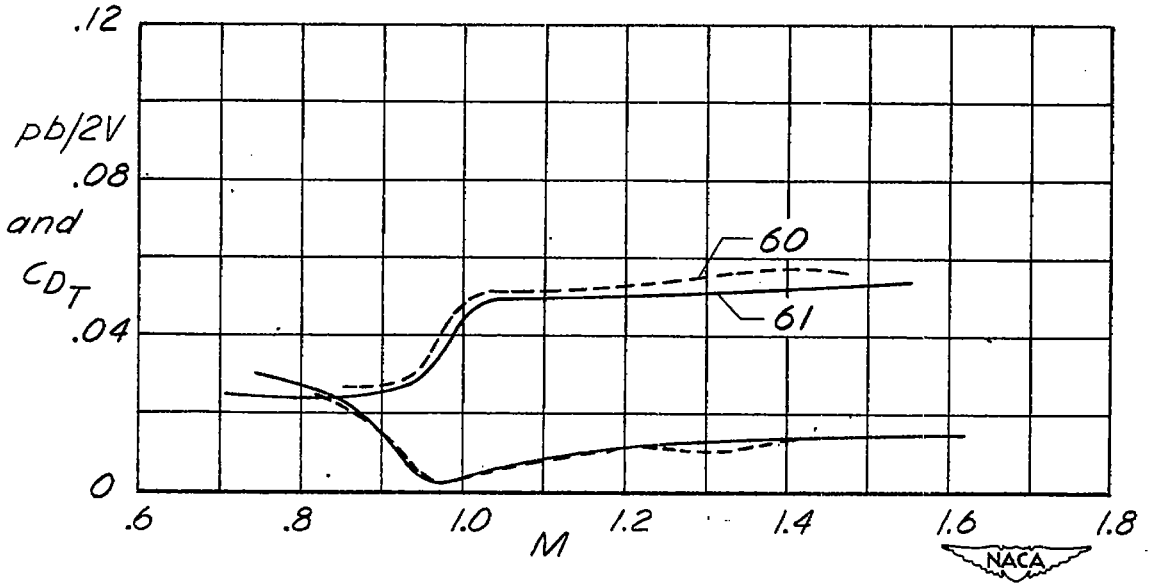

(d) Models 60 and 61.

Figure 7.- Concluded.

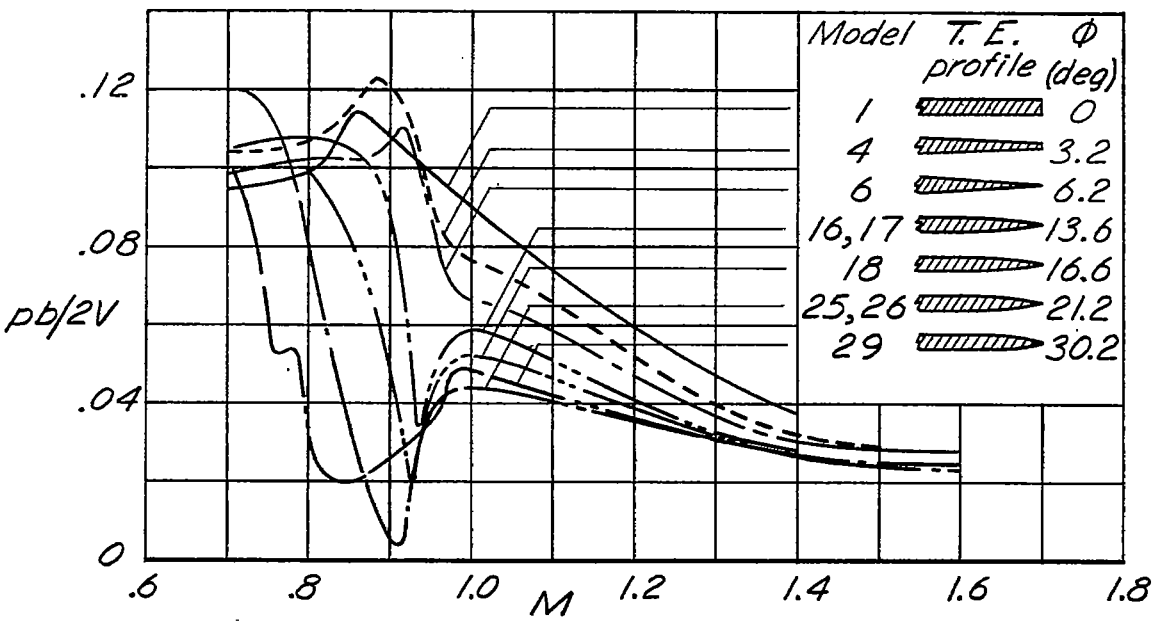

(a) Summary from figure 6.

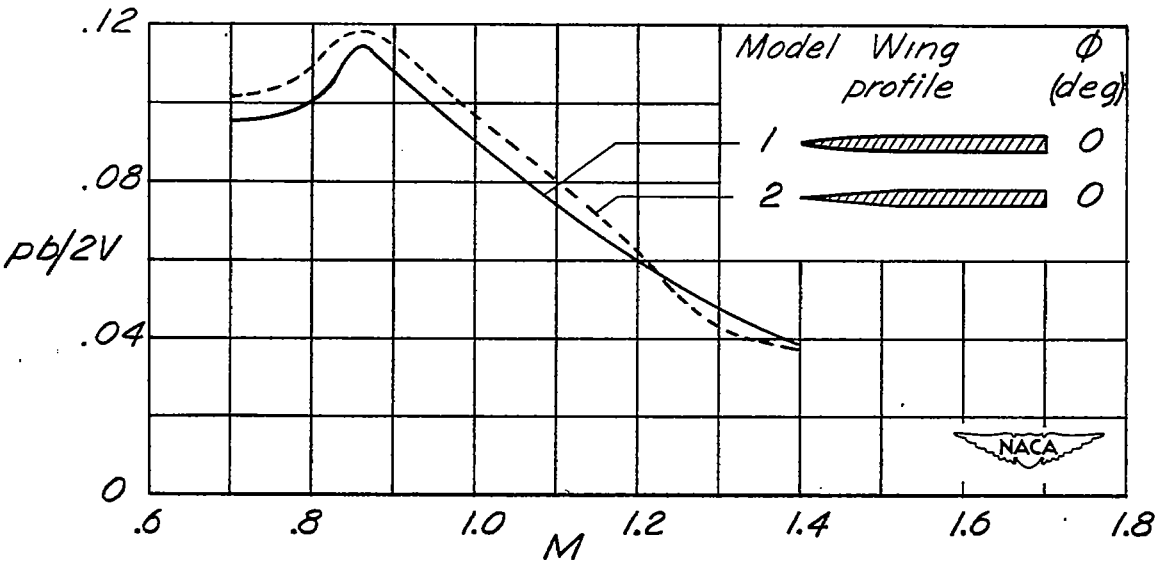

(b) Comparison of effectiveness of models 1 and 2.

Figure 8.- Variation of wing-aileron rolling effectiveness pb/2V with Mach number for unswept wings. $i_w = 0°$ and $\delta_a = 5.0°$; pb/2V corrected to rigid-wing values. Profile sketches show aileron undeflected.

[redacted]

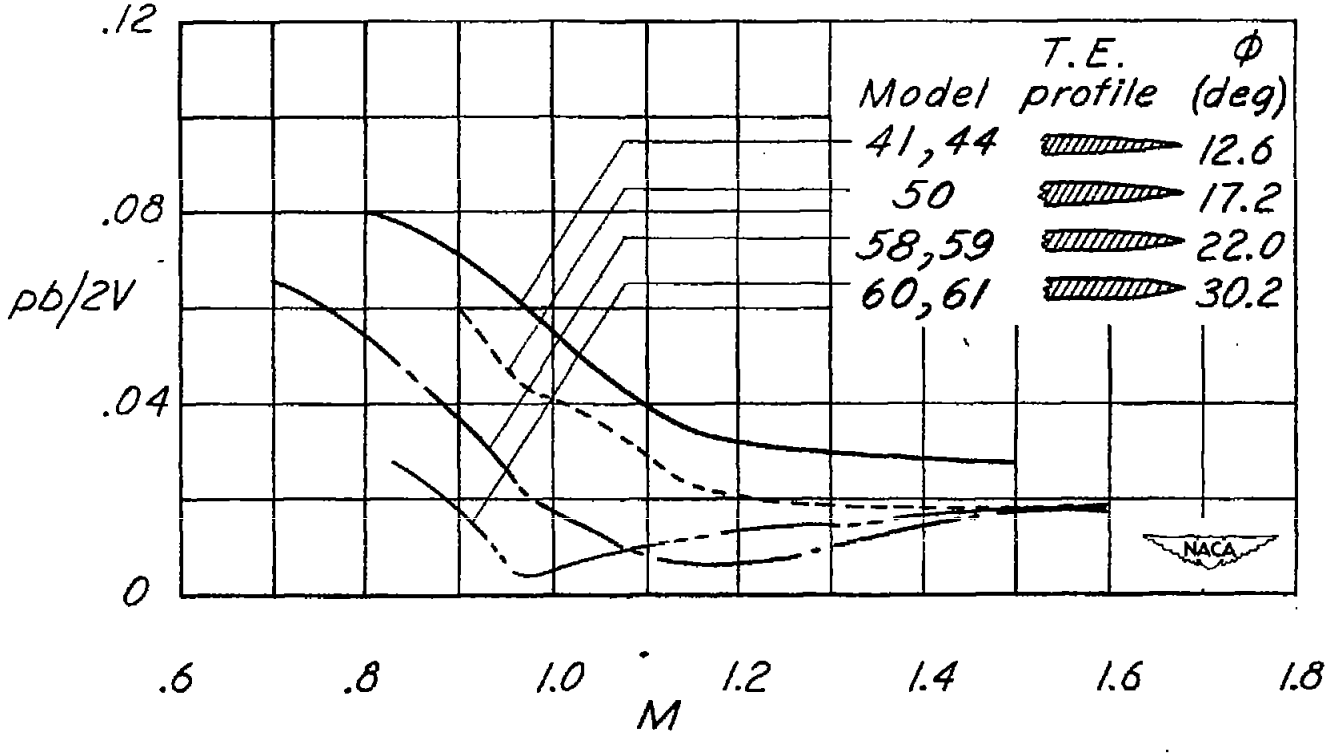

Figure 9.- Variation of wing-aileron rolling effectiveness pb/2V with Mach number for wings swept back 45° (summary from fig. 7), corrected to rigid-wing values. $i_w = 0°$ and $\delta_a = 5.0°$.

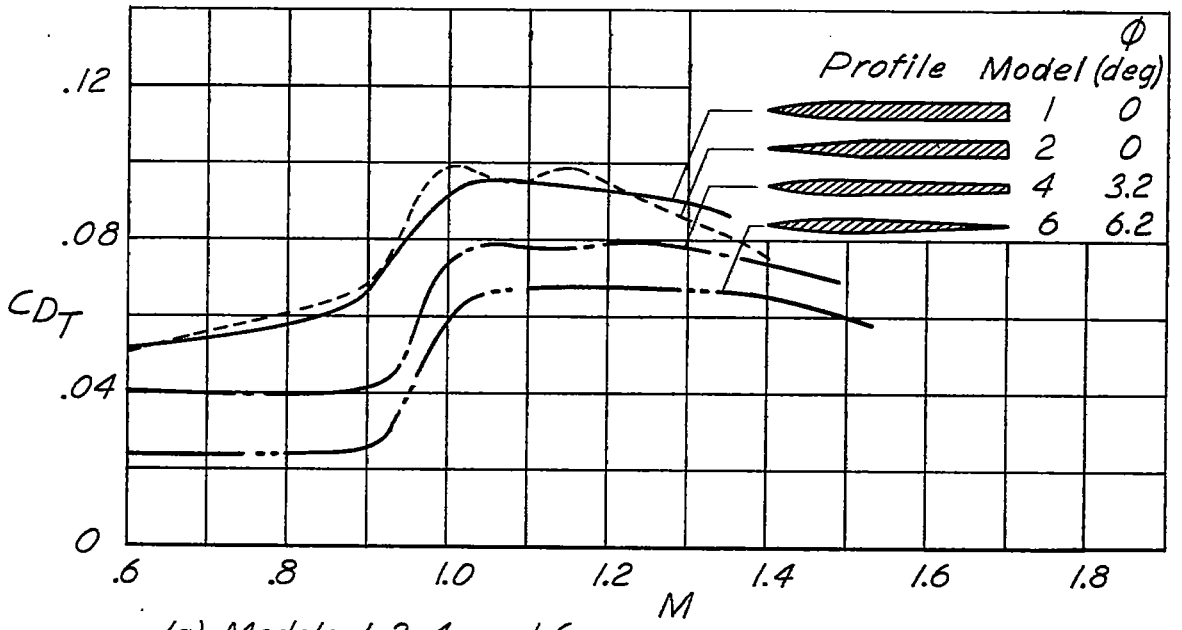

(a) Models 1, 2, 4, and 6.

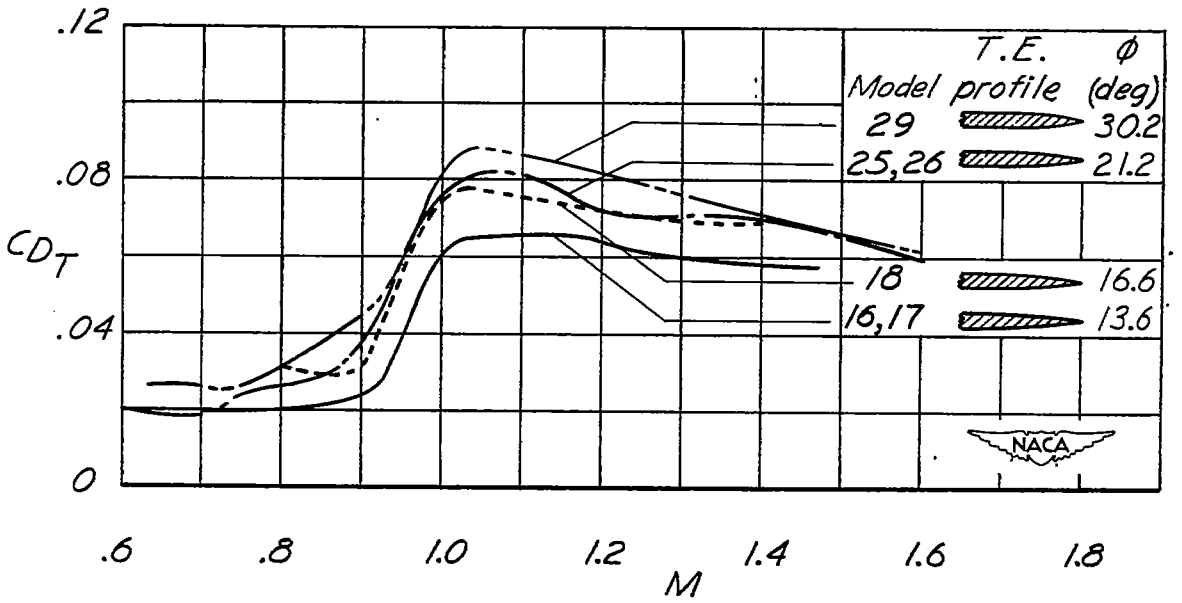

(b) Models 16, 17, 18, 25, 26, and 29.

Figure 10.- Variation with Mach number of test-vehicle total-drag coefficient C_{D_T} for unswept wings (summary from fig. 6).

$\delta_a = 5.0°$.

[redacted]

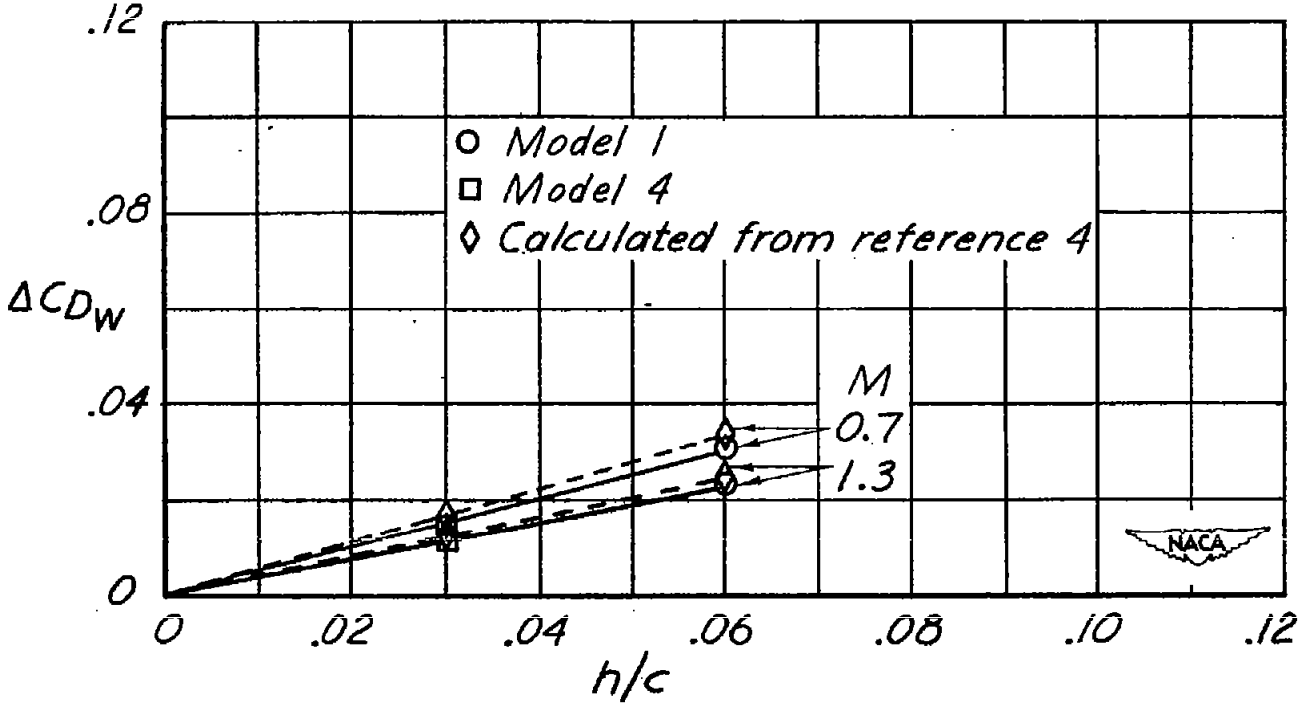

Figure 11.- Test-vehicle total-drag-coefficient increase ΔC_{D_W} due to increase in wing trailing-edge thickness parameter h/c for ailerons with flat sides. For these profiles the trailing-edge angle decreases with increasing h/c.

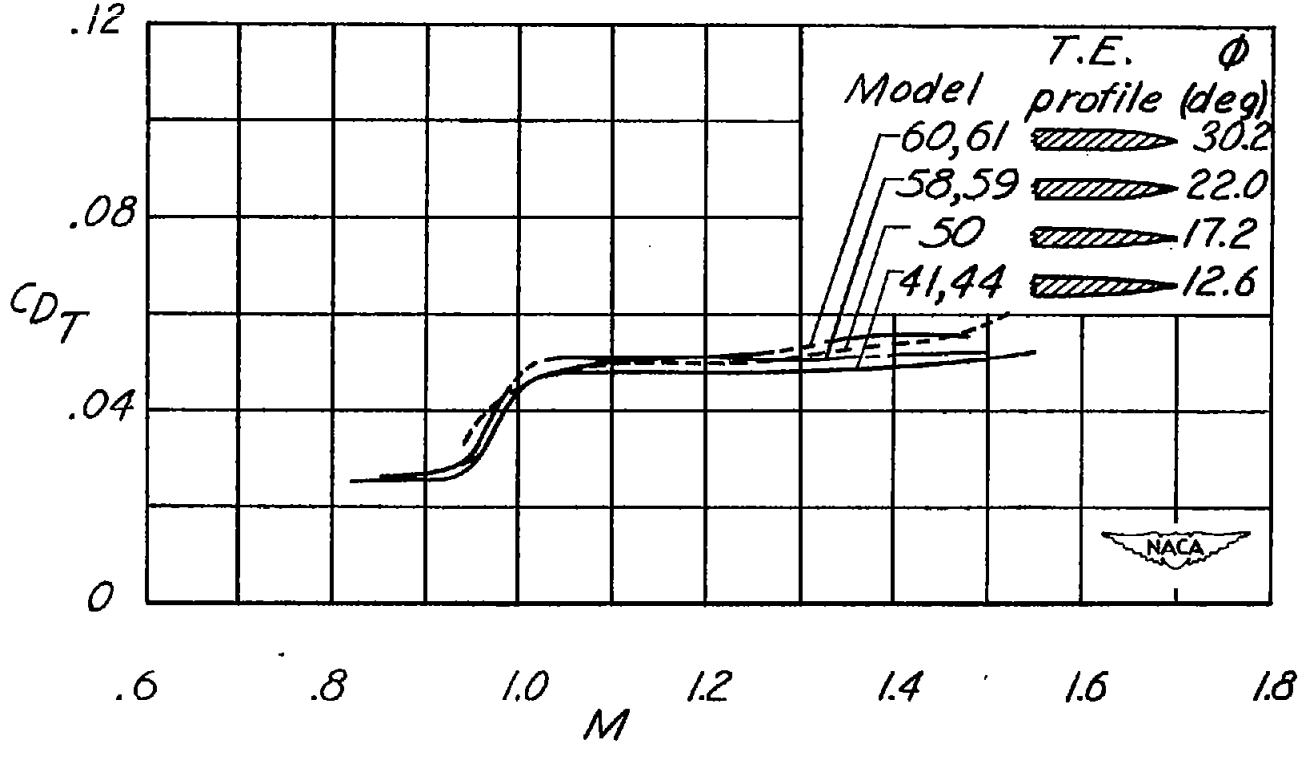

Figure 12.- Variation with Mach number of test-vehicle total-drag coefficient C_{D_T} for wings swept back 45° (summary from fig. 7).

$\delta_a = 5.0°$.

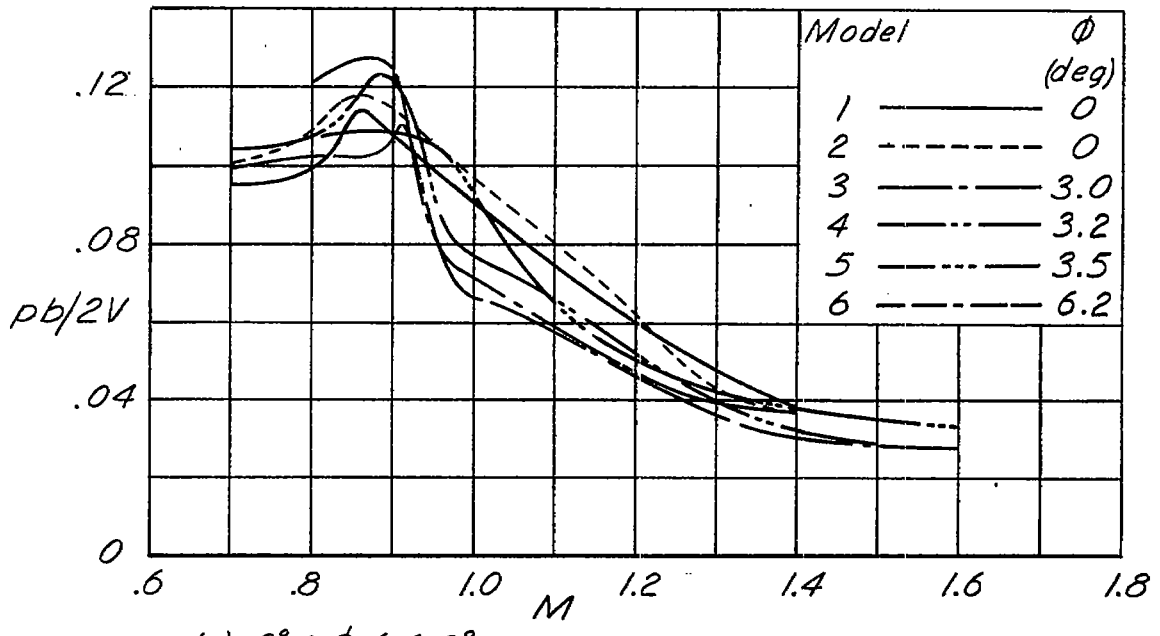

(a) $0° \leq \phi \leq 6.2°$.

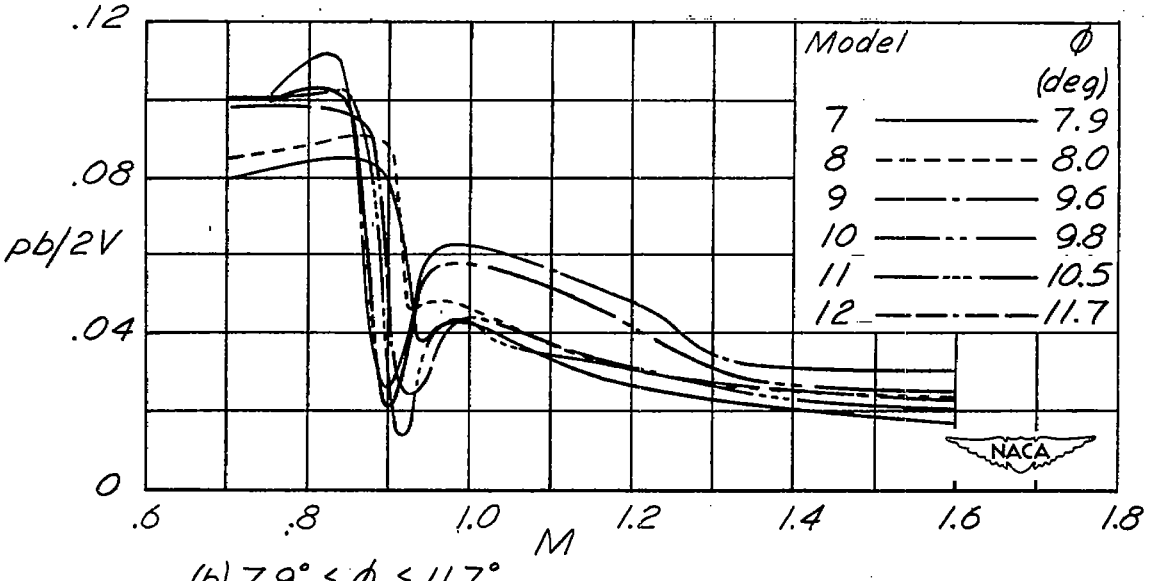

(b) $7.9° \leq \phi \leq 11.7°$.

Figure 13.- Variation with Mach number of wing-aileron rolling effectiveness pb/2V for unswept wings having various profiles and trailing-edge angles ϕ. $C_L \approx 0$; $i_w = 0°$; $\delta_a = 5.0°$; pb/2V corrected to rigid-wing values.

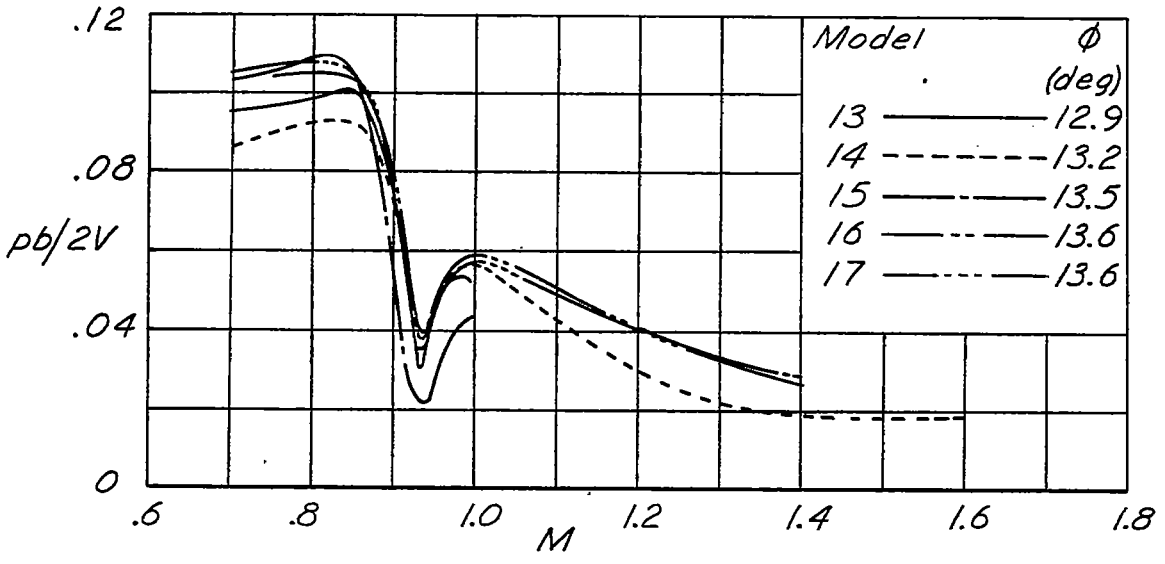

(c) $12.9° \leq \Phi \leq 13.6°$.

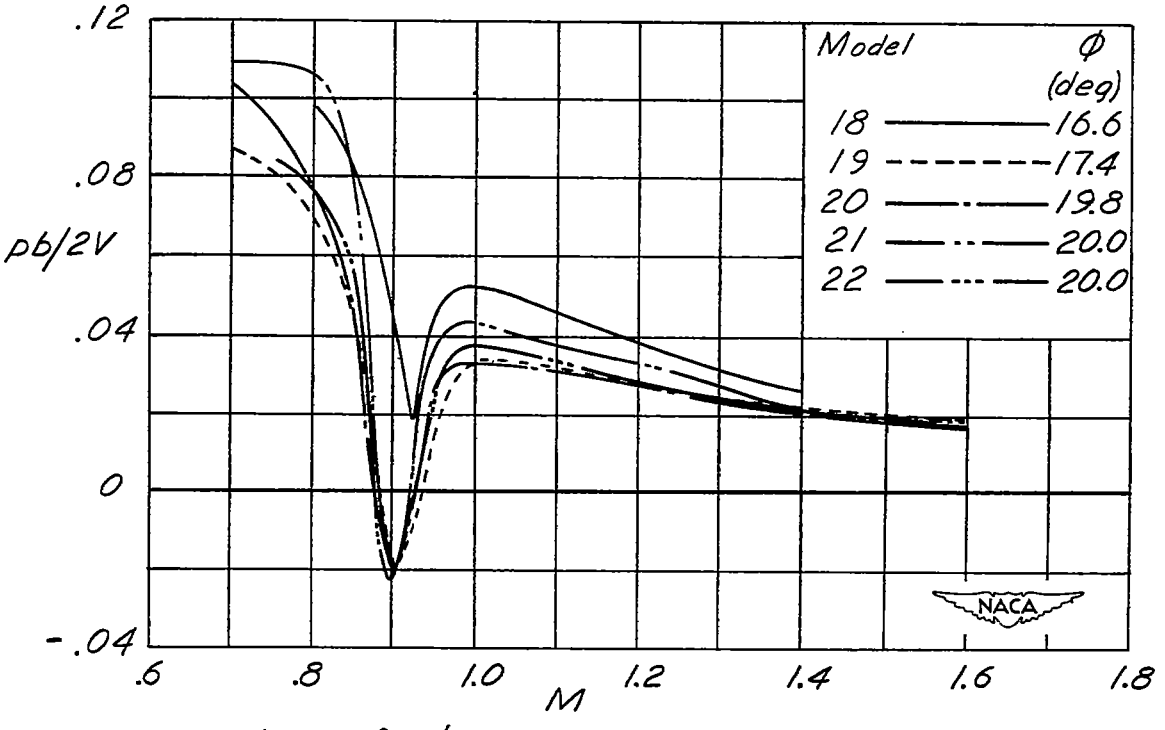

(d) $16.6° \leq \Phi \leq 20.0°$.

Figure 13.- Continued.

[redacted]

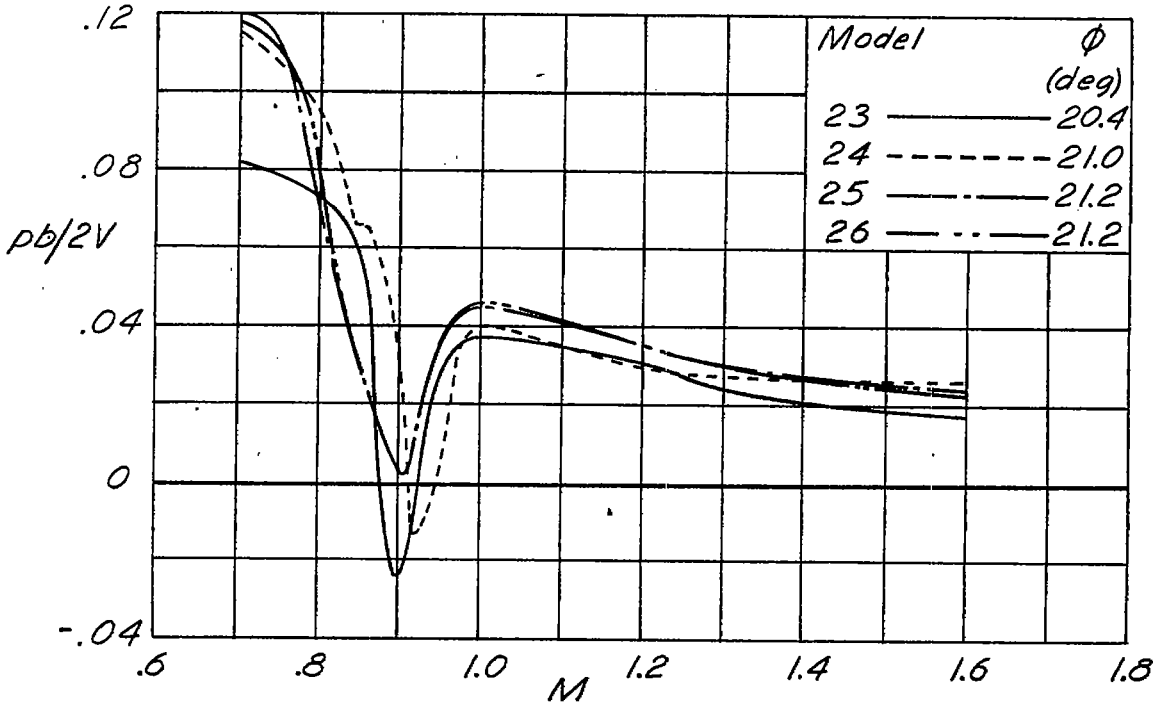

(e) $20.4° \leq \Phi \leq 21.2°$.

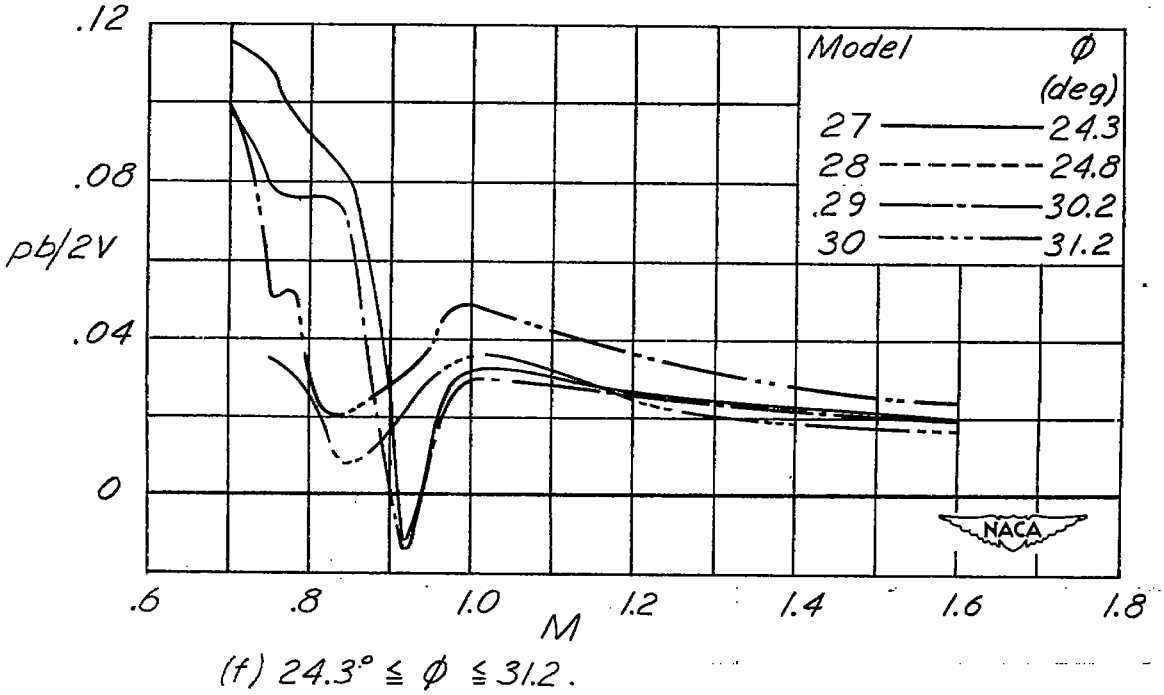

(f) $24.3° \leq \Phi \leq 31.2$.

Figure 13.- Concluded.

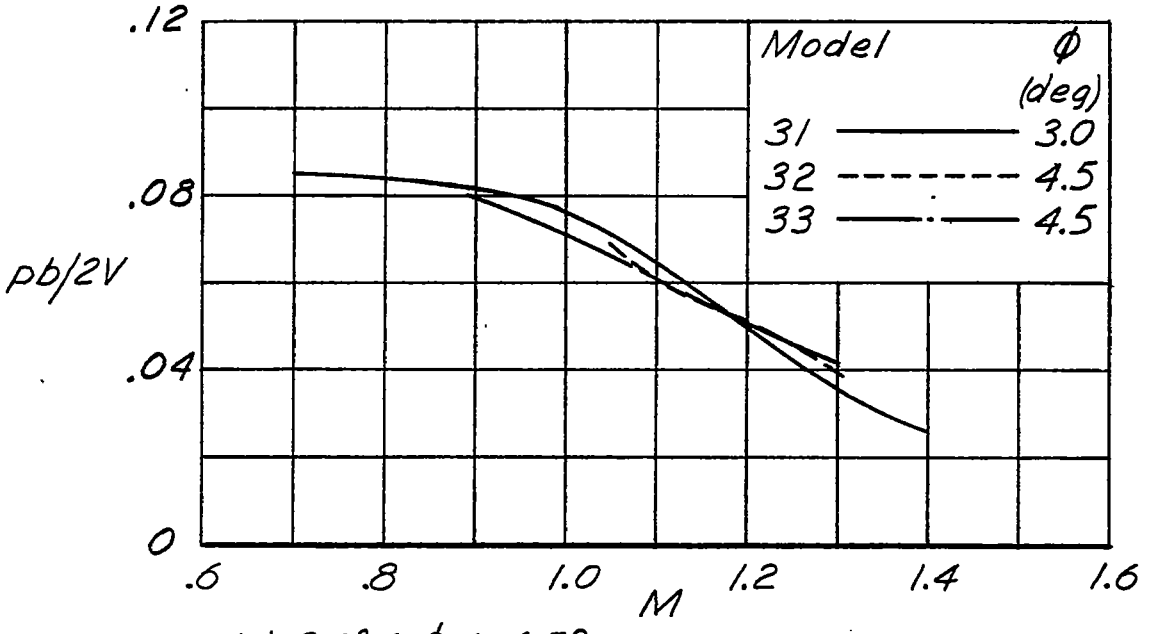

(a) $3.0° \leq \phi \leq 4.5°$.

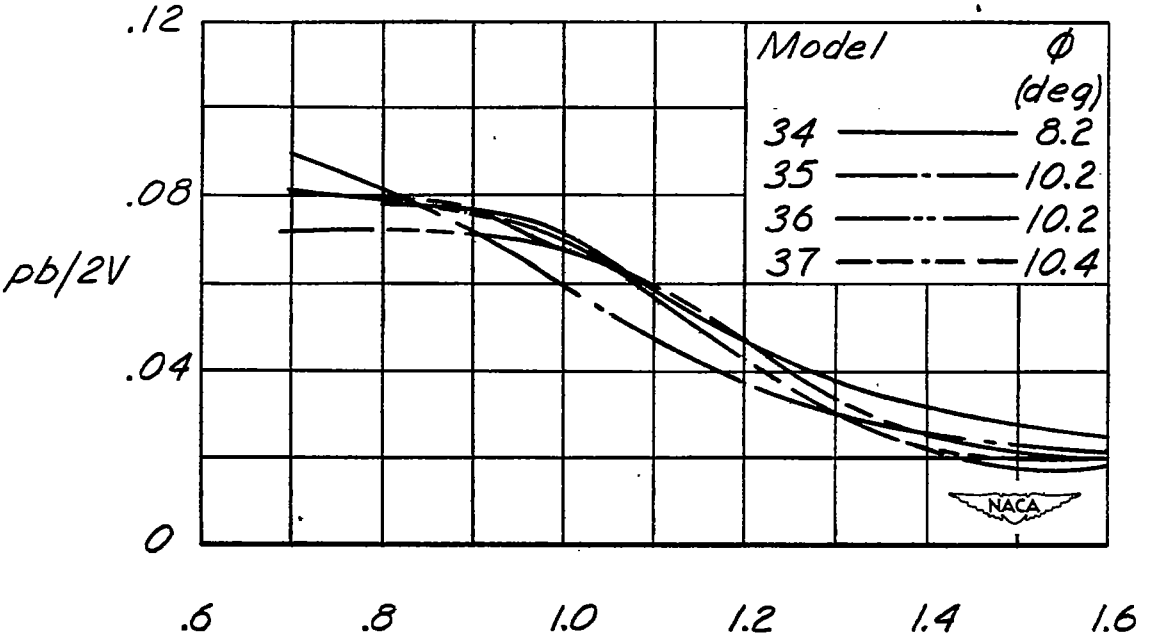

(b) $8.2° \leq \phi \leq 10.4°$.

Figure 14.- Variation with Mach number of wing-aileron rolling effectiveness pb/2V for wings swept back 45° having various profiles and trailing-edge angles ϕ. $i_w = 0°$ and $\delta_a = 5.0°$. $C_L \approx 0$; pb/2V corrected to rigid-wing values.

[redacted]

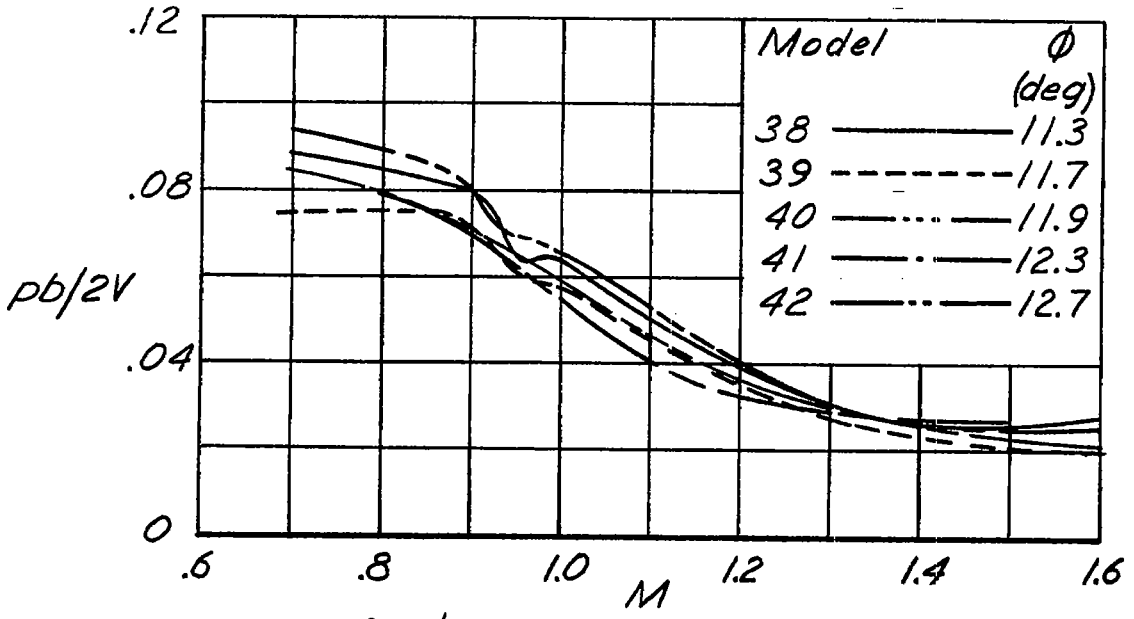

(c) $11.3° \leq \Phi \leq 12.7°$.

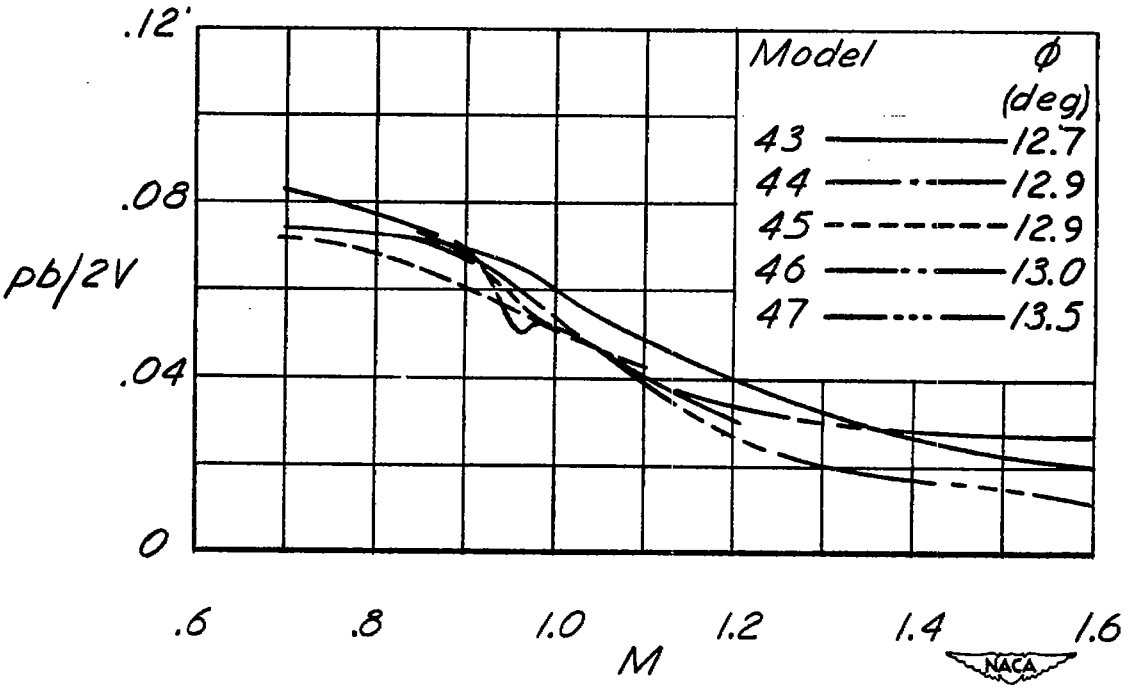

(d) $12.7° \leq \Phi \leq 13.5°$.

Figure 14.- Continued.

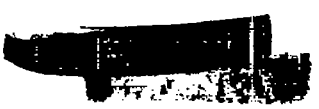

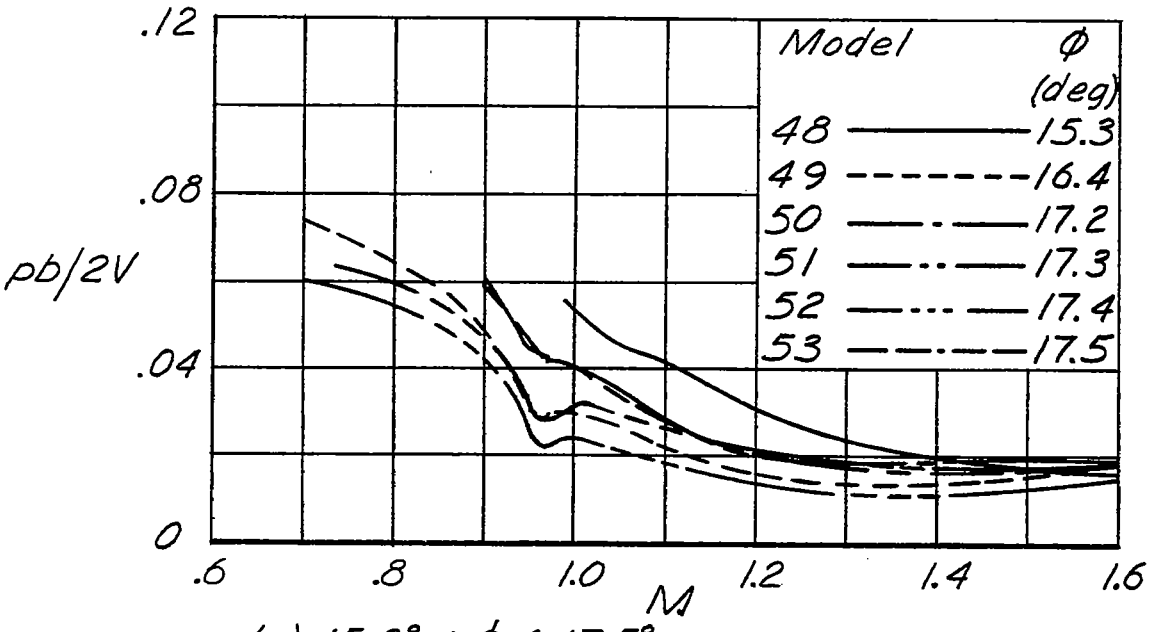

(e) $15.3° \leq \phi \leq 17.5°$.

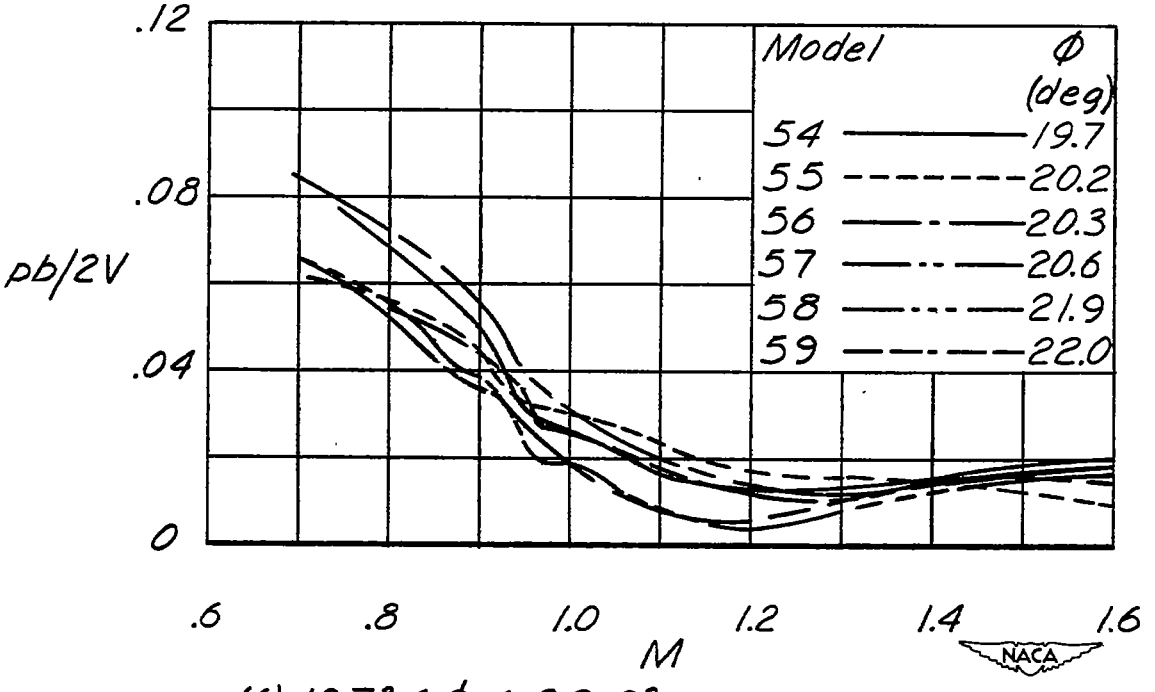

(f) $19.7° \leq \phi \leq 22.0°$.

Figure 14.- Continued.

[redacted]

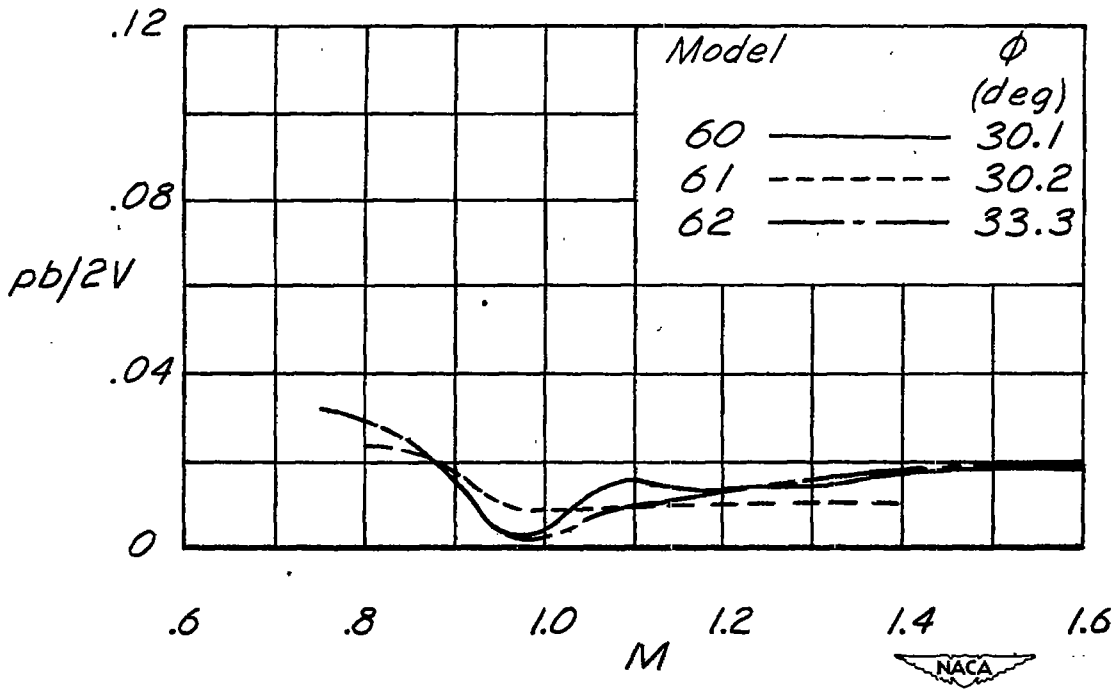

(g) $30.1° \leq \phi \leq 33.3°$.

Figure 14.- Concluded.

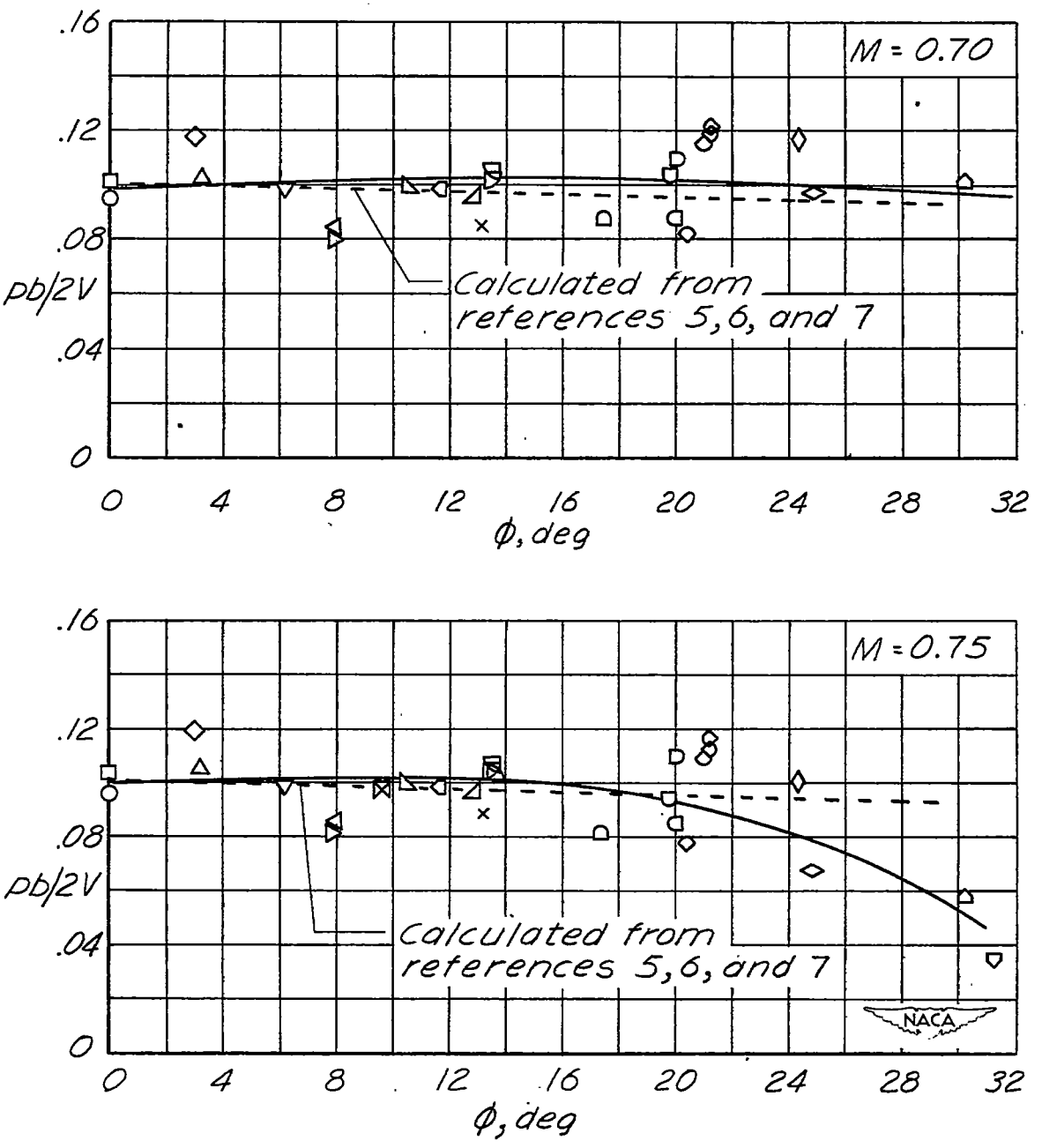

Figure 15.- Effect of trailing-edge angle ϕ on wing-aileron rolling effectiveness pb/2V for rigid unswept wings. $C_L \approx 0$, $i_w = 0^\circ$ and $\delta_a = 5.0^\circ$. (Cross plot of data from fig. 13). See table I for symbols.

[redacted]

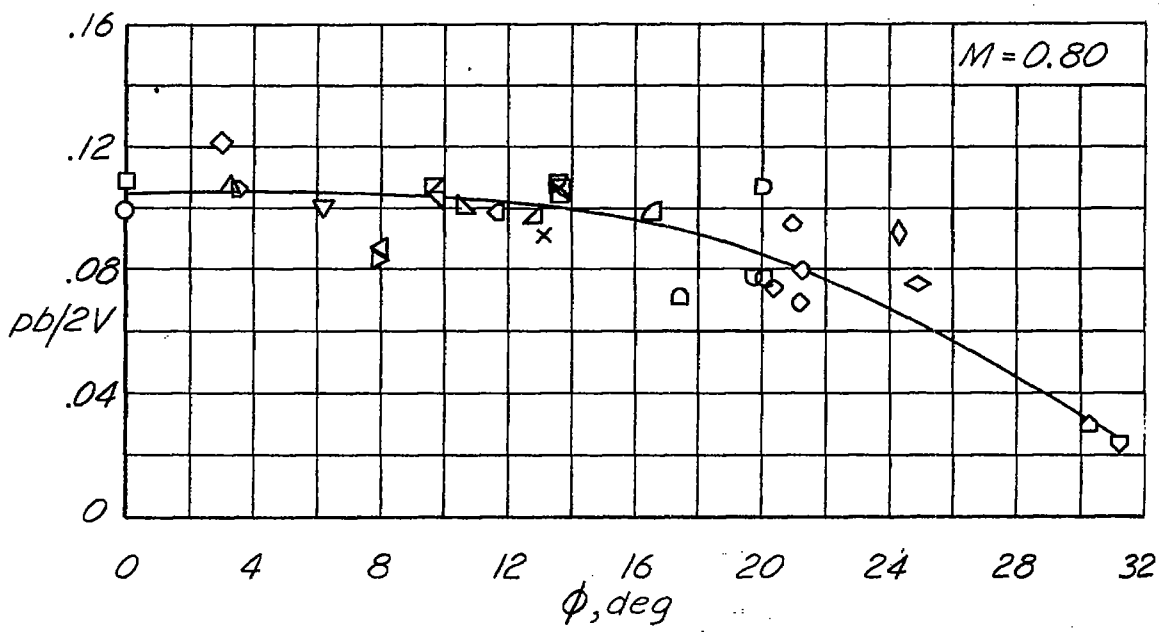

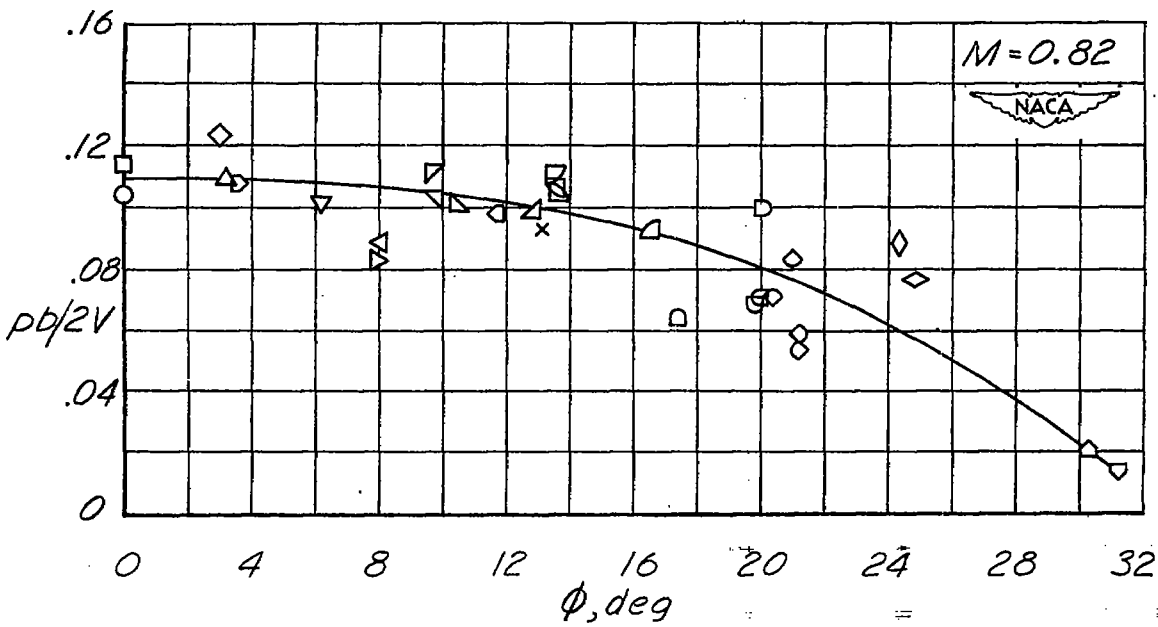

Figure 15.- Continued.

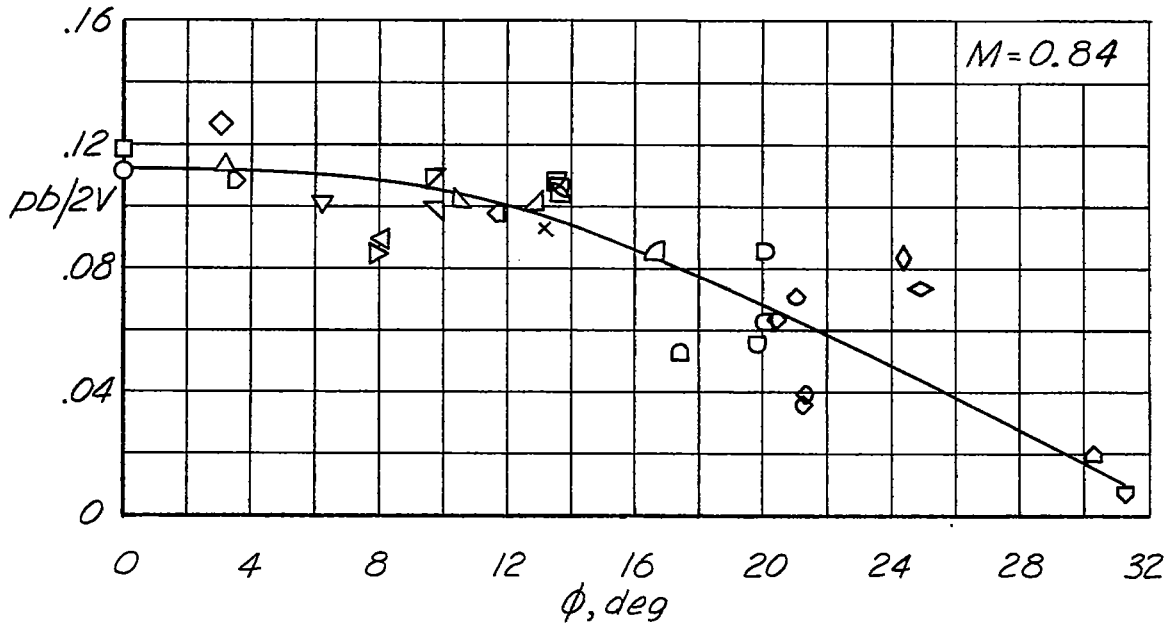

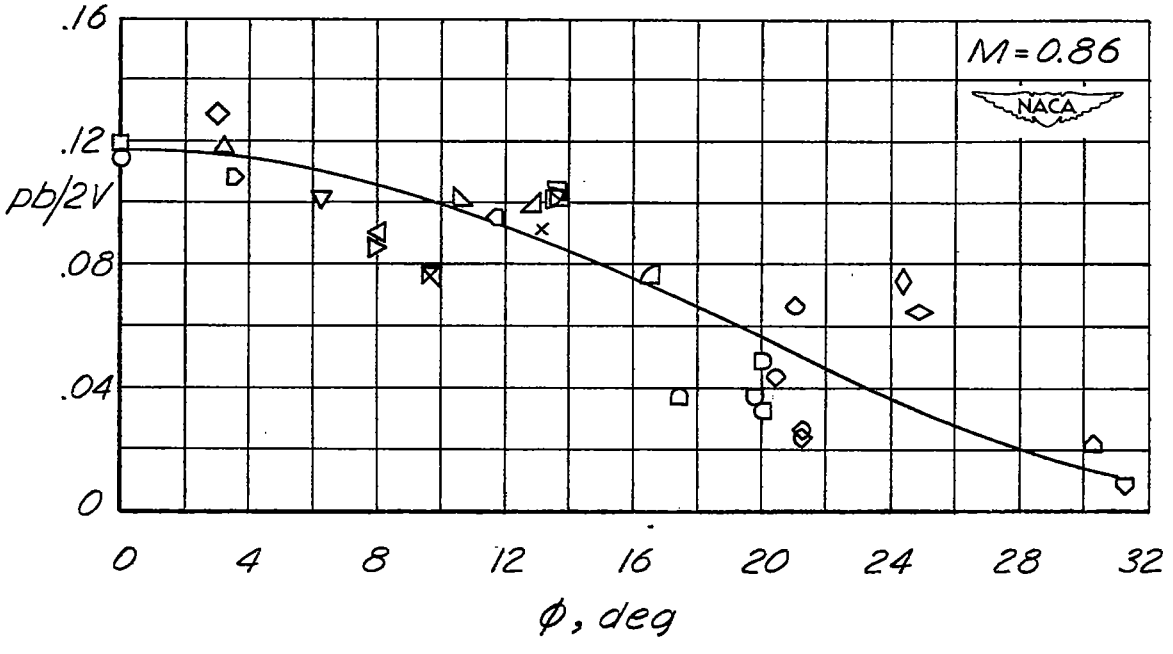

Figure 15.- Continued.

[redacted]

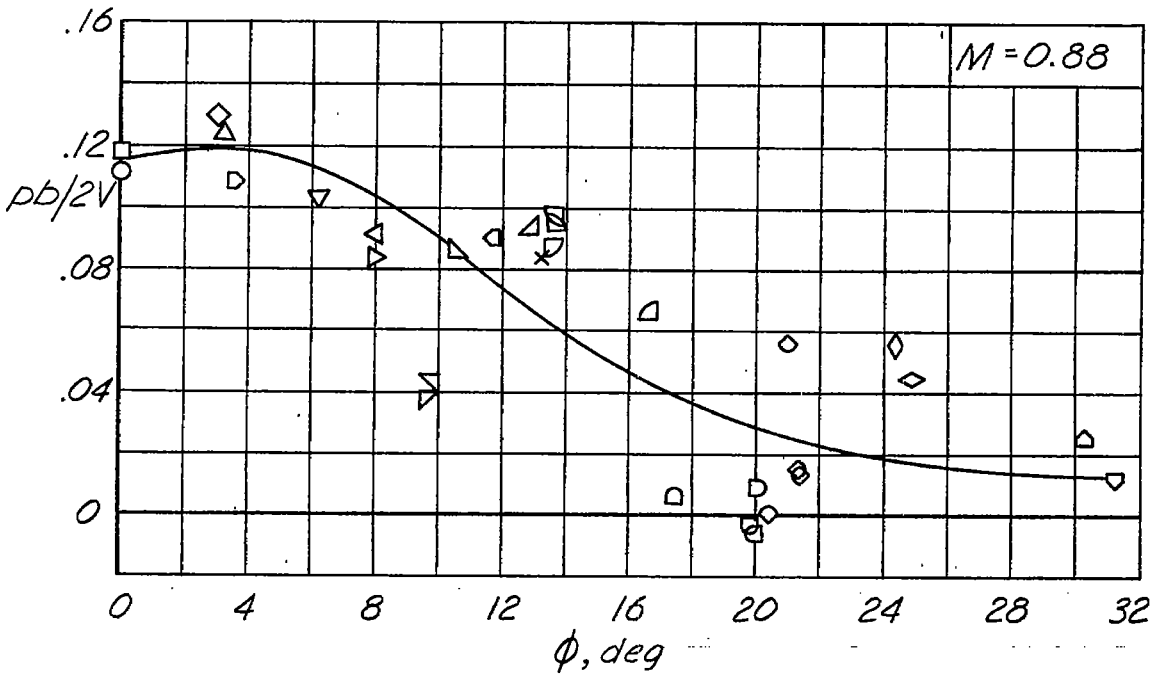

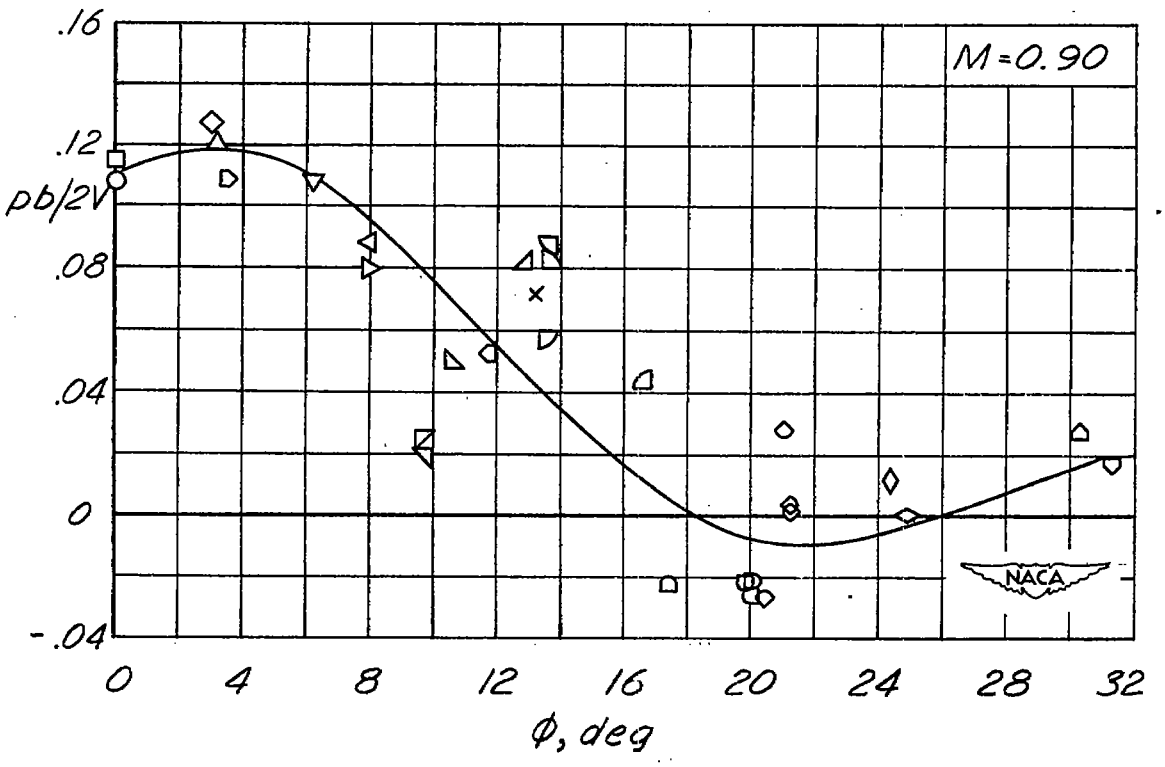

Figure 15.- Continued.

[redacted]

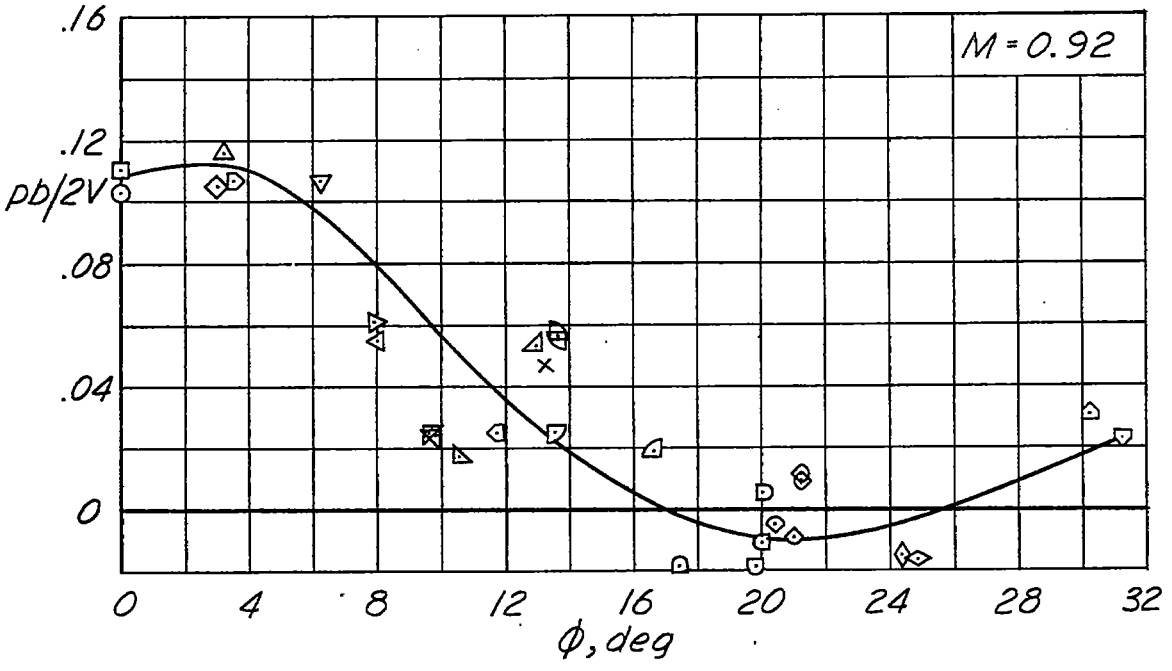

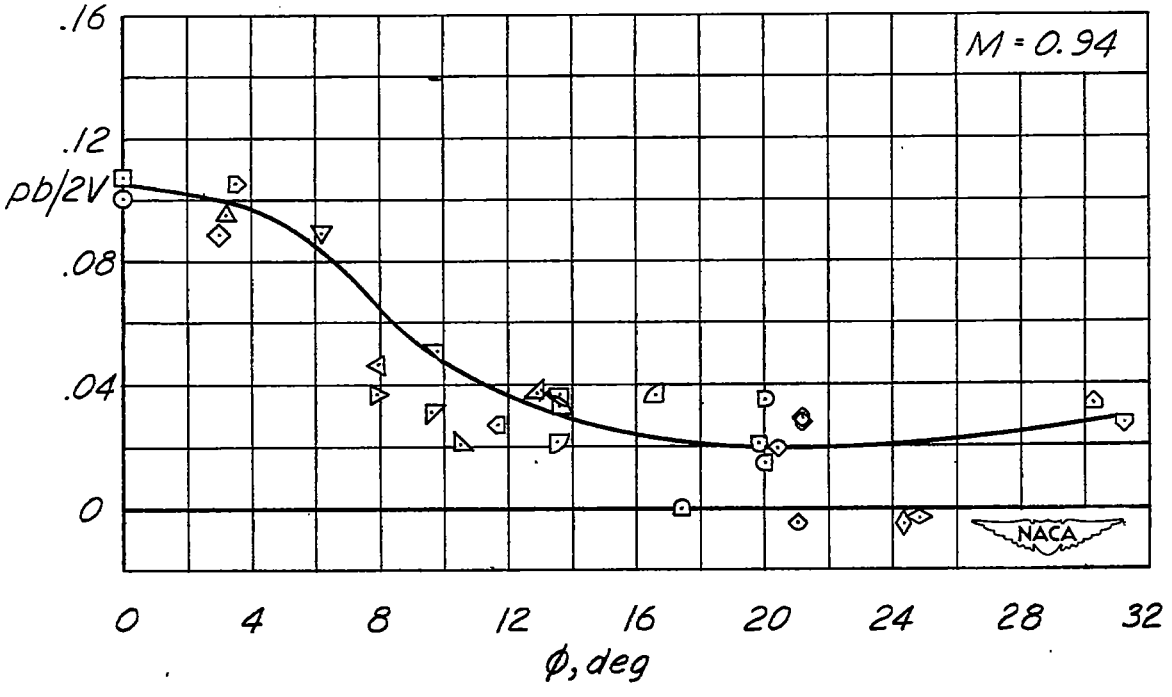

Figure 15.- Continued.

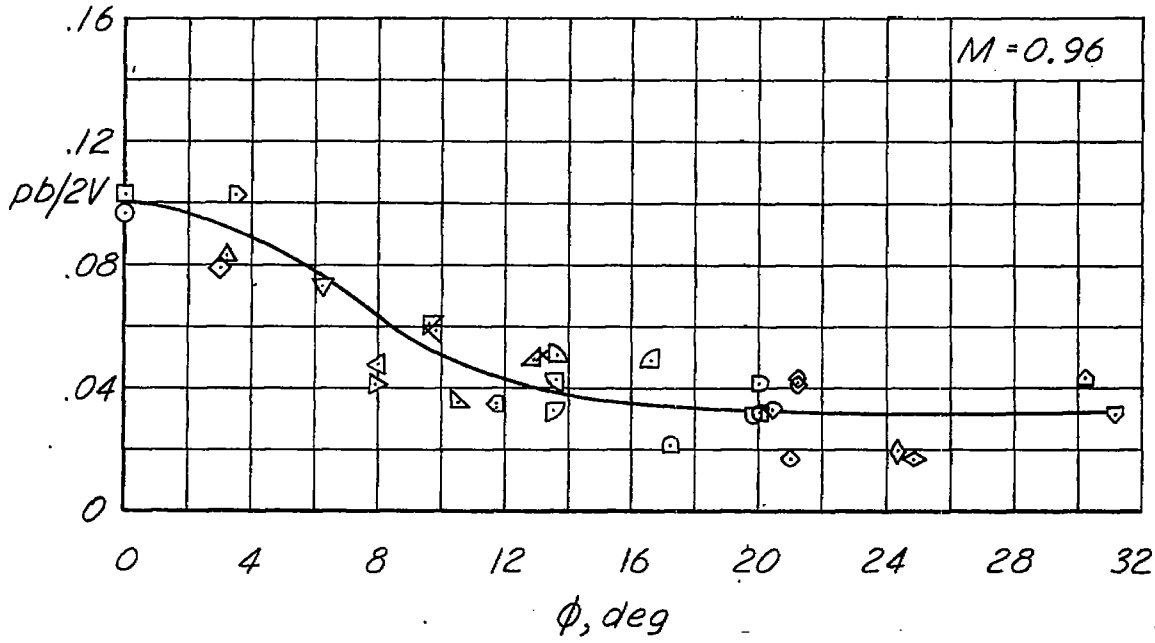

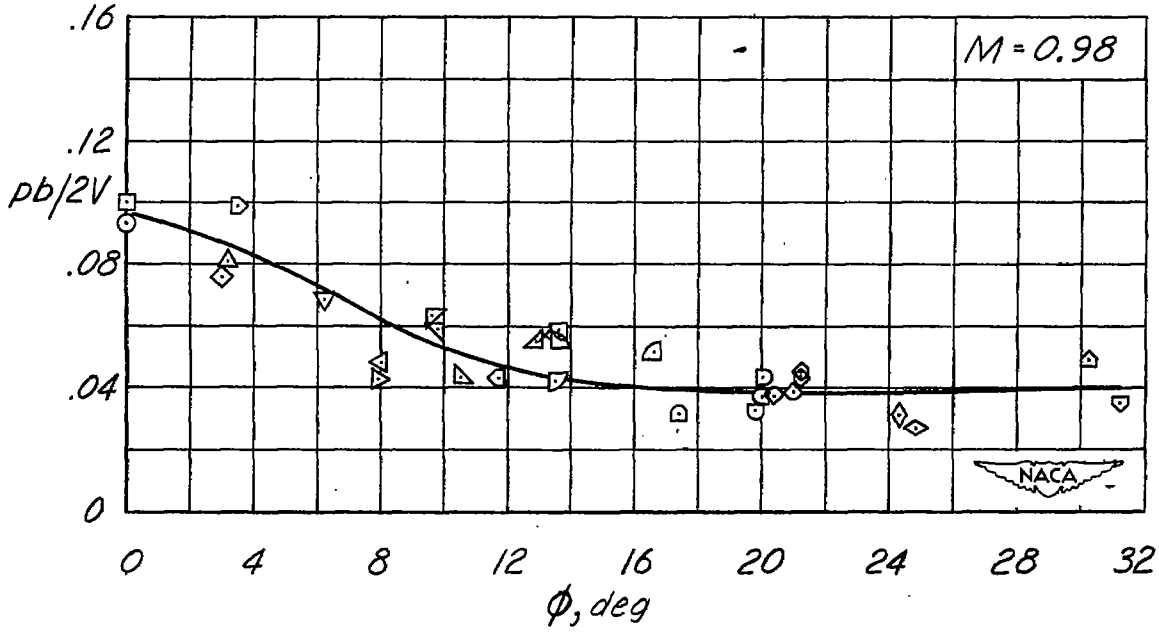

Figure 15.- Continued.

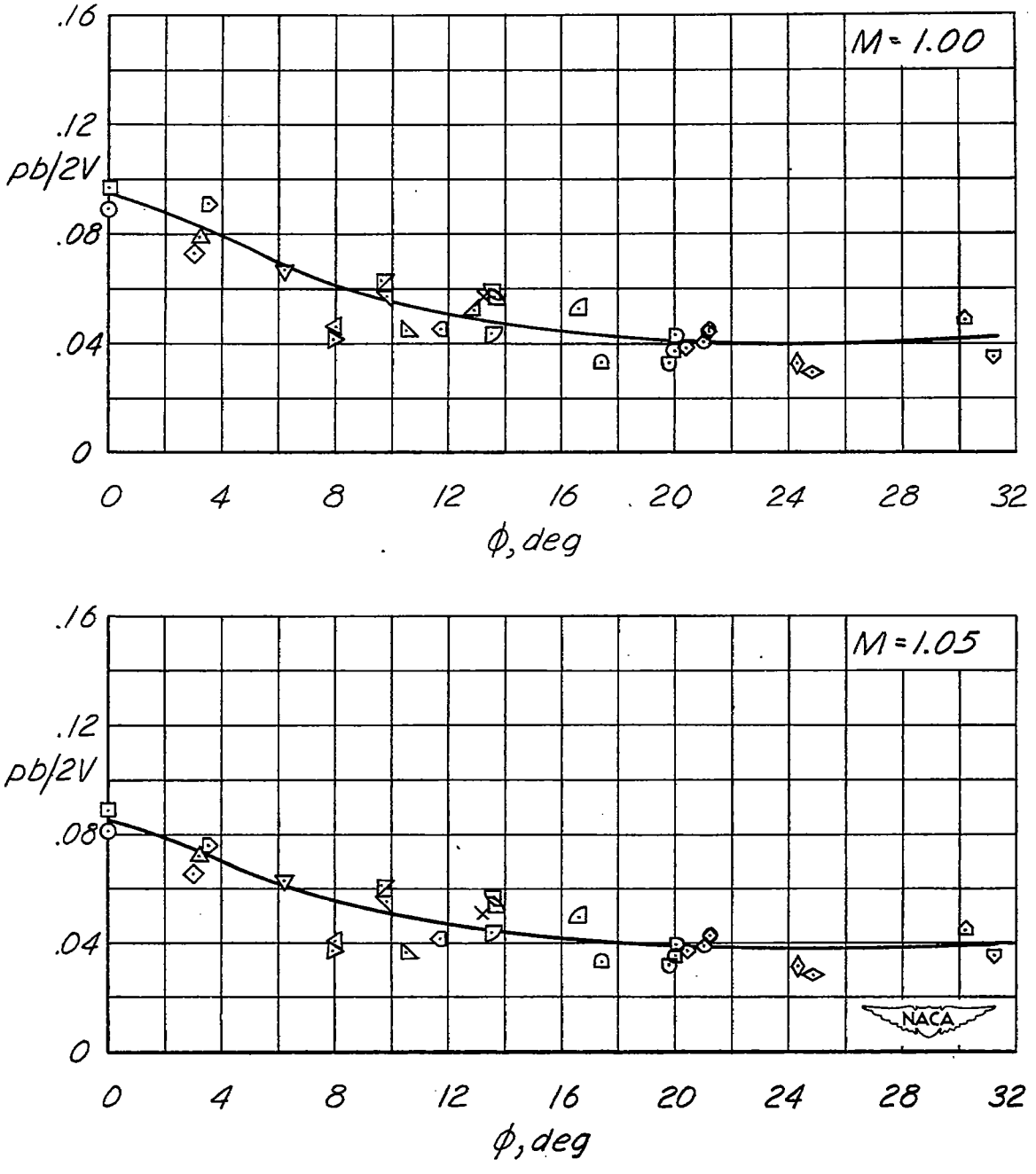

Figure 15.- Continued.

[redacted]

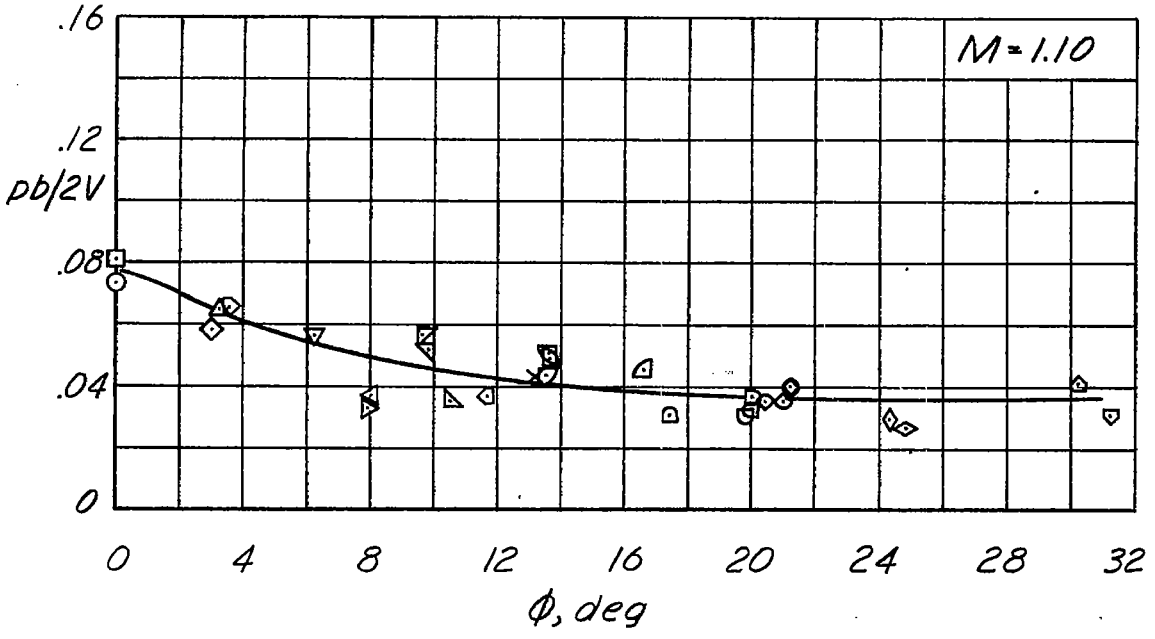

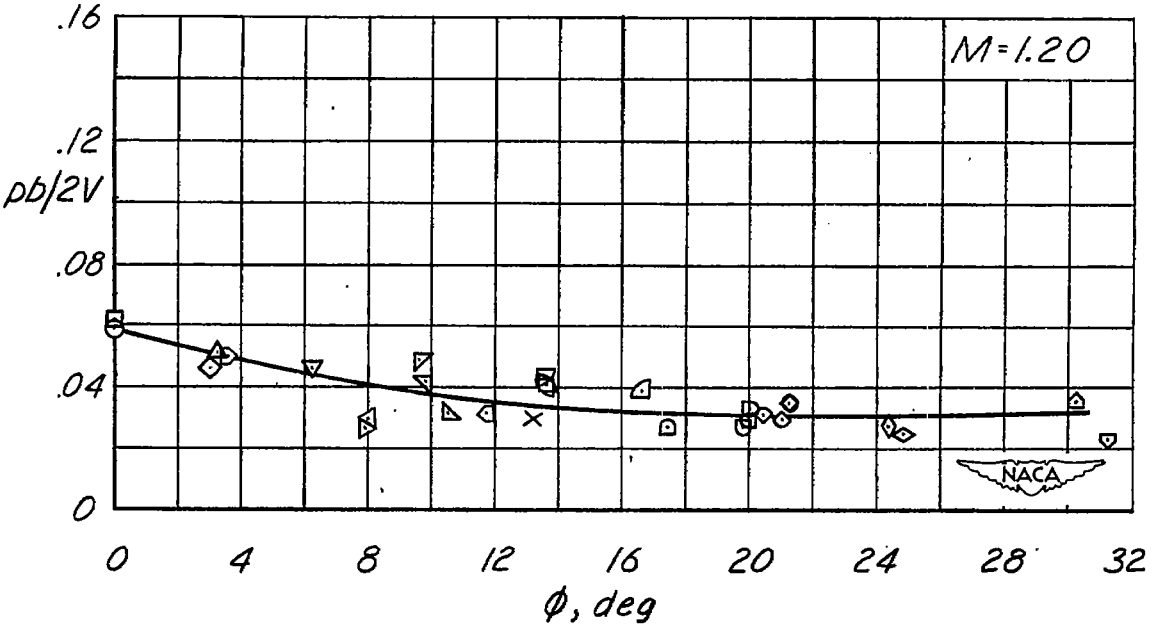

Figure 15.- Continued.

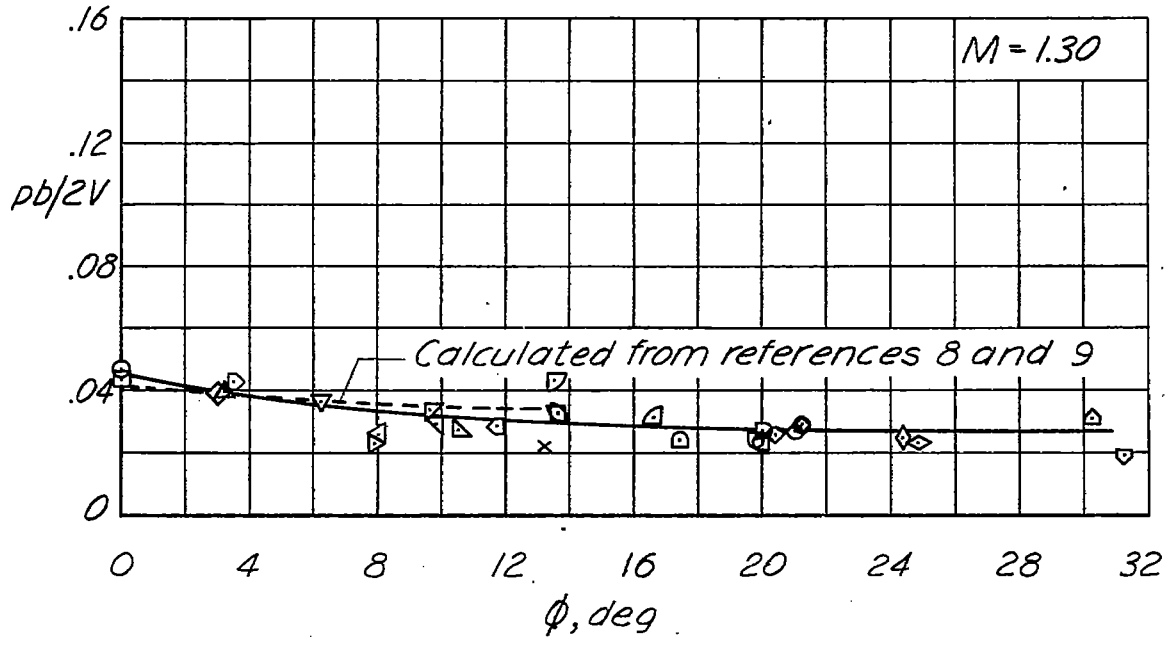

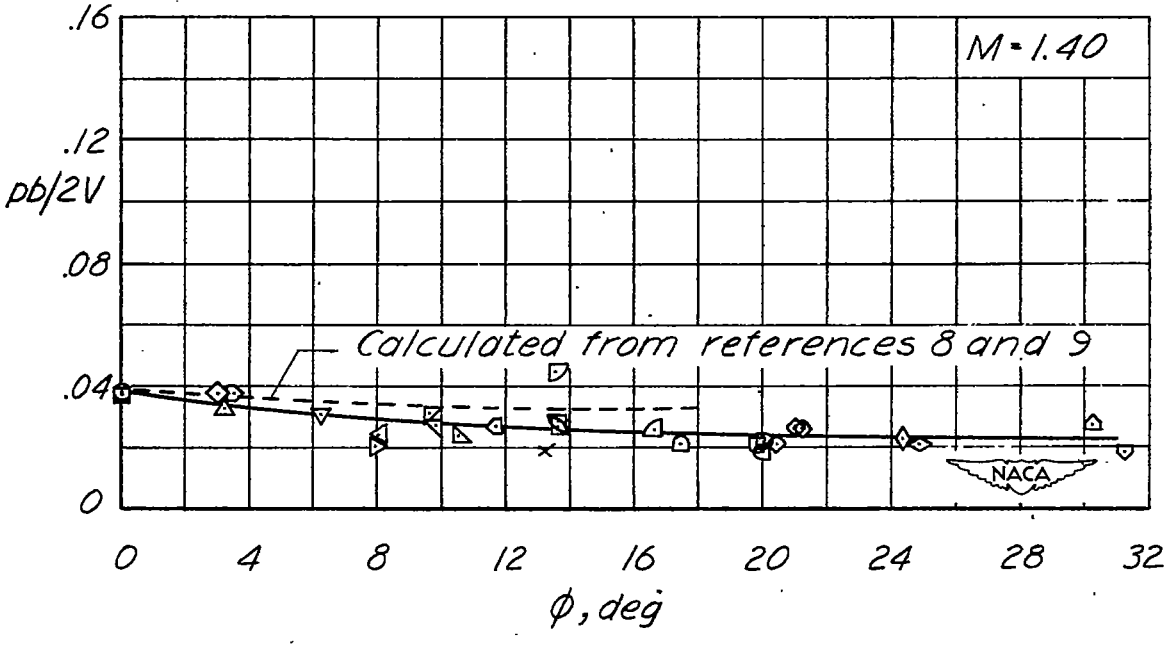

Figure 15.- Continued.

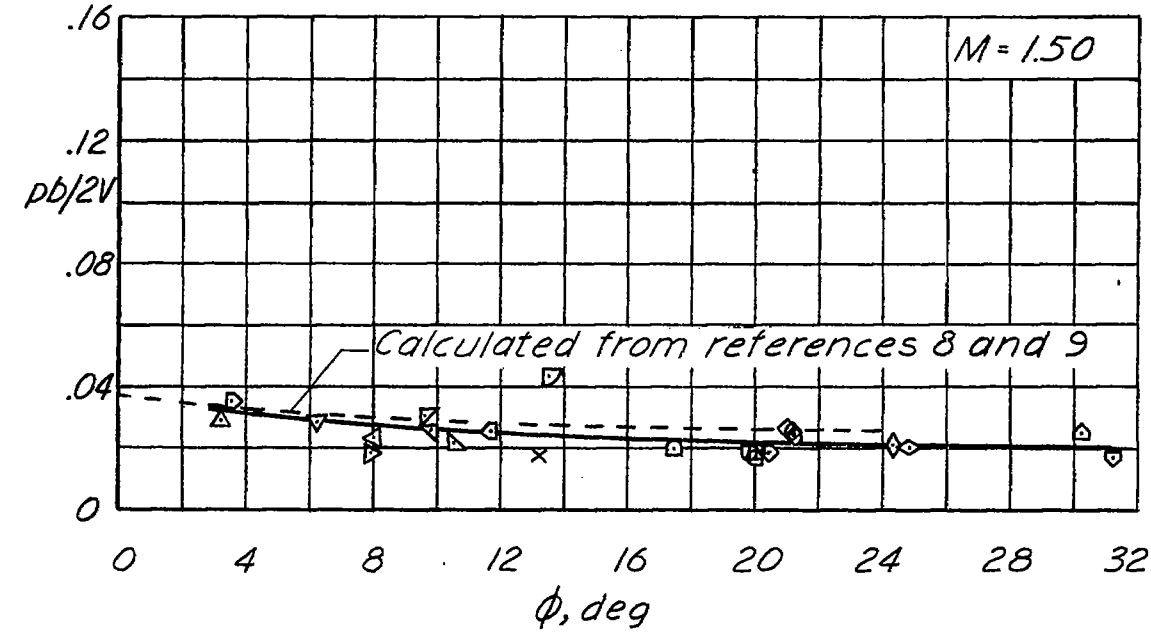

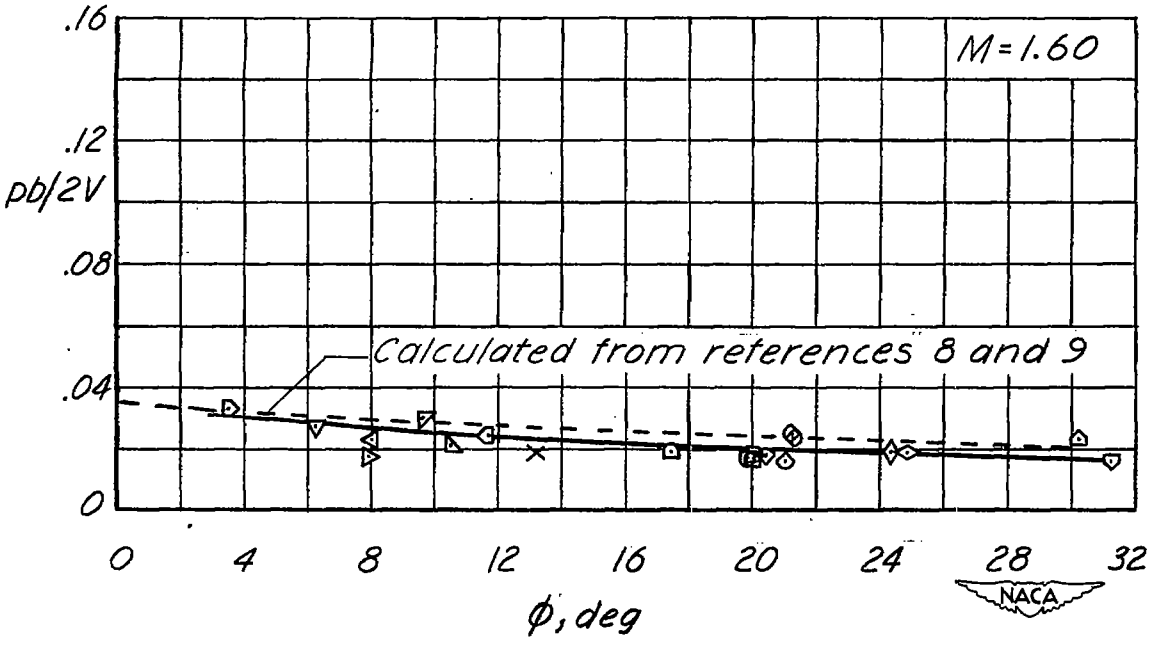

Figure 15.- Concluded.

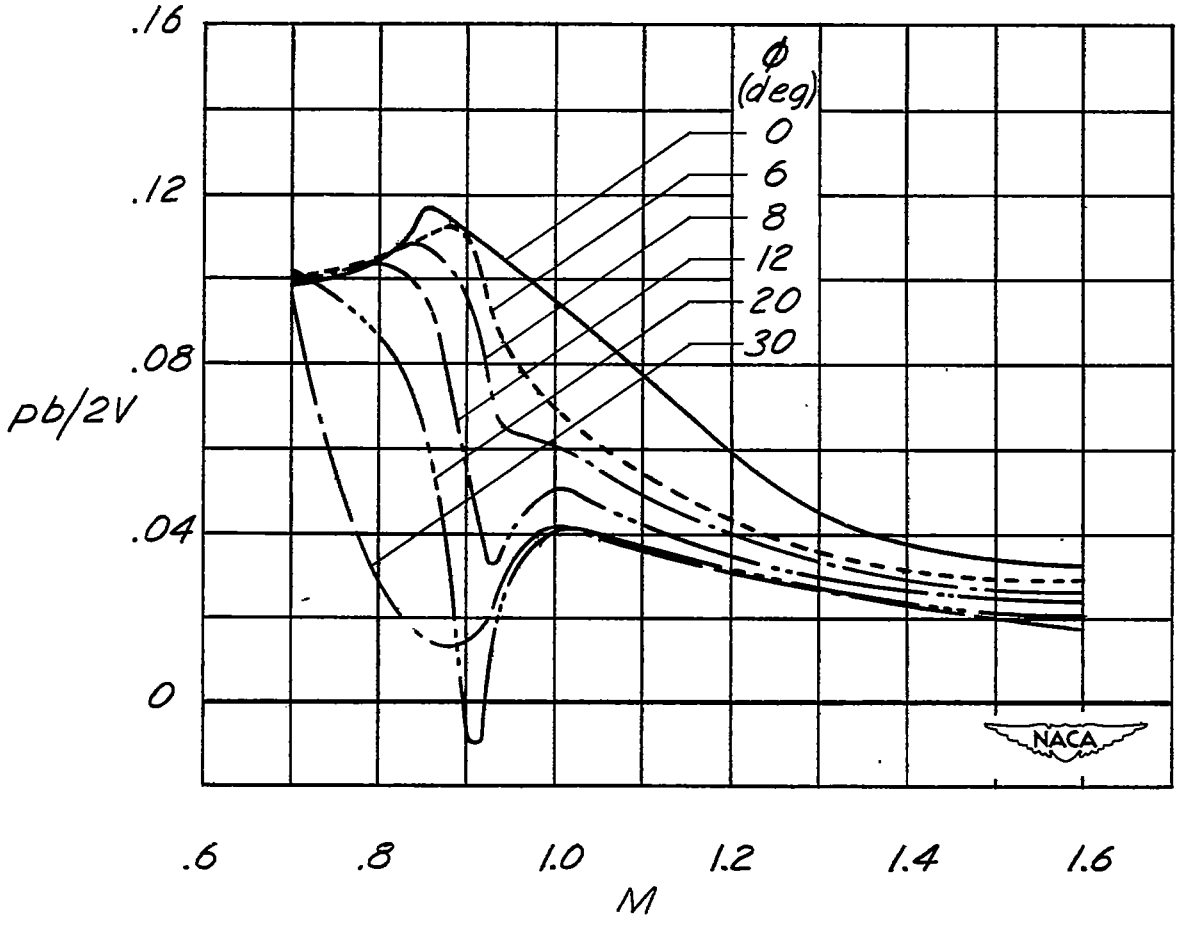

Figure 16.- Variation with Mach number of wing-aileron rolling effectiveness pb/2V for unswept rigid wings; constructed from faired curves of figure 15 for several arbitrary trailing-edge angles. $i_w = 0^\circ$ and $\delta_a = 5.0^\circ$. $C_L \approx 0$.

[redacted]

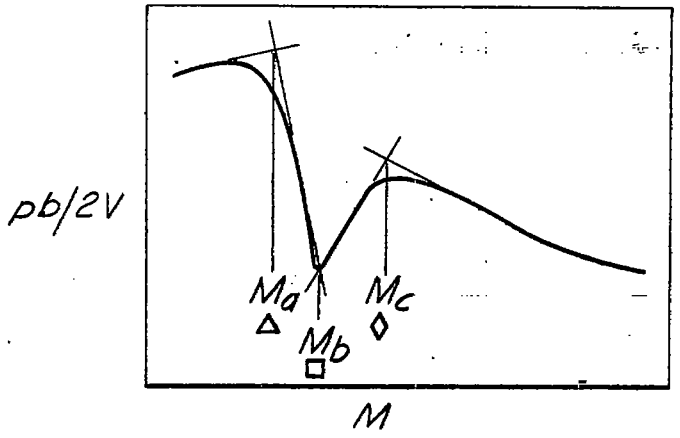

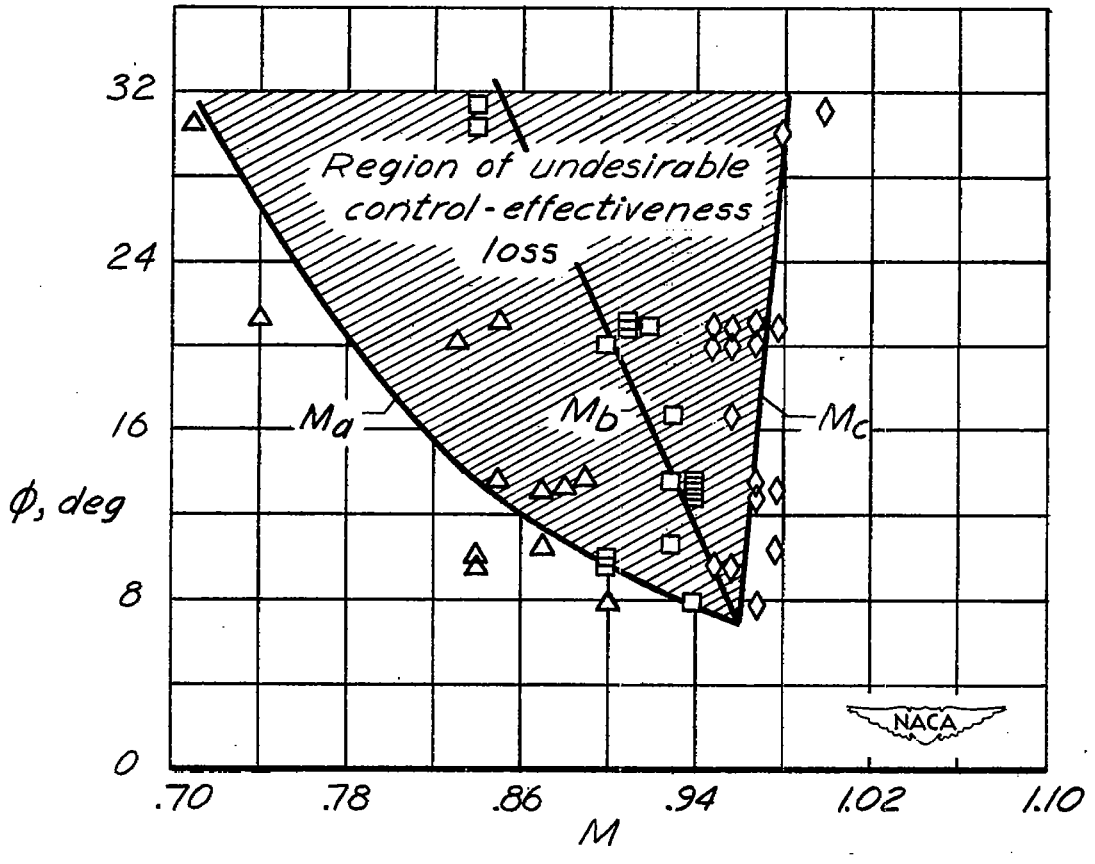

Figure 17.- Effect of trailing-edge angle ϕ on wing-aileron rolling-effectiveness loss for unswept wings at high subsonic speeds. Upper figure defines M_a, M_b, and M_c. $C_L \approx 0$; $i_w = 0^\circ$; $\delta_a = 5.0^\circ$.

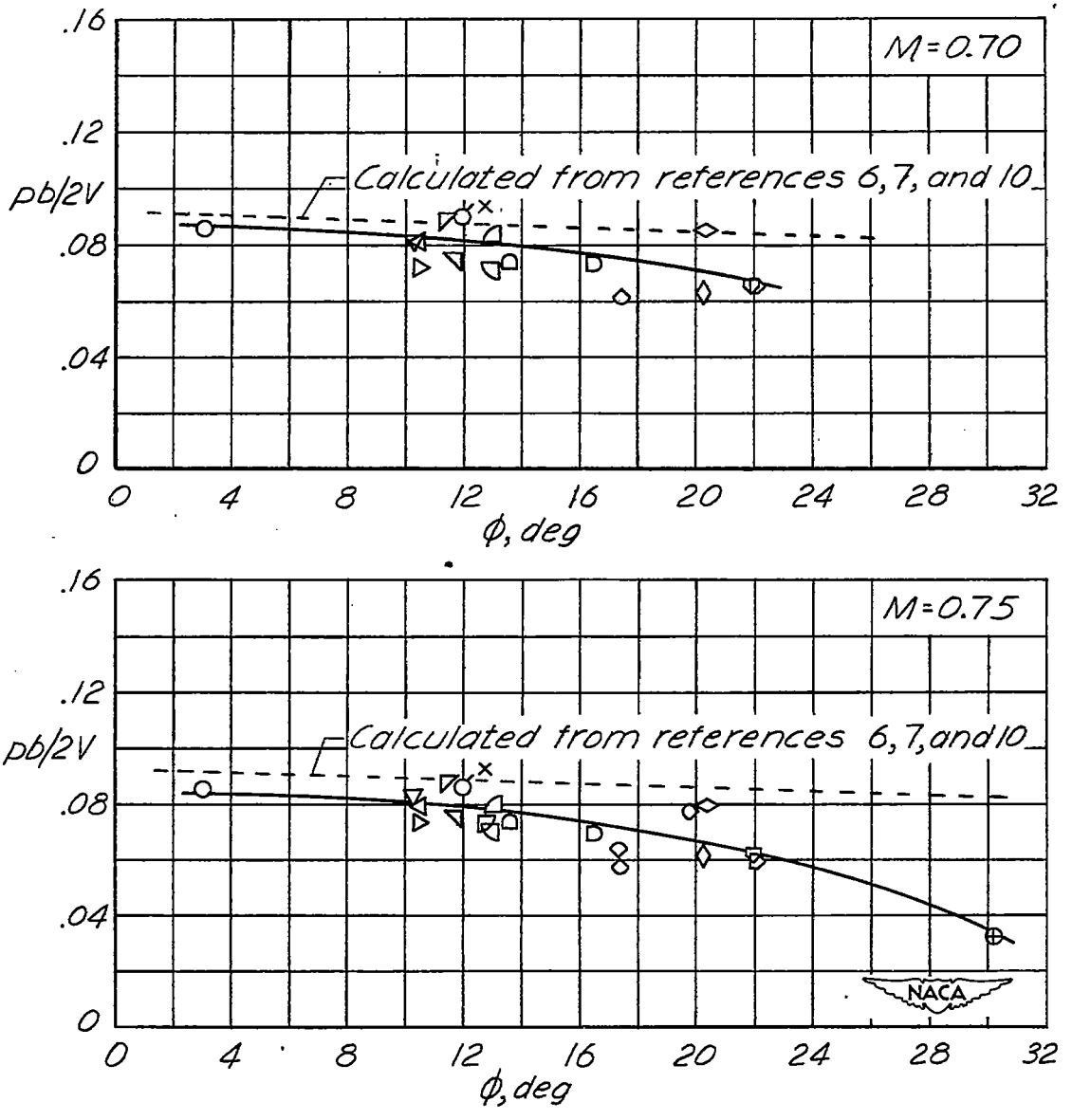

Figure 18.- Effect of trailing-edge angle ϕ on wing-aileron rolling effectiveness pb/2V for rigid wings swept back 45°. Data points are from figure 14. $C_L \approx 0$; $i_w = 0°$; $\delta_a = 5.0°$. See table I for symbols.

[redacted]

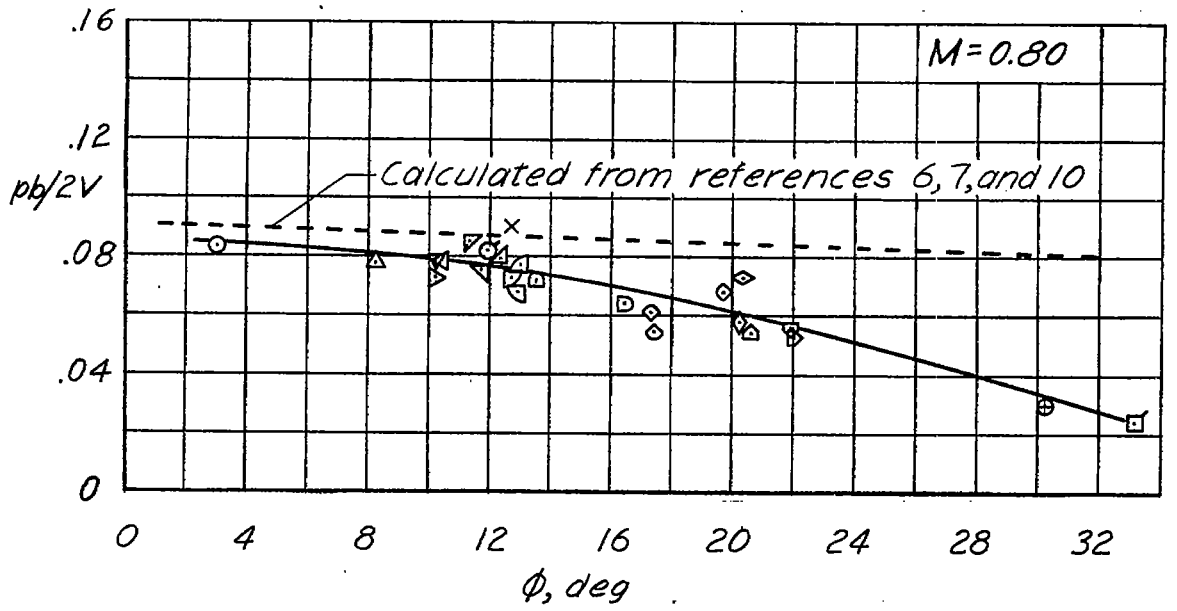

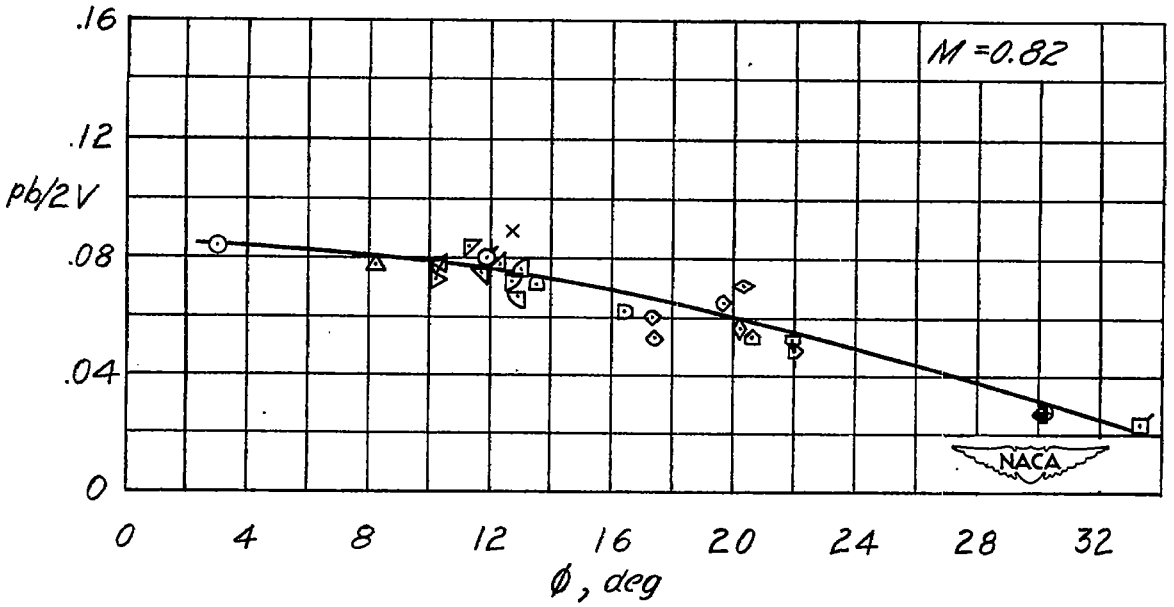

Figure 18.- Continued.

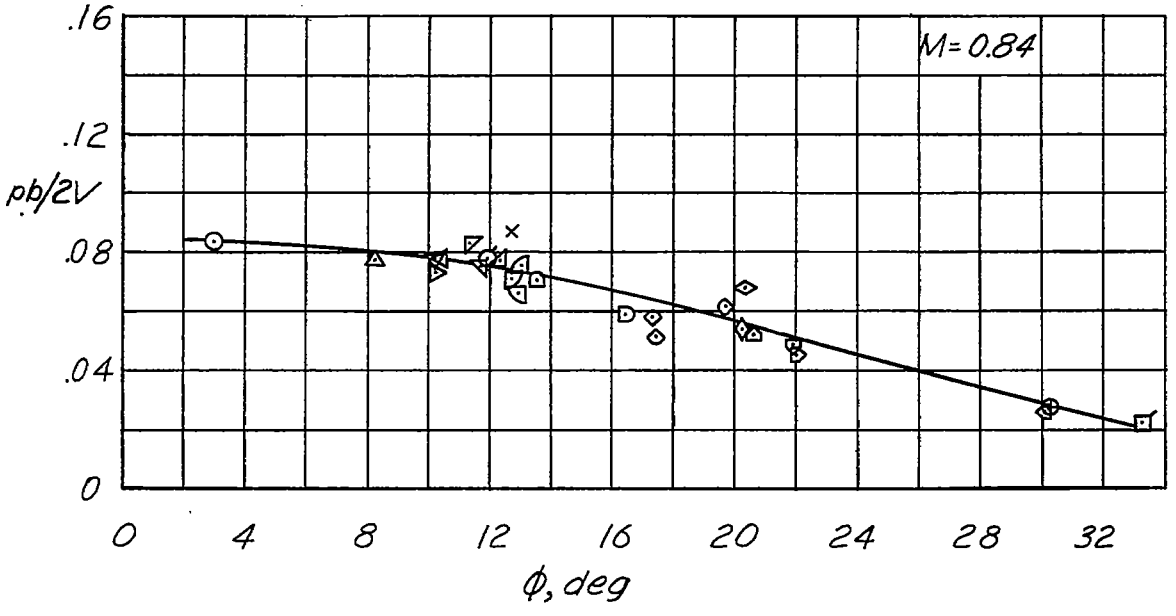

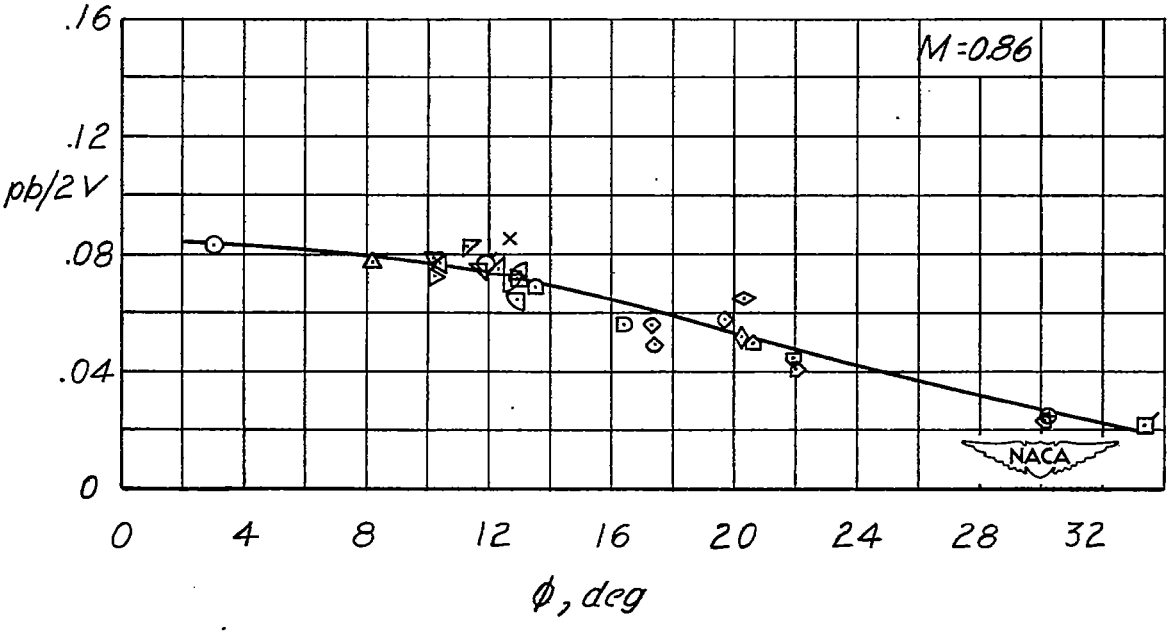

Figure 18.- Continued.

[redacted]

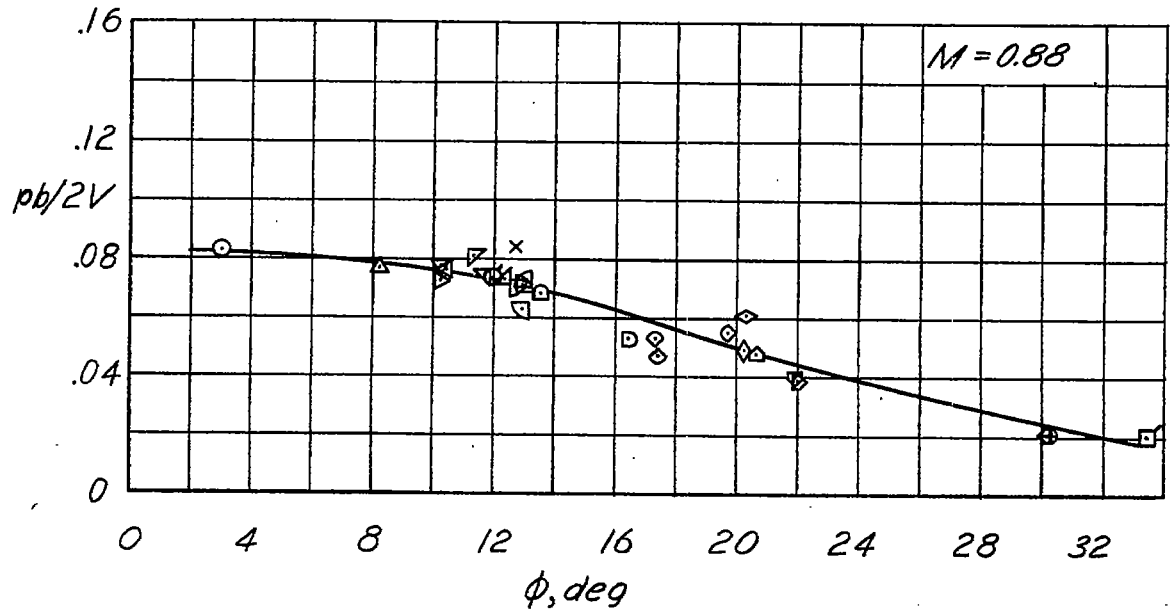

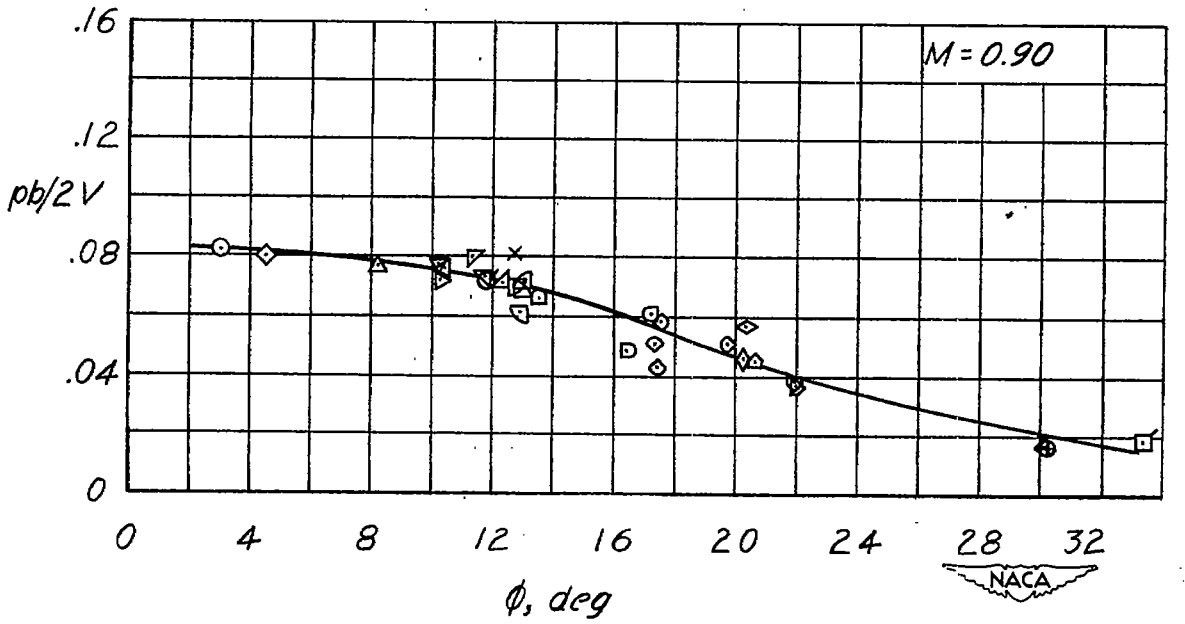

Figure 18.- Continued.

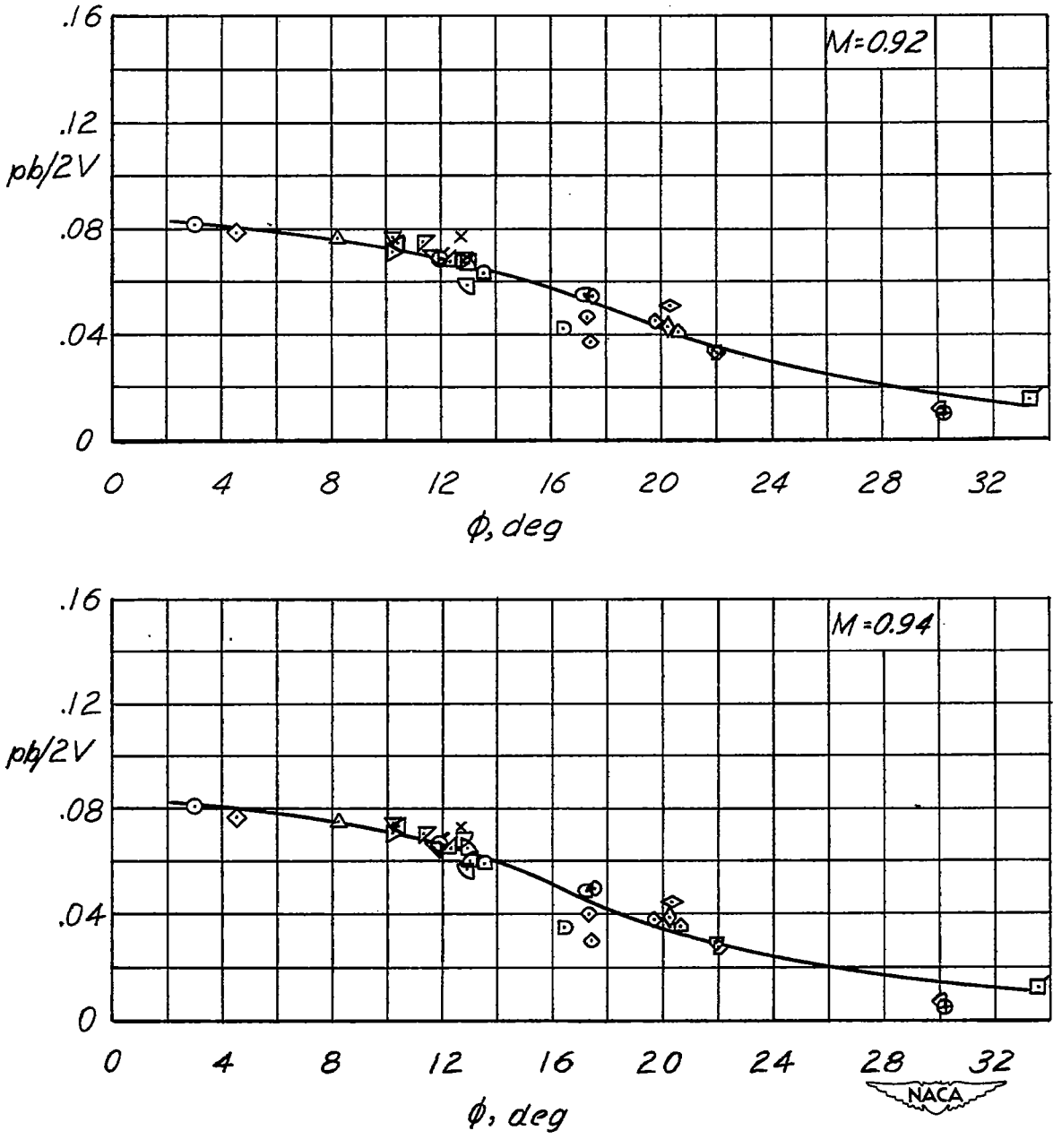

Figure 18.- Continued.

[redacted]

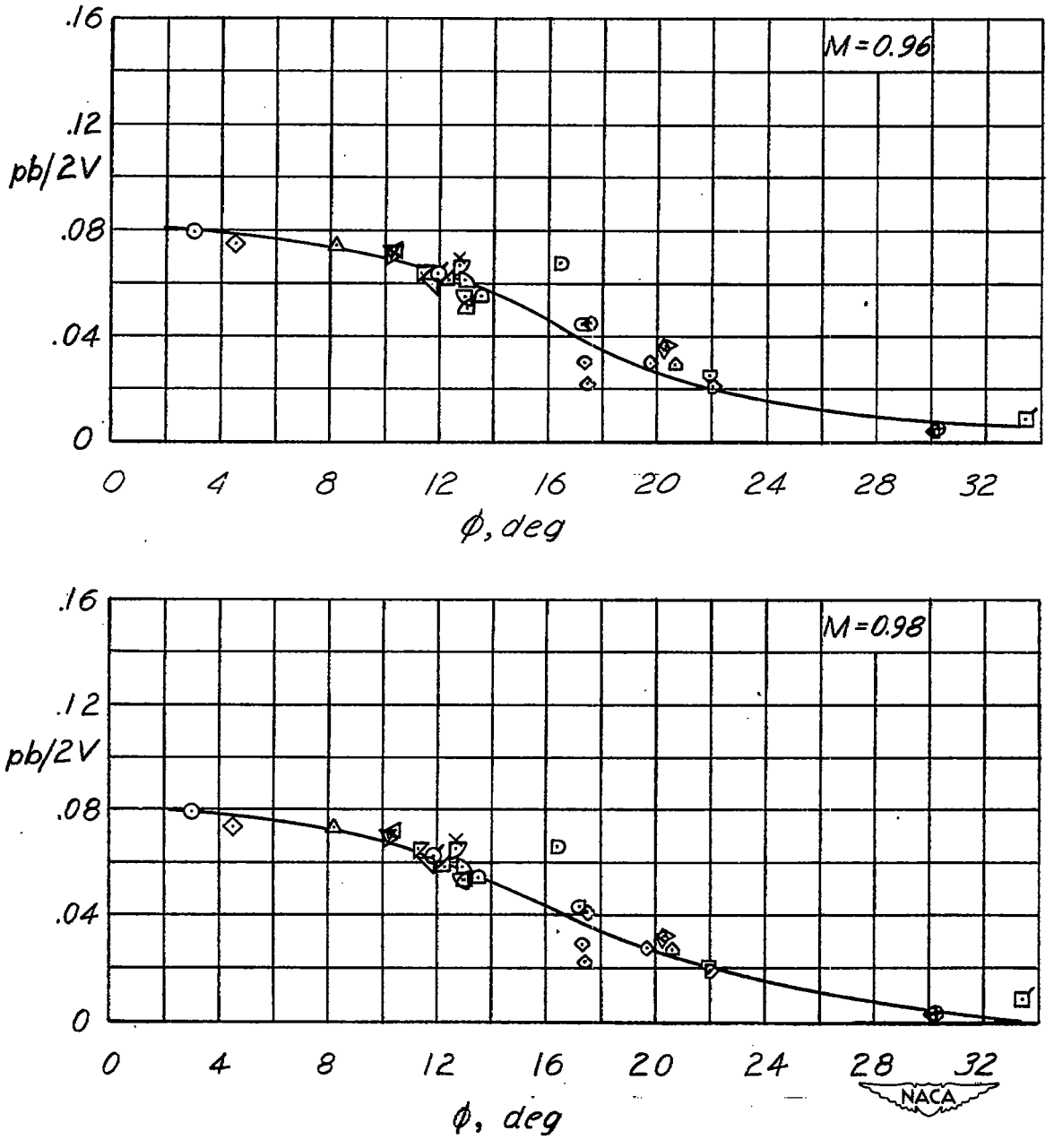

Figure 18.- Continued.

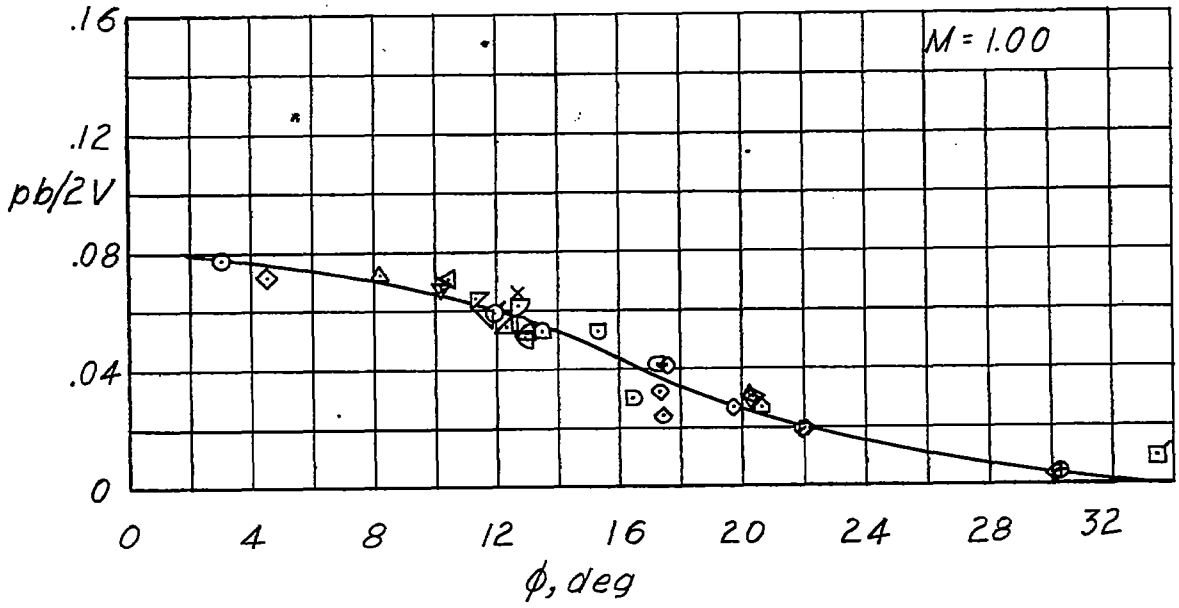

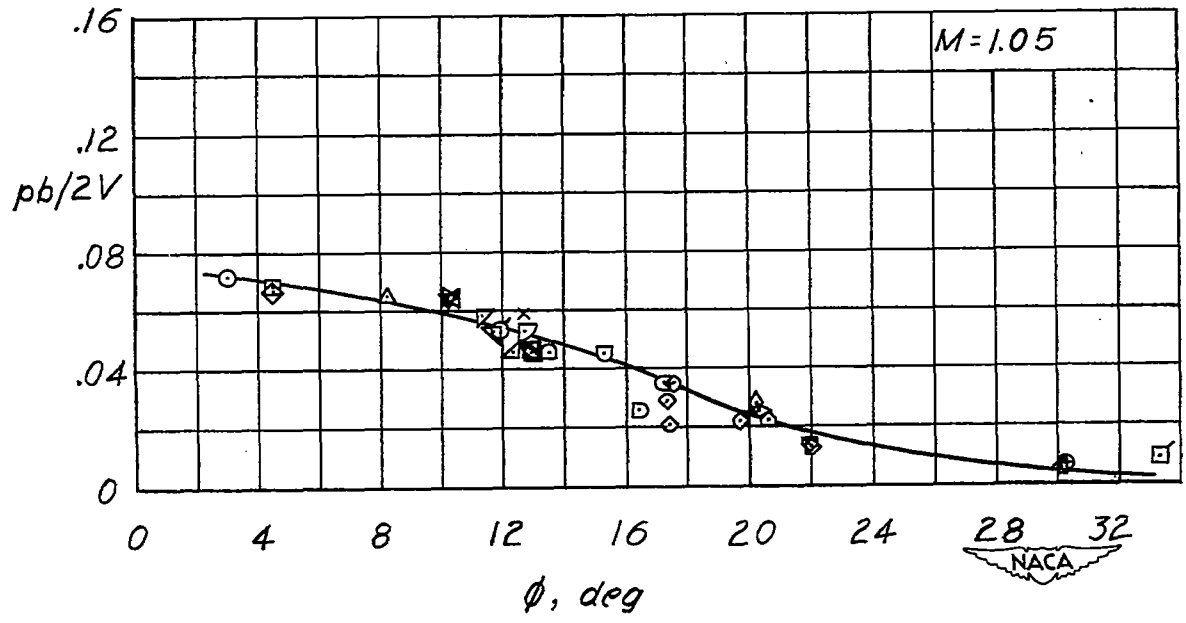

Figure 18.- Continued.

[redacted]

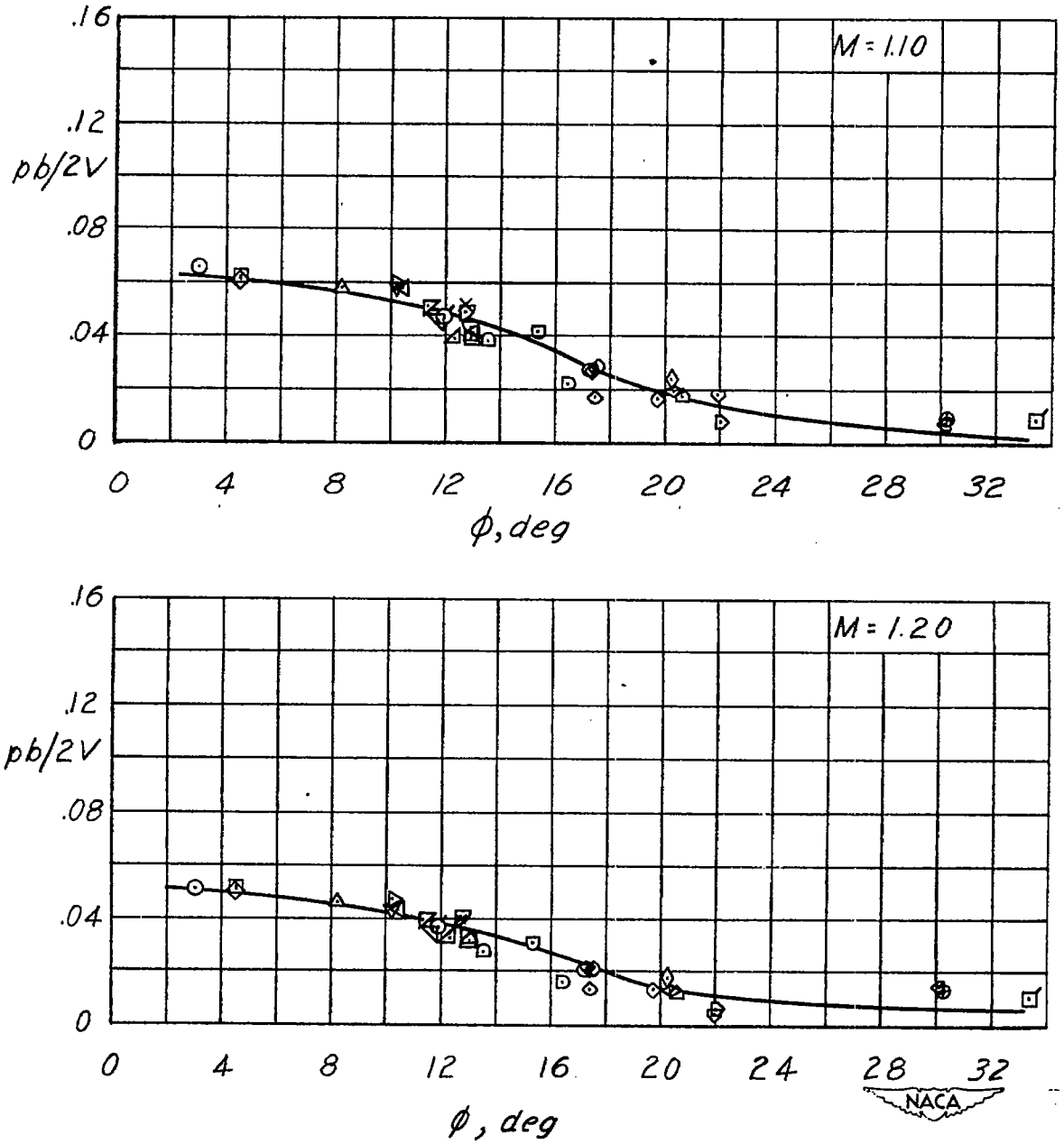

Figure 18.- Continued.

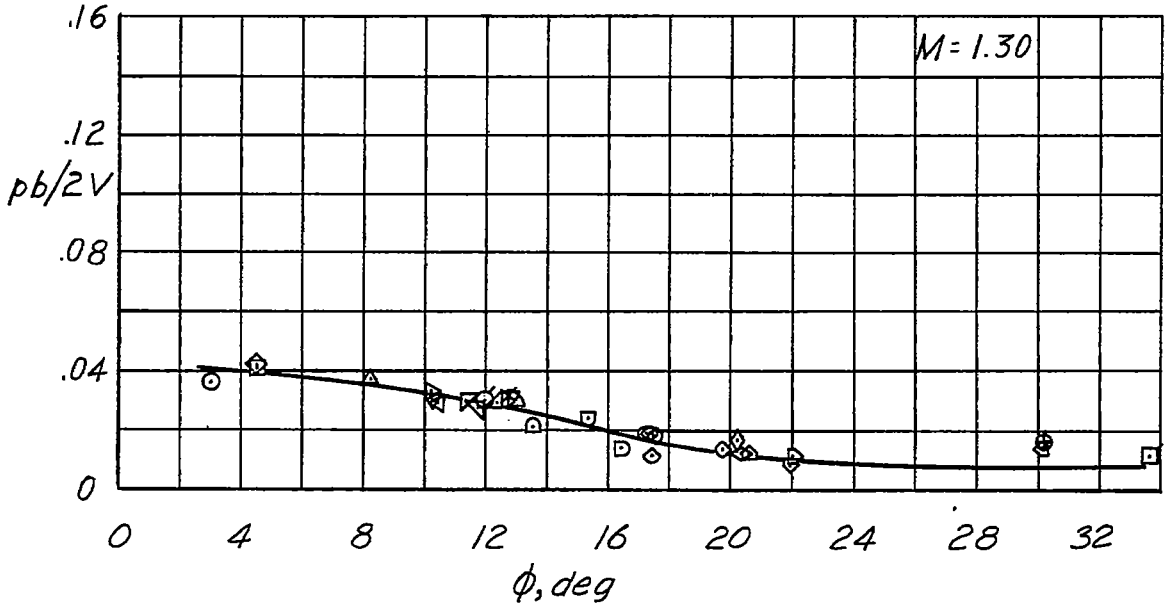

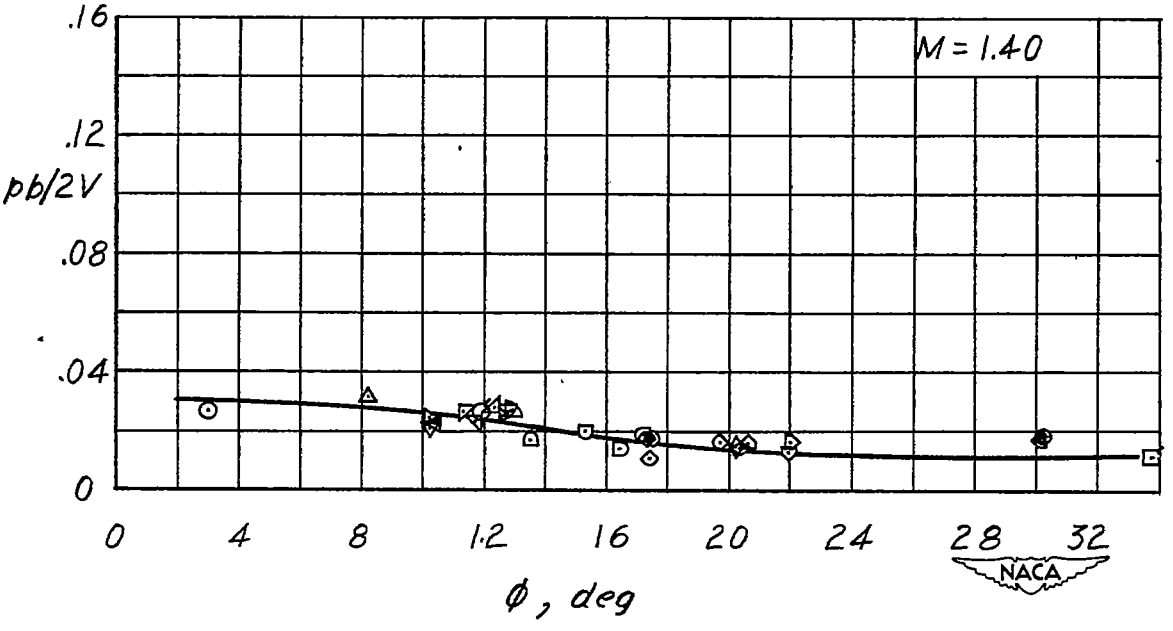

Figure 18.- Continued.

[redacted]

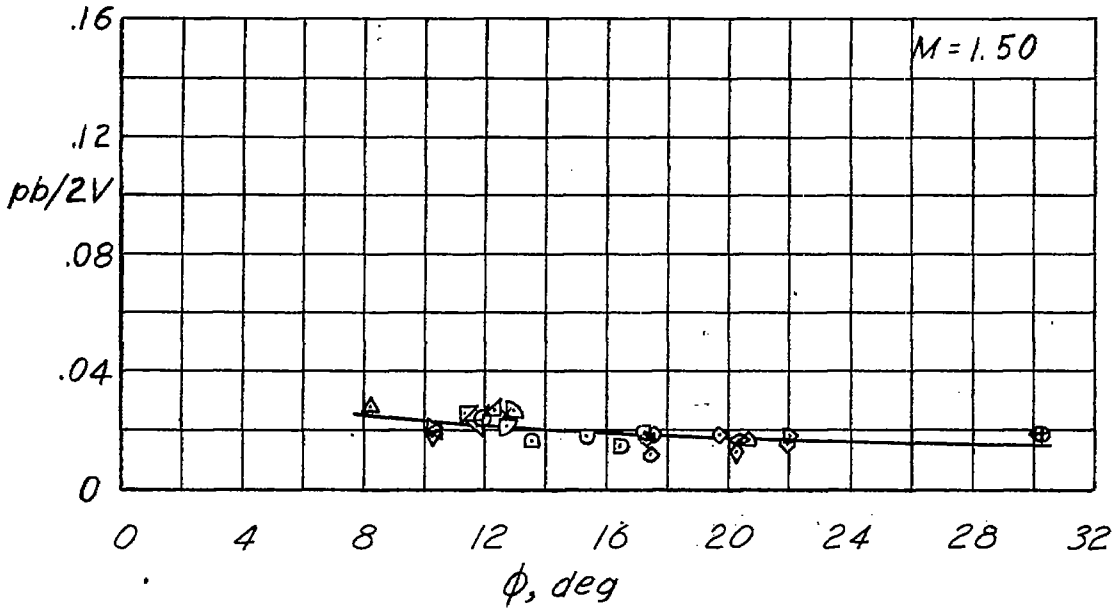

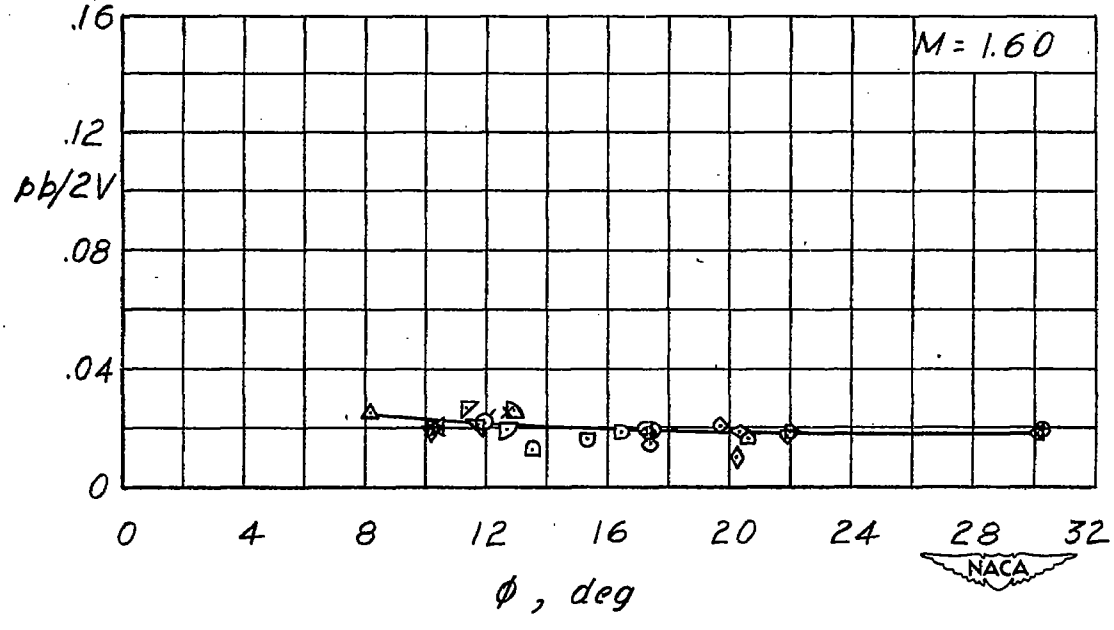

Figure 18.- Concluded.

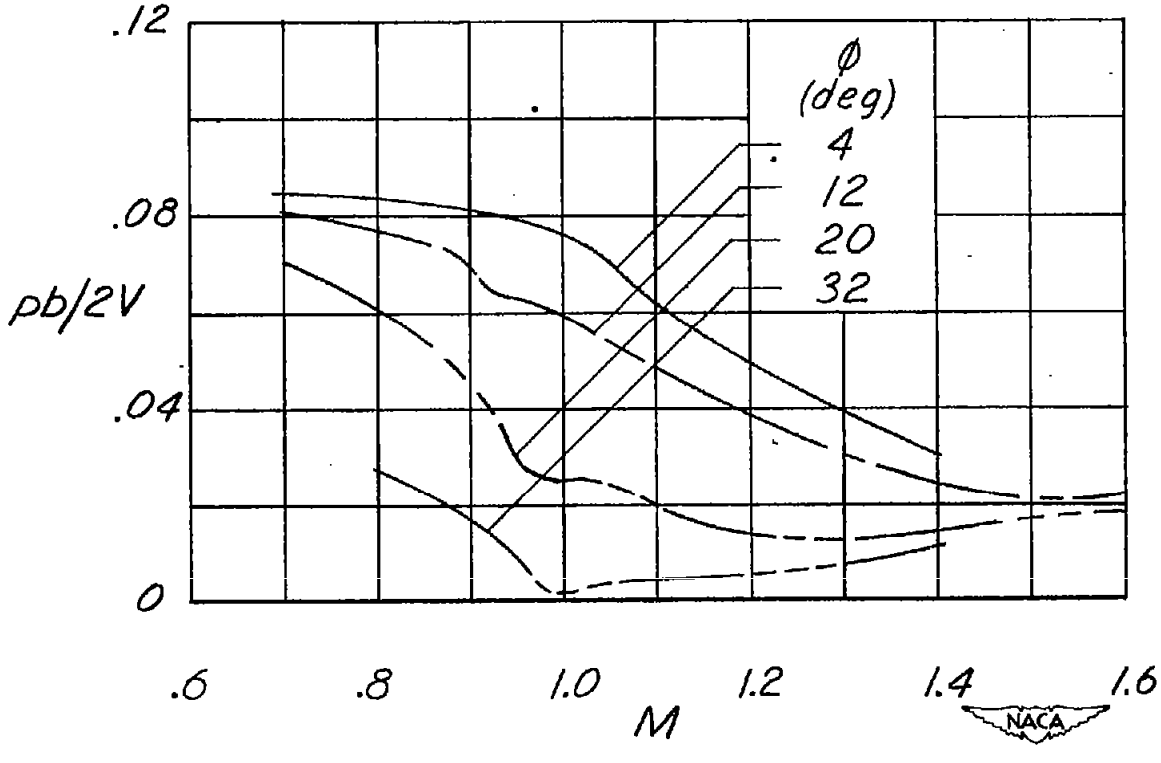

Figure 19.- Variation with Mach number of wing-aileron rolling effectiveness pb/2V for rigid wings swept back 45°; constructed from faired lines of figure 18 for several arbitrary trailing-edge angles. $i_w = 0°$ and $\delta_a = 5.0°$. $C_L \approx 0$.